FORSCHUNGSZENTRUM ROSSENDORF FZR

WISSENSCHAFTLICH-TECHNISCHE BERICHTE
FZR-289
März 2000
ISSN 1437-322X

Institute of Ion Beam Physics and Materials Research

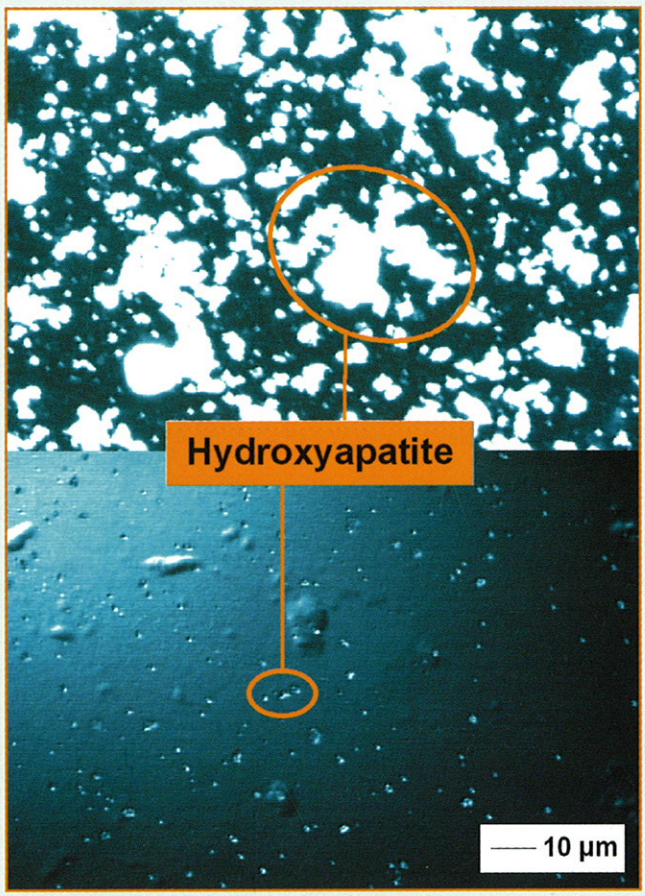

Annual Report 1999

Preface

The Research Center Rossendorf (Forschungszentrum Rossendorf, FZR) represents the largest governmental research institution in the "new" states of the Federal Republic of Germany. Its presently about 600 employees, organized in five institutes, study problems of basic and applied research in the fields of materials science, biomedical and environmental research, and nuclear physics. The FZR is a member of the Gottfried Wilhelm Leibniz Society, with the federal government and the state of Saxony contributing 50 % of the basic funding each.

The Institute of Ion Beam Physics and Materials Research has 74 permanent positions of scientists (32), technicians and engineers (40) and administration personnel (2). In average about 40 additional employees are funded from PhD student and PostDoc programs, guest funds, and governmental and industrial projects. The aim of the institute is to combine basic research and application-oriented studies in the fields of ion surface modification and ion beam surface analysis. According to the recommendations of the German Science Council, the institute represents a national ion beam center, which, in addition to its own scientific activities, offers services and transfers know-how on ion beam techniques to universities, other research institutes, and industry.

For these purposes, a broad range of ion-related equipment is available, delivering ion energies from about 10 eV (plasma treatment) to several 10 MeV (electrostatic accelerators). For the diagnostics of ion-treated surfaces, standard analytical techniques are available such as transmission electron microscopy, X-ray diffraction, Auger and photoelectron spectroscopy, and a number of chemical, optical, electrical, and mechanical diagnostics. Sample preparation is available for a large number of different materials including standard silicon processing within a class 100 clean room.

As shown in the diagram on page 4, the main R&D activities of the institute are grouped into two fields. The development of New Materials comprises the ion-assisted deposition of thin films, the ion- beam modification of semiconductors materials, the ion-assisted generation of nanoclusters and the ion modification of biomedical materials. New Processes include basic investigations and applications using a focused ion beam, plasma immersion and low-energy ion implantation, and the development of high-energy ion beam analysis tools.

It is the purpose of the present Annual Report to document the scientific progress of the institute in 1999 by a few selected extended contributions, numerous short contributions, and a statistical overview on its publications, conference contributions and lectures given by members of the institute. It also reports on the training of young scientists and the external and collaborative actions. We hope to demonstrate a very successful development in all of these areas.

A few important developments and actions deserve special comments. The institute has established itself successfully as a European User Facility according to the funding by the European Commission as a Large Scale Facility (LSF), entitled "Center for Application of Ion Beams in Materials Research" (AIM). More than 20 groups from all over Europe have

conducted their experiments at AIM in 1999. Within the new IHP ("Improving Human Potential") programme, the AIM funding has been extended to the years 2000-2002. Under this programme, also the Rossendorf Beamline ROBL at the European Synchrotron Radiation Facility (ESRF), which is operated in common with the Institute of Radiochemistry at Rossendorf, has been selected as a Large Scale Facility.

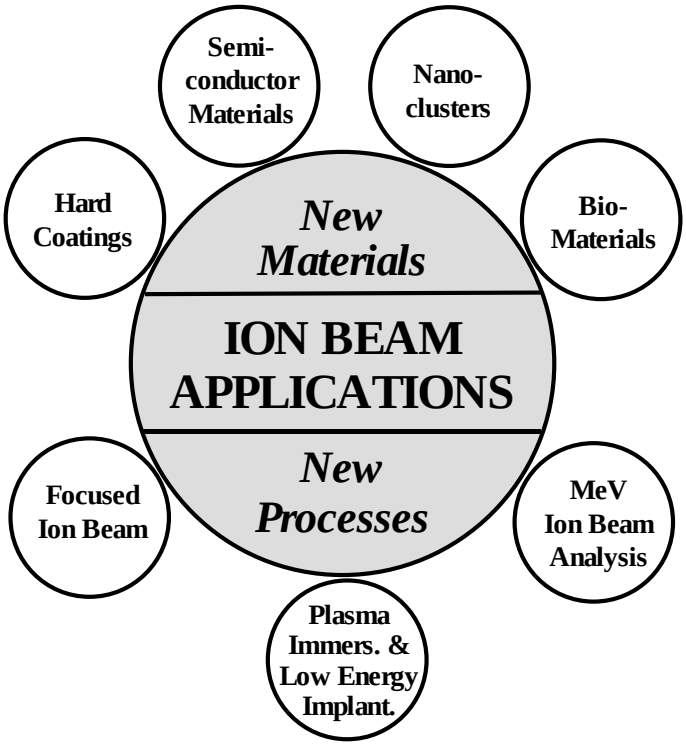

In 1999, the installation of new and combined ion beam facilities has quickly progressed. The 200 keV implanter and the IBAD (ion-beam assisted deposition) devices were transferred to the new experimental hall. Two experimental chambers are available now which allow simultaneous irradiation from the 500 kV implanter and the 3 MV Tandetron, for implantation and in-situ high-resolution ion-beam analysis, and for double implantation, respectively. A new small tandem accelerator (100 kV terminal voltage) has been constructed, for the special purpose of high-level tritium accelerator mass spectrometry.

In 1999, three PhD students finished their theses at the institute and their examinations at the Technical University of Dresden. The third summer school "Nuclear Probes and Ion Beams" was organized in Bad Blankenburg (Thuringia) in cooperation with the Hahn-Meitner Institute, Berlin, whith 40 students and 13 lecturers. In late July, the institute organized the 14th International Conference on Ion Beam Analysis (IBA) in conjunction with the 6th European Conference on Accelerators in Applied Research and Technology (ECAART), for which about 400 researchers and students from 40 countries met at Dresden. The institute also hosted the Second Annual Meeting of the European TMR network on "Carbon Based Hard Coatings", with about 40 participants.

Technology transfer and ion beam service activities of the institute have again been significantly enhanced in 1999. Ion beam analysis services for universities and industry cover a wide

range of materials such as metals, semiconductors, hard coatings, oxides, and perovskites. They are related to a broad spectrum of activities for mechanical and electronic applications in energy research, biomedicine, information technology, geology, and extraterrestrial research. A new beam line has been commissioned at the Tandem accelerator for industrial implantations of semiconductor wafers. Further ion implantation tests and service were performed in cooperation with about 40 partner institutions from research and industry, with particular emphasis on technological applications of plasma immersion implantation for automotive and machine components and different cutting tools.

The institute would like to thank all friends and organisations who supported its progress in 1999. Special thanks are due to the Executive Board of the Forschungszentrum Rossendorf, the Minister of Science and Arts of the Free State of Saxony, and the Minister of Education and Research of the Federal Government of Germany. Our partners from industry and other research institutes play an essential role for the Rossendorf ion beam center. Last but not least, the director would like to thank all members and guests of the institute for their active and often excellent contributions to a successful development in 1999.

Prof. Wolfhard Möller

In Situ Measurement of Stress in Boron Nitride Films

W. Fukarek, C. Fitz and A. Kolitsch

Cubic boron nitride (c-BN) is a wide band gap material (E_g>6 eV) that can be doped *p*- and *n*-type, exhibits a hardness close to that of diamond (40 - 60 GPa), but is resistant to oxidation up to 1300 °C, and does not react with ferrous metals. Thus, c-BN is a promising material for opto-electronics applications and as a super hard (>35 GPa) coating. After more than 30 years of research on BN film deposition, only nanocrystalline c-BN films have been obtained so far which are frequently slightly boron rich and contain impurities (up to some at.%) like Ar, O, C, and others, depending on the deposition technique used. This puts severe limits to electronic device fabrication but not necessarily to the application as a super hard material. The use of c-BN as a hard coating is hindered by high compressive stresses (3-20 GPa) in the films, which cause spalling.

A simple two-beam HeNe laser deflection system for real time *in situ* stress measurement has been set up, which is based on the cantilever bending principle. Cantilevers of 28x5x0.18 mm^3 are etched into 45x15 mm^2 Si <100> samples. Two parallel laser beams are reflected at the freely bending end of the cantilever (measurement beam) and at the surrounding Si frame (reference beam), respectively. Thus, changes in the position of the whole sample, e.g. due to changes in temperature, can be subtracted from the laser deflection caused by cantilever bending. The position of the reflected beam is measured using a linear position sensitive detector (PSD). Fig. 1 shows a sketch of the two-beam laser deflection system; for more details of the setup, see Ref. [1]. The stress measurement system is attached to an ion beam assisted deposition (IBAD) chamber which is installed at a beam line of a 200 kV ion implanter. The setup allows changes in the global stress to be measured in real time during deposition, ion implantation and during thermal processing of samples. The IBAD system employs an electron beam evaporator and a Kaufman ion source. Standard conditions for the deposition of BN films are: ion energy E_{ION}=500 eV, gas flow ratio Ar/N_2=2, substrate temperature T_S=400 °C, and BN growth rate of 2–6 nm/min. Details of the deposition system can be found elsewhere [2]. The chamber is equipped with a real time spectroscopic ellipsometer (RTSE) [3], or alternatively with a high precision single wavelength ellipsometer. Ellipsometry data are recorded at the position of the reference beam in order to avoid the ellipsometry data to be affected by changes in the angle of incidence due to sample bending.

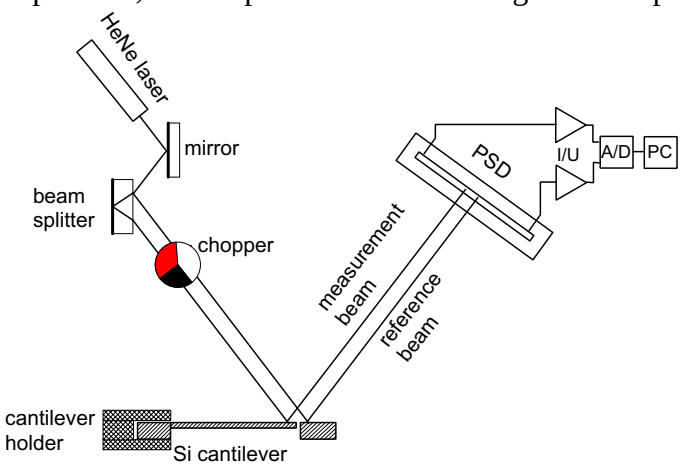

Fig. 1: Sketch of the two-beam laser deflection system. The Si cantilever is mounted on the substrate holder in the deposition chamber, all optical components are installed outside the chamber (not shown here).

The bending radius R (or the curvature $1/R$) of the cantilever is easily calculated from the relative (corrected) laser beam deflection Δx at the detector. Substitution in the modified STONEY's equation yields

$$S \cdot d_f = \int_0^{d_f} \sigma(z)\, dz = \frac{Y \cdot d_s^2}{6 \cdot R} = \frac{Y \cdot d_s^2}{6} \frac{\Delta x}{2lD} \quad , \qquad (1)$$

where S and d_f are global (averaged) stress and film thickness, respectively. $S \cdot d_f$ is called force per unit width (FPUW) and is basically the raw data of the stress measurement ($S \cdot d_f \sim \Delta x$). The constants Y, d_s, l, and D are biaxial elastic modulus, cantilever thickness, effective cantilever length, and distance between cantilever and PSD, respectively. The global stress S is the average over the depth distribution of the instantaneous stress $\sigma(z)$ which is the quantity of physical interest. But, its calculation using Eq. 1 requires not only reliable deflection data but also precise film thickness data to be available in order to allow for the calculation of the derivative with acceptable error bars.

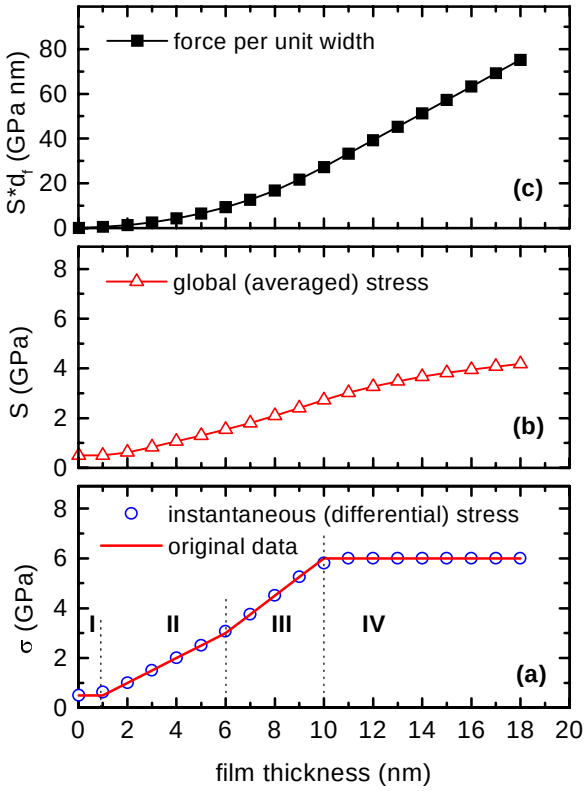

Fig. 2: Instantaneous stress (a), global stress (b), and force per unit width (c) depth profiles of a four-layer film system (computed data).

Fig. 2 shows computed depth profiles of instantaneous and global stress, as well as force per unit width versus film thickness of a 4-layer system to demonstrate the significant difference between those data. From the FPUW spectrum in Fig. 2(c) one would not expect a 4-layer system but rather mainly constant stress with a deviation in the film thickness range up to about 8 nm. In fact, no physical meaningful information can be extracted from a FPUW depth profile without further analysis. The global stress profile in Fig. 2(b) indicates a layered structure, but abrupt changes in the stress are not apparent in that data and the absolute numbers of the stress are too low (~50% at d_f =10 nm) due to averaging over regions with low and higher stress. The instantaneous stress data (hollow circles in Fig. 2(a)), as calculated from the FPUW profile in Fig. 2(c) deviate little from the original data (grey line) only at the interfaces of the regions. This example demonstrates that only the instantaneous stress data can provide the information of physical interest, and that precise FPUW- and d_f-data with a small data spacing are required.

Investigations on the stress in BN films have been performed by *in situ* measurement of the global stress [4,5] and *ex situ* in combination with stepwise etching [6]. An analysis of the instantaneous stress depth profile in BN films has not been reported before, although it has been noticed that the global stress increases with increasing film thickness due to the layered structure of BN films and higher stress in c-BN [6]. Fig. 3 shows the depth profile of the instantaneous stress in a BN film deposited under standard conditions for c-BN film growth. The thicknesses of the layer sequence t-BN / transition t-BN+c-BN / c-BN have been extracted from a TEM micrograph and correspond well to regions in the depth profile of the instantaneous stress. The origin of the increase in compressive stress during growth of the t-BN interfacial layer is not understood up to now. It can result from gradual changes in the crystalline structure of the t-BN layer, like increasing crystallite size. Also, c-BN might start to nucleate before it becomes visible in TEM analysis. Another possible explanation is that the modulus of elasticity in the t-BN layer increases gradually, while the strain induced by ion bombardment during growth remains largely constant. But information on the modulus of very thin t-BN films is missing up to now. In the transition region from t-BN to c-BN, where

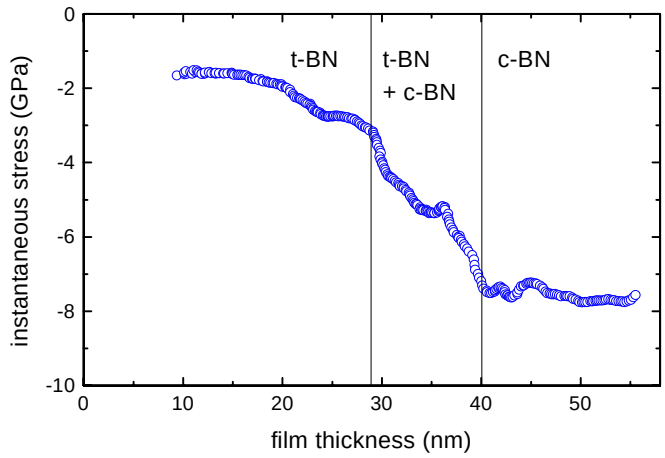

Fig. 3: Instantaneous stress versus film thickness in a c-BN film with the characteristic t-BN/c-BN layered structure.

t-BN and c-BN coexist but the volume fraction of c-BN increases with film thickness, the stress increases more rapidly. This can be explained on the basis of a phase mixing model of two phases with lower and higher stress, respectively. The constant stress in c-BN is expected for steady state film growth. The depth profile of the instantaneous stress in Fig. 3 differs markedly from global stress versus film thickness data reported recently [5], although the deposition systems and parameters are very similar. Moreover, in the experiments reported here, tensile stress has never been observed. Without the sample position correction employed here, bending data that would imply tensile stress have been recorded. This is an artifact resulting from an increase in temperature of the substrate holder in the beginning of the growth process due to energetic particle fluxes and IR radiation from the evaporator.

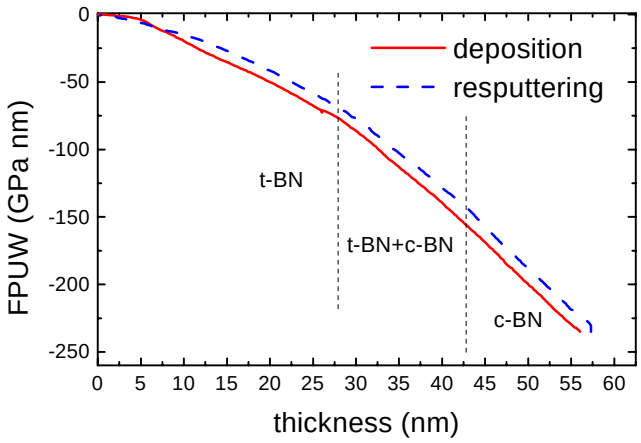

Fig. 4: Force per unit width versus film thickness in a c-BN film recorded *in situ* during growth and re-sputtering.

It has not been checked in any report on measurements of stress in BN films if the substrate and film are still in the elastic region or if they suffer from plastic deformation (PD). The occurrence of PD does not depend primarily on the stress but it depends on the film force, the thickness of the substrate, the temperature during processing, the nature of defects, etc. There is clear evidence for plastic deformation in Si substrates coated with thick (0.5 – 1 μm) c-BN films, as the substrates remained visibly bent after film delamination [7]. Information on plastic deformation of the Si substrate can be obtained from the cantilever bending (FPUW) after removal of the film. Fig. 4 shows the FPUW versus film thickness recorded during growth and sputtering off a c-BN film using 1 keV Ar ions. After re-sputtering there is no residual bending of the cantilever. This is the proof that the cantilever does not undergo plastic deformation up to the film forces accessible by the stress measurement setup. The data in Fig. 4 also show that there was no detectable stress relaxation in the film during or after growth. The offset in film thickness results from deposition of about 2 nm boron onto the film after termination of the growth process.

The relation between ion/atom arrival ratio and stress can be investigated dynamically by measuring the effect of a temporary increase in ion current density on the instantaneous stress. Fig. 5 shows the instantaneous stress versus film thickness for a t-BN deposition process. The temporary increase in the ion current density results in an immediate increase in instantaneous stress. This is in agreement with results reported for t-BN deposition using magnetron sputtering, where an increase in global stress with increasing I/A ratio has been observed [8]. It has to be pointed out, that the affected layer is only about 4 nm thick, and that the general

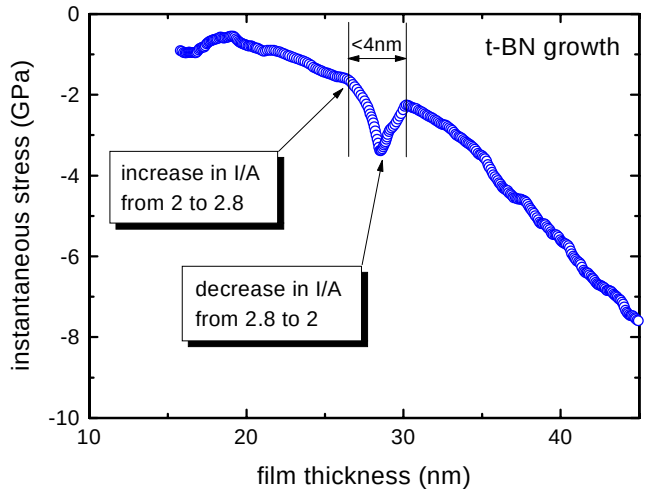

Fig. 5: Instantaneous stress versus film thickness in a t-BN film with a temporary increase in I/A ratio.

trend of increasing stress in the t-BN layer is not affected by the short-time increase in current density and instantaneous stress.

Ion implantation can be employed to reduce the compressive stress in c-BN films [9]. The results indicate plastic flow to be the predominating mechanism. A critical fluence for the transformation of c-BN to sp^2 bonded BN has been determined. Only very little information is available on the dynamics of the stress reduction, as only the effect of certain fluences and ions has been investigated. Fig. 6 shows the global stress in a c-BN film recorded dynamically during implantation of 35 keV Ar^+ ions at an angle of incidence of 34° to a fluence of $2x10^{14}$ cm^{-2}. Up to $2x10^{13}$ cm^{-2} an increase in global stress is clearly observed followed by the expected decrease in stress. The initial increase in stress has never been observed using *ex situ* analytical techniques. The data reveal that at least two mechanisms are involved: First defect formation and accumulation seem to be predominating before plastic flow becomes effective and results in stress relaxation. The inset in Fig. 6 shows s-polarised PIRR spectra recorded from the sample before and after the implantation. The spectra clearly show a decrease in the c-BN related absorption around 1080 cm^{-1} after implantation revealing sp^3 bond destruction. Summarising, ion implantation into c-BN results not only in stress relaxation by plastic flow, but in an increase in stress at low fluences, indicative of damage accumulation.

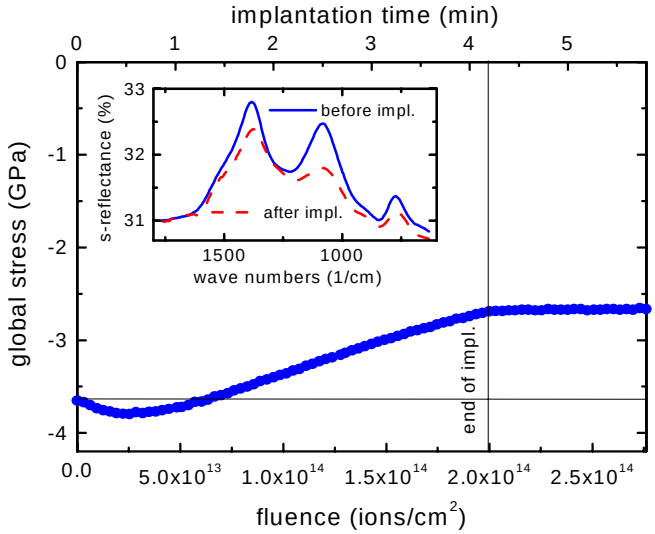

Fig. 6: Global stress in a c-BN film versus implanted fluence of 35 keV Ar^+ ions.

References

[1] C. Fitz, W. Fukarek, A. Kolitsch, W. Möller, accepted for publication in Surf. Coat. Technol.

[2] M.F. Plass, W. Fukarek, A. Kolitsch, U. Kreissig, Surf. Coat. Technol. 84 (1996) 383

[3] M-44 ellipsometer delivered by J.A. Woollam Co., Inc. Lincoln, NE, USA 68508

[4] D.R. McKenzie, W.D. Fall, W.G. Sainty, C.A. Davies, R.E. Collins, Diamond Relat. Mater. 2 (1993) 970

[5] M. Zeitler, S. Sienz, B, Rauschenbach, J. Vac. Sci. Technol. A 17 (1999) 597

[6] Y. Yamada, Y. Tatebayashi, O. Tsuda, T. Yoshida, Thin Solid Films 295 (1997) 137

[7] c-BN films produced by HKBV deposition in the group of A. Lunk, IPF, Univ. Stuttgart

[8] H. Ehrhardt, Proceedings of the 4th International Symposium on Advanced Materials (ISAM ´97), Tsukuba, Japan (1997) 34

[9] P. Widmayer, P. Ziemann, S. Ulrich, H. Ehrhard, Diamond Relat. Mater. 6 (1997) 621

Improvement of Ta-Based Thin Film Barriers for Copper Metallization by Ion Implantation of Nitrogen and Oxygen

E. Wieser, J. Schreiber**, C. Wenzel*, J.W. Bartha*, B. Bendjus**, V. Melov**,
M. Peikert, H. Reuther, A. Mücklich, B. Adolphi*, and D. Fischer*
* Technische Universität Dresden
** Fraunhofer Institut für Zerstörungsfreie Prüfverfahren, Aussenstelle Dresden

The continuous trend to reduce line widths in integrated circuits creates the necessity to decrease the thickness and simultaneously improve the stability of diffusion barriers in particular for copper metallization. Barrier thicknesses as low as 20 nm are required. The effectiveness of a diffusion barrier is strongly degraded by structural layer defects like grain boundaries and pores. Therefore a critical thickness of the barrier layer exists below about 30 nm to stop the diffusion of elements effectively. One effective way to reduce fast diffusion paths is the modification of the barrier into a nanocrystalline or amorphous and chemically [1] modified material by high dose ion implantation. In this paper we present results obtained by TEM, XRD and XPS for the structural modifications and their thermal stability in 100 nm Ta and Ta-Si films, deposited by long-throw RF magnetron sputtering on silicon (100) wafers, and modified by ion implantation of nitrogen and oxygen [2]. The functionality of modified 50 nm Ta barriers on Cu after thermal stress between 650 and 750 °C for 1 h is demonstrated by AES depth profiling.

The as-deposited 100 nm Ta layer is polycrystalline (predominantly β-Ta). The XTEM image of Fig. 1a shows clearly its columnar growth. After implantation of $1x10^{17}$ N^+/cm^2 the Ta film contains about 10 at.% nitrogen and an X-ray amorphous microstructure is formed. The implantation of $3x10^{17}$ N^+/cm^2 (about 25 at.%. nitrogen) results in partial formation of tantalum nitrides. As proved by XTEM the original columnar structure of the tantalum film is destroyed also in the case of nitride formation. The same fluence of O^+ ions leads to amorphization which is observed up to concentrations of about 50 at.% without significant indication of oxide formation in the diffraction pattern. The XTEM investigations show that layers characterized as amorphous by XRD still contain crystalline contributions. This is demonstrated in Fig. 1b for the implantation of $3x10^{17}$ O^+/cm^2. In the upper region of the Ta layer a contrast due to residual crystalline structures is observed. In the high resolution image (HRTEM) of such features lattice spacings indicating β-Ta have been identified. The central part of the Ta layer shows no significant contrast, as expected for an amorphous structure. At the interface to the silicon substrate a crystalline band of about 20 nm width is visible. Fourier analysis of a HREM image from this band (see inset of Fig. 1b) allows the identification of (202) and (114) lattice planes of the tetragonal Ta_5Si_3 phase with $c/a > 1$. XPS measurements indicate that oxidic bindings are formed. For all O^+-implantation doses the Ta 4f photoelectron peaks show additional peaks chemically shifted by 1.5 eV and 4.9 eV, respectively. These peaks can be assigned to Ta^{1+} and Ta_2O_5 . The difference to the bulk value for Ta_2O_5 of 4.5 eV can be explained by the amorphous structure. Ta_2O_5 arises only at the highest O^+ dose.

The thermal stability of the modified Ta layers was investigated by XRD measurements on annealed samples. The amorphization induced by oxygen implantation remains stable up to about 650 °C. Annealing at 750 °C results in significant crystallization. The most likely interpretation of the observed diffraction peaks is a superposition of contributions from the non-stoichiometric phase $Ta_{3.28}Si_{0.72}$ and TaO, i.e. the crystallization is correlated with interdiffusion of silicon into the implanted tantalum layer. The N^+-implanted sample ($3x10^{17}$

N^+/cm^2) which did form nitride already during implantation shows after annealing at 650 °C the superimposed reflections of Ta_4N and Ta_2N without diffuse intensity distributions from amorphous or nanocrystalline structures. By annealing at 750 °C the diffraction peaks become more narrow and shift to the positions of the Ta_2N reflections. This observation indicates that Ta_4N is transformed to Ta_2N.

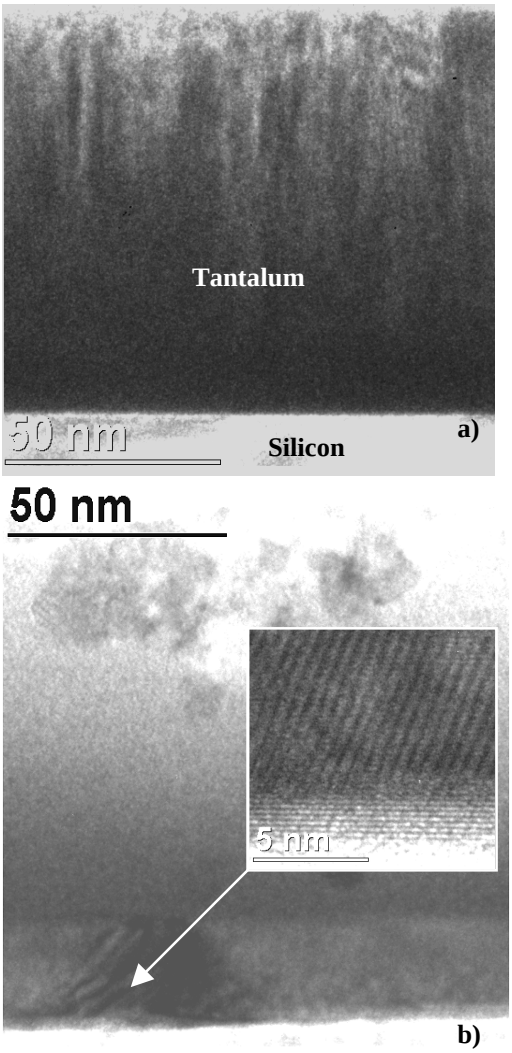

Fig. 1: XTEM images of 100 nm Ta layers: a) as deposited, b) implanted with $3x10^{17}$ O^+/cm^2. The inset presents a HREM image from the Ta_5Si_3 band at

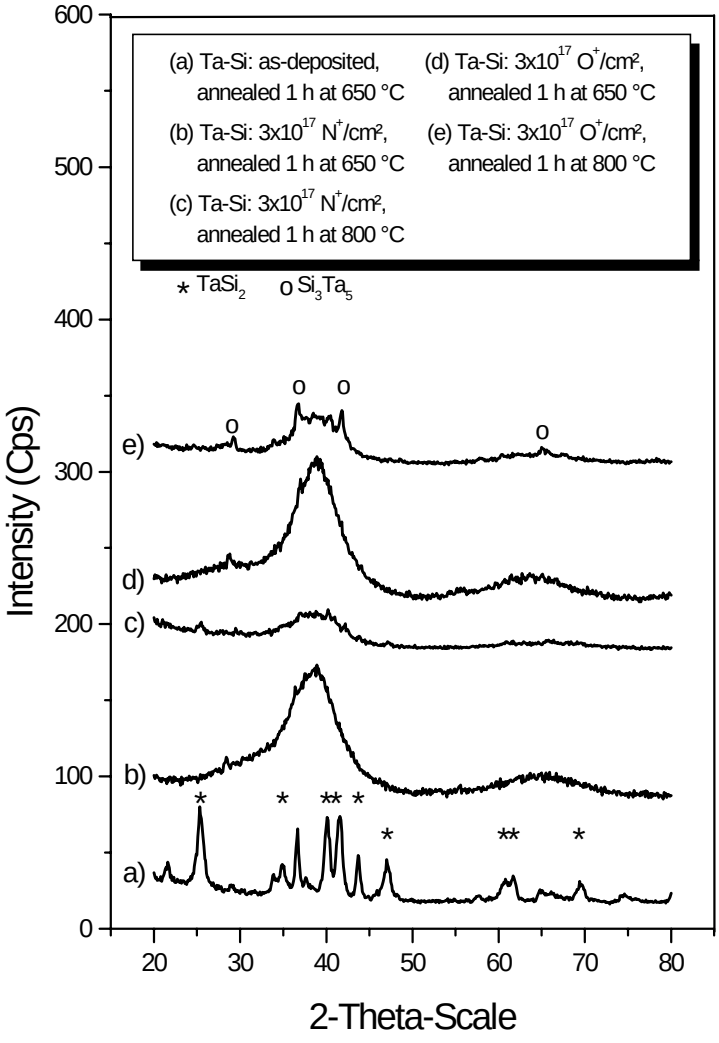

Fig. 2: XRD pattern of 100 nm Ta-Si layers as-deposited and implanted with $3x10^{17}$ cm^2 O^+ or N^+ ions after annealing at 650 °C and 800 °C, respectively.

The 100 nm Ta-Si layers are already X-ray amorphous after deposition. Here the intention of O^+ or N^+ implantation is an enhancement of thermal stability of the amorphous structure. This effect is demonstrated by the XRD pattern of post-annealed samples presented in Fig. 2. The unimplanted Ta-Si film recrystallizes already during annealing at 650 °C by formation of silicides. Most diffraction peaks in Fig. 2a correspond to reflections of $TaSi_2$. The formation of this silicon-rich phase can be explained only by interdiffusion of additional silicon from the substrate. The implantation of both species, N^+ or O^+, rises the crystallization temperature. After annealing at 650 °C the amorphous structure is conserved for both implantations. Even after annealing at 800 °C 1 h the N^+-implanted film is almost amorphous or nanocrystalline.

The layer implanted with $3x10^{17}$ O^+/cm^2 reveals much more pronounced crystallization features.

For testing the barrier integrity, multilayers were prepared consisting of 50 nm Ta / 1000 nm Cu / 50 nm Ta on a (100) Si substrate. Ion implantation of nitrogen ($5x10^{16}$ and $1x10^{17}$ N^+/cm^2 at 30 keV) or oxygen ($1x10^{17}$ or $3x10^{17}$ O^+/cm^2 at 35 keV) was carried out. The substrate temperature during implantation was held below 100 °C. Due to sputtering during the implantation the thickness of the top Ta layer is reduced to about 40 nm for the low, and to about 30 nm for the high oxygen dose. The thermal stability of the Ta layers against penetration of copper from the underlaying sheet was studied by annealing in vacuum of 1 to

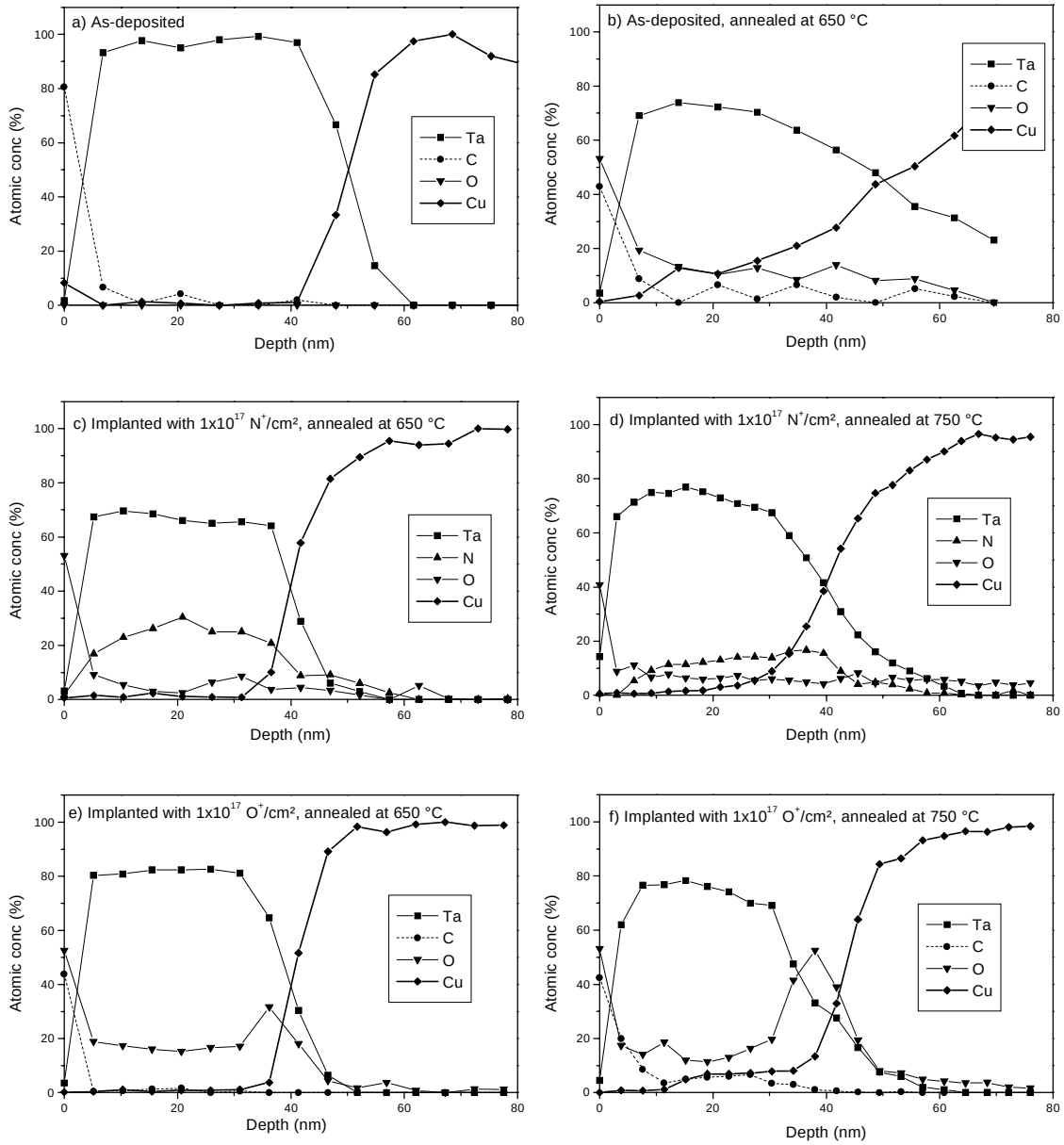

Fig. 3: Comparison of AES depth profiles of as-deposited and nitrogen and oxygen implanted multilayers annealed at 650 and 750 °C, respectively.

$3x10^{-4}$ Pa at temperatures from 650 and 750 °C for 1 h. The depth distribution of Ta, Cu and the implanted species was measured by Auger Electron Spectroscopy (AES) in combination with sputter etching by 3 keV Ar^+ ions. XRD of Cu-K_α radiation in gracing incidence was used to detect amorphization or formation of tantalum nitride. For all implantations the XRD patterns are characteristic for amorphous structures. The nitrogen dose of $1x10^{17}$ cm^2 resulting in about 20 at.% nitrogen is at the transition to nitride formation. After annealing at 650 °C weak nitride reflections are observed.

The non-implanted Ta barrier is not stable at 650 °C. A comparison of the AES depth profiles of Figs. 3a and 3b shows a significant penetration of copper into the Ta layer after annealing at 650 °C for 1 h. The intermixing with Cu increases by annealing at 750 °C especially in the interface near region. An AES mapping of the Ta surface after sputter removal of about 20 nm shows an inhomogeneous Cu distribution within the Ta layer indicating copper admixture starting from the grain boundaries of the columnar structure. For both nitrogen implantations a significantly improved barrier behavior is observed. Figs. 3c and 3d show corresponding depth profiles for the implantation of $1x10^{17}$ N^+/cm^2 corresponding to about 20 at.% nitrogen. The differences to the lower dose (about 10 at.% nitrogen) are within the error limits. After annealing at 650 °C no change in the interface region can be stated. However, a small Cu contamination (2 – 3 at.%) is detected within the Ta layer. By annealing at 750 °C the intermixing at the interface and the Cu contamination in the lower part of the Ta film are enhanced, although the Cu content in the top 10 nm remains unchanged. An oxygen contamination of the Ta layer with about 10 at.% is observed for both annealing temperatures. At 650 °C the copper penetration is completely impeded by oxygen implantation as demonstrated for about 20 at.% oxygen in Fig. 2e. The beginning of intermixing of Ta and Cu by annealing at 750 °C is somewhat more pronounced compared to the nitrogen implantation, with, however a negligible amount of Cu within the first 10 nm. Tempering at 750 °C leads also to a strong redistribution of oxygen from the Ta layer to the interface and to a penetration of oxygen into Cu. The redistribution starts already at 650 °C. This effect and the deterioration of the barrier properties can be attributed to the transformation of amorphous material to crystalline Ta oxides observed for the oxygen implanted Ta after annealing at 750 °C.

The presented results indicate that implantation of nitrogen and oxygen ions can change the microstucture of thin Ta films from polycrystalline to an amorphous-like. This structural change improves significantly the barrier effect in the temperature range from 650 to 750 °C. At 650 °C oxygen implantation is advantageous, compared to implantation of nitrogen.

References

[1] Y.-J. Lee, B.-S. Suh, Sa-K. Rha, C.-O. Park, Thin Solid Films 320 (1998) 141

[2] E. Wieser, J. Schreiber, C. Wenzel, J.W. Bartha, B. Bendjus, V. Melov, M. Peikert, W. Matz, B. Adolphi, D. Fischer, Advanced Metallization Conference (AMC), Orlando, Florida, Sept. 28-30, 1999

Prediction of the Morphology of the As-Implanted Damage in Silicon by a Novel Combination of BCA and MD Simulations

M. Posselt

In order to improve the knowledge on type and amount of defects created by ion implants which are typical of Si technology a novel combination of computer simulations based on the binary collision approximation (BCA) with classical molecular dynamics (MD) calculations has been developed.

The connection of BCA and MD simulations requires the description of ballistic processes in dependence on time. Since this is not accomplished in conventional BCA codes, the new time-ordered BCA program Crystal-TCAS was developed which is based on the Crystal-TRIM code (cf. [1] and refs. therein). The new program allows the time-ordered simulation of the collision cascades of incident ions. At sufficiently high energy transfer (above the displacement threshold) between projectiles and target atoms empty lattice sites and moving recoils are created. Otherwise target atoms are only hit. In the Crystal-TCAS code a collision cascade is followed until the energy of the moving recoils becomes less than a threshold of 100 eV. The time and position of the creation of empty lattice sites, the time and position of the generation of hit target atoms as well as their momentum, and the position and momentum of moving recoils at the time when their energy falls below 100 eV are stored. These data are used as inputs for subsequent MD calculations. In order to calculate the average as-implanted damage formed per incident ion statistically reliably, sufficiently many ion impacts have to be considered by the time-ordered BCA simulations. Fig. 1 illustrates the simulation region. The incidence points are randomly distributed within the irradiated area which is chosen large enough so that in the middle stripe all physical quantities related to ion irradiation depend only on the depth coordinate. This corresponds to conditions realized in common large-area implantations. In the middle stripe cubic cells are defined in which the relevant data on the state of collision cascades obtained after the termination of time-ordered BCA simulations of ion impacts are recorded. The size of a registration cell is $10a_o \times 10a_o \times 10a_o$ where a_o is the lattice constant, i.e. the cell is smaller than the entire volume of a collision cascade but larger than the distance between nearest neighbour atoms.

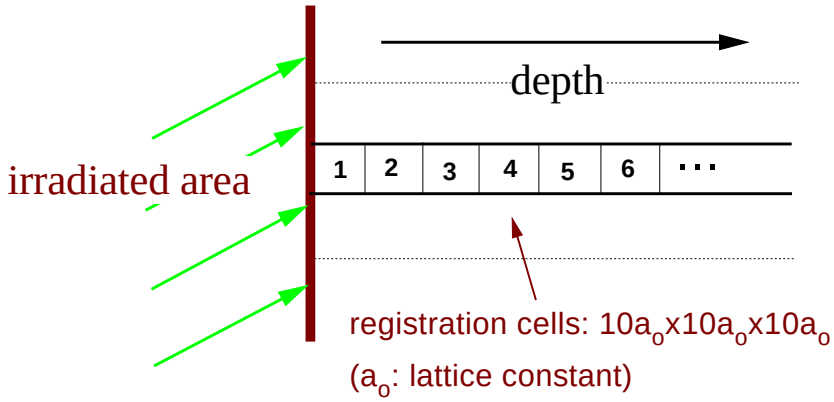

Fig. 1: Region of time-ordered BCA simulations and definition of registration cells.

The athermal and rapid thermal processes as well as the first stage of the thermally activated

processes initiated by the collision cascade of an individual ion in the registration cells are treated by MD calculations. Details of the MD code can be found in [2]. In all calculations the target temperature was 300 K (R.T.). The defect creation and evolution caused by various ions in the different registration cells is investigated. From the large amount of input data for the MD calculations produced by time-ordered BCA simulations such characteristic cases are selected where the energy deposition takes place mainly near the center of a cell. In this manner the error introduced by the limited cell size can be minimized. The selection procedure is possible due to the occurrence of well-separated subcascades. The investigations by MD simulations shows that 5-15 ps after ion impact the athermal and rapid thermal processes are finished, and a metastable defect structure is formed. Its further change due to thermally activated processes at R.T is in the order of few per cent. In the following the damage structure found after 18 ps is analyzed and defined as the as-implanted defect structure. Different damage analysis methods were employed: The first procedure identifies atoms the potential energy of which is at least 0.2 eV above the ground state value. These atoms are called disordered atoms. The threshold of 0.2 eV is chosen since in the perfect crystal atoms with higher potential energy do not exist at 300 K. The second method used to analyze the metastable damage structure formed is the Wigner-Seitz-cell-Voronoy-polyhedron analysis [2] which allows the identification of vacancies (*V*) and interstitials (*I*). The average number of disordered atoms per *V* and per *I* is found to be about 10 in all cases studied. The different as-implanted defect structures found 18 ps after ion impact were further subjected to a quantitative cluster analysis: A disordered atom is considered to be a part of a cluster if its distance to at least one of the other disordered atoms is less than the cut-off radius of the Stillinger-Weber potential which is used in the MD code. The cluster analysis was carried out in connection with the Wigner-Seitz-cell-Voronoy-polyhedron analysis. Therefore, it is not only possible to perform cluster statistics for disordered atoms but also to determine the number of *V* and *I* in each cluster. The cluster analysis demonstrated that not only isolated *V* and *I* are created but also medium-sized clusters consisting of *V*- and *I*-agglomerates like di-*V* and di-*I*, etc., and large clusters with up to some hundred disordered atoms. This variety of defect types is an important characteristic of the damage structure formed by ion bombardment. The analysis of the metastable defect states produced by different ions showed that the as-implanted damage created by a part of a collision cascade of a certain ion in a registration cell is completely determined by the nuclear energy deposition by the ion into this cell. There is almost no additional dependence on the depth of the cell and the species of the ion. Consequently, the combined simulation method can be significantly simplified since MD simulations need to be performed only in one cell for different values of nuclear energy deposition by a certain ion into this cell, regardless of the ion species and depth. Fig. 2 shows results of the analysis of 40 different cases of nuclear energy deposition into a cell. The total number of *V* and *I* grows almost linearly in the range of nuclear energy deposition considered (Fig. 2a). The number of isolated *I* is shown in Fig. 2b. It increases about linearly for low values of nuclear energy deposition. At higher values it is approximately constant. Fig. 2c depicts the increase of the number of atoms in clusters with more than 10 disordered atoms. In the following such clusters are called complex defects because they do not contain isolated *V* or *I*. Fig. 2c illustrates that complex defects are observed only above a threshold value for the nuclear energy deposition of about 640 eV. In a similar manner, the dependence of the number of atoms in clusters with more than 20 disordered atoms on the nuclear energy deposition into the cell was determined. Such clusters are called amorphous pockets because of the strong deviation of the atomic arrangement inside these clusters from that in a perfect crystal. Amorphous pockets are found above a threshold of about 1000 eV. The relatively large scattering of the data points in Fig. 2 is due to the fluctuations of the individual properties of collision cascades of different ions.

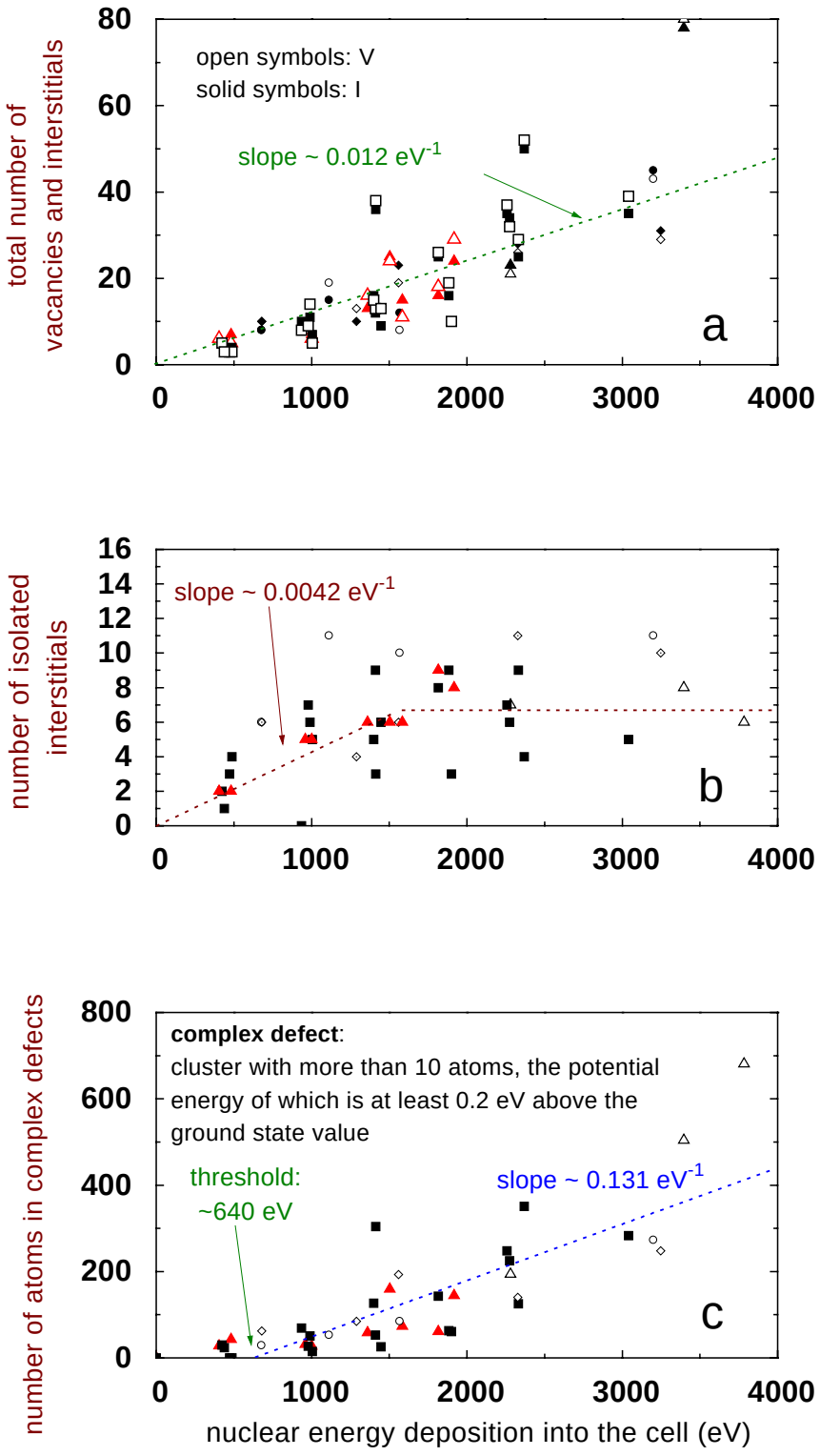

Fig. 2: Total number of vacancies and interstitials (a), number of isolated interstitials (b), and number of disordered atoms in complex defects (c) in dependence on the nuclear energy deposition by a certain ion into a registration cell. The symbols depict results of MD simulations (symbol types were chosen arbitrarily), the dotted lines show analytical approximations for the dependence of the number of defect species h^D (D: *V*, isolated *I*, number of atoms in complex defects) on the nuclear energy deposition E into the cell.

In order to use the results of MD calculations to determine the type and amount of defects

created on average per incident ion cascade statistics has to be considered. For this purpose the large amount of data generated by the time-ordered BCA simulations is analyzed with respect to the different values of nuclear energy deposition by a collision cascade of a certain ion into a cell i (at given depth, cf. Fig. 1). The number of events per incident ion $g_i(E)dE$, at which the nuclear energy deposition is between E and $E + dE$ is determined. The normalization of $g_i(E)$ with respect to the total number of deposition events N_i in cell i per incident ion ($N_i = \int g_i(E)dE$) leads to the probability $q_i(E)dE$ for a given nuclear energy deposition at a certain event. The dependence of $q_i(E)$ on E is depicted in Fig. 3 for 30 keV P^+ implants. It is found that $q_i(E)$ is nearly independent of the depth of the cell i, i.e. $q_i(E) \approx \mathrm{q}(E)$. This allows a great simplication in the calculation of $g_i(E)$

$$g_i(E) \;\approx\; N_i \; \mathrm{q}(E) \tag{1}$$

where N_i can be easily obtained from the depth profile of the nuclear energy deposition per incident ion. The probability $\mathrm{q}(E)$ was found to be an important characteristic of each ion species at given implantation conditions: Since heavy ions like As^+ form much denser cascades than light ions like B^+ a high nuclear energy deposition by a certain As^+ ion in a given cell is much more probable than by a certain B^+ ion. This difference is the cause for the fact that for each ion species a characteristic damage morphology is obtained as discussed below. The average number of defect species K_i^D (D: *V*, *I*, isolated *I*, disordered atoms, atoms in complex defects or amorphous pockets, etc.) produced per incident ion in cell i can be calculated by

$$K_i^D \;=\; \int h_i^D(E)\; g_i(E)\; dE \tag{2}$$

where $h_i^D(E)$ is the number of such defects created in cell i if the nuclear energy deposition at a certain event is E (cf. Fig. 2). Since it was found that $h_i^D(E)$ is nearly independent of the depth of cell i: $h_i^D(E) \;\approx\; \mathrm{h}^D(E)$, and because of equation (1) the determination of K_i^D becomes rather simple. Analytical fits to the values of $\mathrm{h}^D(E)$ and $\mathrm{q}(E)$ are used to calculated K_i^D. The fit functions are depicted by the dotted lines in Figs. 2 and 3. Equation (2) was applied to determine the depth profiles and the total number of different defect species produced on average per incident ion in 15 keV B^+, 30 keV P^+, and 15 keV As^+ implantations. The values of latter quantities are given in Tab. 1. These data are shown together with the total nuclear energy deposition and the total number of atomic displacements per incident ion. It is clear that the ratio of the latter quantities is about the same in the three examples due to the modified Kinchin-Pease relation [3]. But also the ratio of the total number of disordered atoms and the nuclear energy deposition per incident ion is nearly equal. This holds for the ratio of the total number of *V* or *I* and the nuclear energy deposition per ion, too. Thus, some quantities characterizing the as-implanted damage structure created by an incident ion are almost completely determined by the nuclear energy deposition per ion. However, this does not hold for all characteristics of the damage morphology: The ratio of the number of disordered atoms in complex defects and the nuclear energy deposition per ion is very different in the three cases due to the difference in the probability function $\mathrm{q}(E)$. The difference still increases if the ratio between the number of disordered atoms in amorphous pockets and the nuclear energy deposition per ion is considered. In the case of 15 keV B^+ implantation most of the complex defects are di-*V* and di-*I*, i.e. clusters with up to 20 disordered atoms containing exactly two *V* or two *I*. On the other hand, most of the complex defects formed by 15 keV As^+ implants are amorphous pockets.

In summary, a promising new method to quantify the morphology of the as-implanted damage has been presented. It is expected to have a great potential of applications in the field of fundamental investigations on implantation defects in Si as well as in future process simulators

for the Si technology. The principles of the method are also applicable to investigations of ion implantation into other materials.

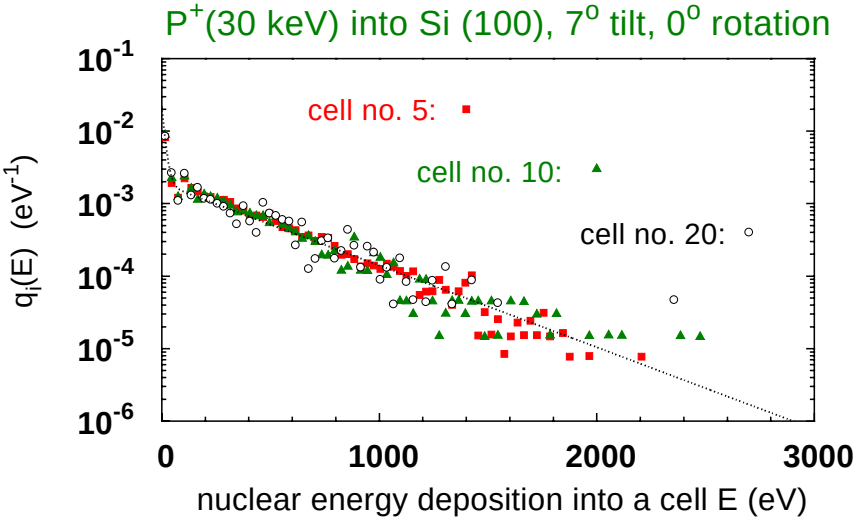

Fig. 3: Probability function $q_i(E)$ calculated for registration cells at different depths.

	15 keV B^+ 7° tilt, 0° rotation	30 keV P^+ 7° tilt, 0° rotation	15 keV As^+ 6° tilt, 0° rotation
nuclear energy deposition (eV)	3690	9650	7840
atomic displacements	107	290	237
disordered atoms (total)	927	2133	1821
disordered atoms in complex defects	73	441	607
disordered atoms in amorphous pockets	21	222	398
V or *I* (total)	93	213	182
isolated *I*	32	73	61

Tab. 1:
Total number of different defect species produced on average per incident ion for three examples. The total number of displacements and the total nuclear energy deposition per ion impact are also given.

References

[1] M. Posselt, Br. Schmidt, C.S. Murthy, T. Feudel, K. Suzuki, J. Electrochem. Soc. 144 (1997) 1495

[2] M. Posselt, in: Process Physics and Modeling in Semiconductor Technology, C.S. Murthy, G.R. Srinivasan and S.T. Dunham (eds.), The Electrochemical Society Proceedings Series, Pennington, NJ, USA (1999), PV 99-2, p.58

[3] P. Sigmund, Rad. Eff. 1 (1969) 15

Phase Formation due to High Dose Aluminium Implantation into SiC

V. Heera, H. Reuther, J. Stoemenos* and B. Pécz**,
*Aristotle University of Thessaloniki, Physics Department, 54006, Thessaloniki, Greece
**Research Institute for Technical Physics and Material Science, H-1525, Budapest, P.O.B. 49, Hungary

The physical and chemical behaviour of aluminium (Al) in silicon carbide (SiC) is of current interest for semiconductor physics and materials science. Al is the most important acceptor atom in the wide-band-gap semiconductor SiC that exhibits excellent properties for high power and high temperature electronics [1]. In comparison to Si based electronics, much higher acceptor concentrations are necessary in order to achieve comparable electrical conductivities. The Al concentrations often exceed the equilibrium solubility which is less than 0.5 at% at 1800 °C. It can be assumed that under critical annealing conditions the oversaturated Al/SiC system undergoes a phase separation or even transformation which will dramatically influence its physical properties. High Al concentrations are also needed for p-type ohmic contact formation on SiC. Furthermore, the study of the evolution of Al implanted single crystalline SiC as a function of Al concentration can contribute to a better understanding of the elementary Al-SiC reactions in more complex systems like SiC based solid solutions (e.g. $(SiC)_{1-x}(AlN)_x$), ceramics, SiC reinforced Al matrix composites and Al/a-SiC:H multilayers [2]. In the present paper the results of a detailed analysis of the structure and composition of SiC implanted with Al at 500 °C are reported. In addition, a reaction model is developed that explains the atomic depth profiles as a function of the Al concentration.

(0001) oriented hexagonal (6H) SiC wafers (n-type, Si-terminated surface) from Cree Research Inc. were implanted with Al doses of 3×10^{17} cm^{-2}, at an ion energy of 350 keV and a substrate temperature of 500 °C. This implantation temperature was chosen in the interesting range between 300 °C, above which amorphization of the SiC matrix is avoided, and 1000 °C, below which surface degradation can be neglected [3]. The morphology and lattice structure of the implanted layer were studied by cross section (X) and plan view (PV) transmission electron microscopy (TEM). Atomic concentration depth profiles were measured by Auger electron spectrometry (AES) in combination with sputtering.

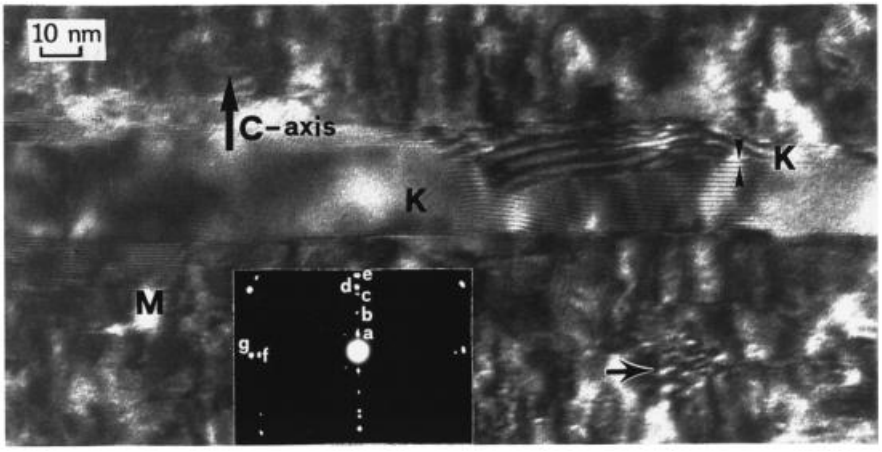

Fig. 1: High magnification XTEM micrograph from a band of Si and Al_4C_3 precipitates in the 6H-SiC matrix. The moiré patterns denoted by the letters K and M are attributed to the reflections (000.12) Al_4C_3 // (0006) 6H-SiC and (220) Si // (0006) 6H-SiC, respectively. Stacking faults are found in the SiC matrix below the band of precipitates as marked by the arrow. The selected area diffraction pattern in the inset shows the superposition of the 6H-SiC (d, g) and Al_4C_3 spots (a, b, c, e, f) from the precipitate K .

As demonstrated by the XTEM investigation the SiC matrix remains crystalline at the implantation temperature of 500 °C. In Fig. 1 a cross sectional micrograph of the centre of the implanted zone is shown. Within this zone a narrow band of large crystalline precipitates is formed around the Al maximum at about 450 nm depth. The most prominent precipitate has a laminar shape, about 150 nm long and 30 nm thick. Selected area diffraction patterns (SADP) taken from the zone of precipitates reveal the presence of Al_4C_3 and Si in the 6H SiC matrix. The diffraction spots (inset of Fig. 1) denoted by the letters d and g correspond to the 0006 and $2\bar{1}\bar{1}0$ reflections of the 6H-SiC matrix and the extra spots denoted by the letters a, b, c, e and f are identified to be the 0003, 0006, 0009, 000.12 and $2\bar{1}\bar{1}0$ reflections of the Al_4C_3 compound, respectively. As evident from the diffraction pattern the Al_4C_3 precipitates are in perfect epitaxial relation with the SiC matrix ([0001]SiC//[0001]Al_4C_3 and [11$\bar{2}$0]SiC//[11$\bar{2}$0]Al_4C_3). In addition to the Al_4C_3 precipitates, Si precipitates were found with an orientation of [0006]SiC//[111]Si and [220]Si. The presence of Al_4C_3 and Si is also confirmed by moiré patterns denoted by the letters K and M in Fig. 1. The moiré fringes are formed by interference of the imaging electron beams originating from the two superimposed lattices. The precipitates were further studied by plan view TEM after thinning the specimen from both sides so that only the precipitated zone was left. As shown by the bright and dark field images in Fig. 2 the precipitated zone has a morphology similar to a system after spinodal decomposition. It consists of a network of interpenetrating Si and Al_4C_3 grains with wavy boundaries.

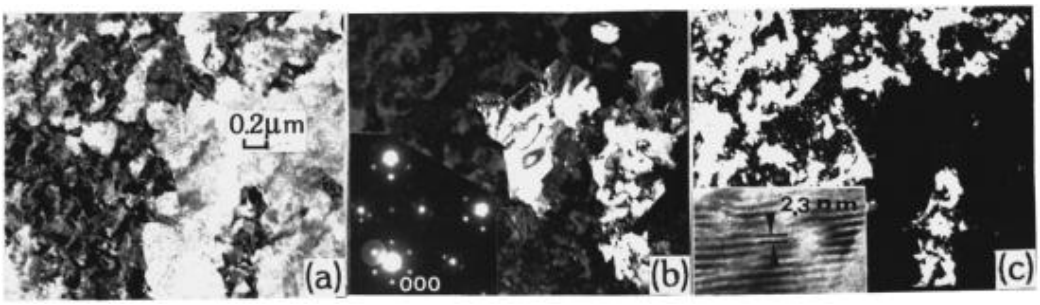

Fig. 2: Plane view TEM of the precipitate layer. (a) bright field, (b) dark field from the 220 silicon spot with the corresponding SADP in the inset, (c) dark field from the common 11$\bar{2}$0 6H-SiC and Al_4C_3 reflection. Moiré pattern due to the 11$\bar{2}$0 6H-SiC//11$\bar{2}$0 Al_4C_3 reflections is shown in the inset.

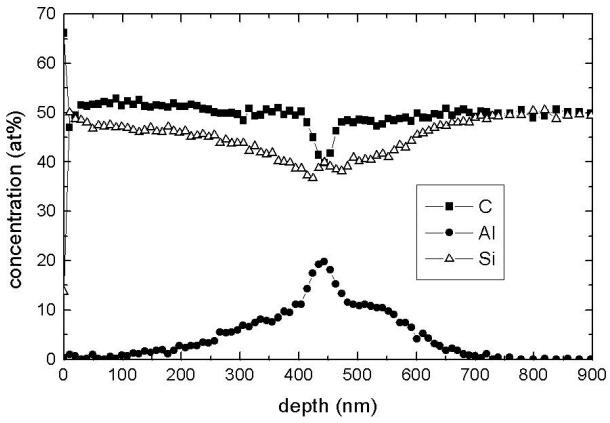

Fig. 3: Atomic depth profiles measured by AES.

Obviously, the Al/SiC system is unstable above a certain Al concentration, and precipitates of Si and Al_4C_3 are formed as demonstrated by the TEM results. However, the TEM analysis does not reveal the critical concentration above which the precipitation process starts. Moreover, it is not clear whether this phase separation leads to changes in the as-implanted Al depth profile. Therefore, sputter depth profiling by AES has been carried out. The Al depth profiles measured by AES are shown in Fig. 3. The formation of an Al peak at the depth of about 450 nm is an indication for compound formation in

this region. The band of precipitates found by XTEM is obviously correlated with the Al peak found in the AES profile.

From Fig. 3 it is evident that the Al peak is associated with a dip in the C concentration. In the more complex shape of the Si depth distribution a considerable feature is the local maximum which coincides with the C minimum in depth and concentration. The atomic concentration profiles may be understood in the frame of the following simple model:
(i) At low concentrations, the implanted Al atoms preferentially occupy Si lattice sites and produce Si interstitials. Most of these interstitials are mobile under the conditions of high temperature implantation and diffuse out of the implanted region.
(ii) Above a critical Al concentration $c_{Al,cr}$ of about 10 at%, chemical driving forces lead to the decomposition of the SiC matrix [4]. In the concentration range $c_{Al,cr.} \leq c_{Al} \leq 0.4$ this decomposition process is described by the chemical reaction

$$SiC + m\ Al \rightarrow m/4\ Al_4C_3 + (1\text{-}3/4\ m)\ SiC + 3/4\ m\ Si \qquad (1)$$

with $m \leq 4/3$. The Al fraction m is given as the ratio of the densities of Al atoms and SiC molecules in the Al/SiC system. Aluminium carbide and silicon are formed inside the silicon carbide matrix. The Si atoms which are kicked out in the chemical reaction are accumulated in Si precipitates. Additionally, Si atoms are bound in the remaining SiC matrix. This precipitation is accompanied by Al accumulation and volume swelling.

The following conclusions can be drawn from the model:
(i) As long as the Al concentration is less than the critical one, the implanted layer has the stoichometry $Si_{1-y}Al_yC$. This means that for any depth x the condition

$$c_{Al}(x) + c_{Si}(x) = 0.5 \qquad (2)$$

is fulfilled.
(ii) Considering the reaction (1) and the stoichometry of the resulting phases the following relations are obtained between the concentrations of Si atoms in the Si precipitates ($c_{Si,\ Si}$) and the total atomic concentrations which have been measured by AES:

$$c_{Si}(x) = 1/2 + 1/2\ c_{Si,Si}(x) - 7/8\ c_{Al}(x) \qquad (3)$$

$$c_C(x) = 1/2 - 1/2\ c_{Si,Si}(x) - 1/8\ c_{Al}(x)\ . \qquad (4)$$

Assuming that the Si atoms kicked out in the chemical reaction stay in their original depth we obtain

$$c_{Si,Si}(x) = 3/4\ c_{Al}(x) \qquad (5)$$

and with eqs. (3,4)

$$c_{Si}(x) = c_C(x) = 1/2\ (1 - c_{Al}(x)). \qquad (6)$$

As evident in Fig. 3, eq. (6) is only valid at the depth of the Al maximum. Therefore, it can be concluded that a mass transport occurs in normal direction away from the Al concentration peak. This mass transport is caused by the displacement of SiC by the precipitates. In particular a dramatic swelling is associated with the formation of Si precipitates since the

atomic density in Si is only half that of SiC. The total swelling can be calculated from the chemical reaction equation (1) and the atomic densities of the phases. It is

$$\Delta V/V = 1.94\, c_{Al}/(1-c_{Al}) \quad \text{for } 0.10 < c_{Al} < 0.40. \tag{7}$$

In Fig. 4 the AES depth profiles are analysed in terms of the model described above. In general, this analysis confirms the model. Obviously, the sum of the Al and Si concentration profiles fulfills equation (2) in good approximation as long as the Al concentration does not exceed 10 at%. According to the model this value should be the critical concentration for aluminium carbide formation and precipitation. In agreement with the XTEM results a narrow band of Si precipitates with a FWHM of 30 nm is found within the region of aluminium carbide precipitates. The local Si maximum in Fig. 3 is caused by these Si precipitates. Outside this band all Si atoms belong to the SiC phase.

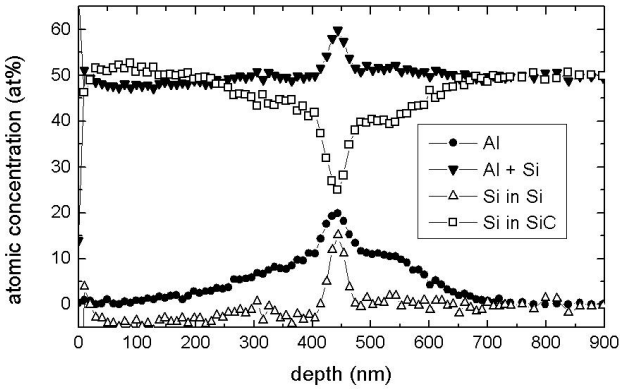

Fig. 4: Profiles of the noncarbon atoms calculated by eq. (3) from the AES results shown in Fig. 3

In conclusion, the phase formation due to high dose Al implantation into hexagonal 6H-SiC single crystals at 500 °C was studied by transmission electron microscopy (TEM) and Auger electron spectrometry (AES). A critical Al concentration of about 10 at% was found below which the 6H-SiC structure remains stable. The Al atoms occupy preferentially Si sites in the SiC lattice. The replaced Si atoms appear to be mobile under the implantation conditions and diffuse out. At higher Al concentrations the SiC matrix is decomposed and precipitates of Si and Al_4C_3 are formed. The Al_4C_3 precipitates have a perfect epitaxial orientation to the SiC matrix. The phase transformation is accompanied by atomic redistribution and strong volume swelling. The resulting changes in the atomic depth profiles can be accounted for by a simple chemical reaction model.

Acknowlegements

One of the authors (V.H.) would like to acknowledge the financial support by Deutsche Forschungsgemeinschaft (Contract No. HE 2604/2).

References

[1] T. Troffer, M. Schadt, T. Frank, H. Itoh, G. Pensl, J. Heindl, H.P. Strunk, M. Maier, phys. stat. sol. (a) 162 (1997) 277
[2] V. Heera, H. Reuther, J. Stoemenos, B. Pécz, J. Appl. Phys. 87 (2000) 78
[3] V. Heera, W. Skorupa, Mat.Res.Soc.Symp.Proc. 438 (1997) 241
[4] K. Yoshii, S. Inoue, S.Inami, H. Kawabe, J. Mater. Sci. 24 (1989) 3096

Simulations for Impurity Gettering in Silicon by Ion Implantation Induced Defects

K.-H. Heinig and H.-U. Jäger

Deep implantation of impurity atoms by high-energy ion implantation is interesting in at least three disparate areas. MeV ion implantation is adopted by industry for fabrication of retrograde wells of dopants. The second area is the fabrication of Silicon-On-Insulator (SOI) wafers for large scale integration by high-energy high-dose oxygen implantation (SIMOX process) or high-dose hydrogen implantation (Smart-Cut technique). The third area is gettering of deleterious impurities, such as Fe, at defects produced by high-energy ion implantation. Despite of the growing effort devoted to MeV ion implantation techniques [1-6], systematical theoretical studies of the formation and the evolution of high-energy ion implantation defects are rare. However, the ability to predict the depth distribution and evolution of defects is an important need for microelectronics industry. Therefore, numerical simulations of the formation as well as the thermal annealing of MeV ion implantation damage were performed. The predicted depth profiles are compared with SIMS profiles of gettered metallic impurities.

Although TRIM simulations predict the depth distribution of implanted ions reliably, the predictive power for ion implantation damage is much worse. This is due to the facts that (i) most displacements in a cascade are produced by low energy collisions which are not adequately described within the binary collision approximation and that (ii) the in-beam annealing of damage is not included. Despite these facts a good agreement has been generally found between the damage remaining after annealing and "excess defects" predicted by TRIM. This somewhat

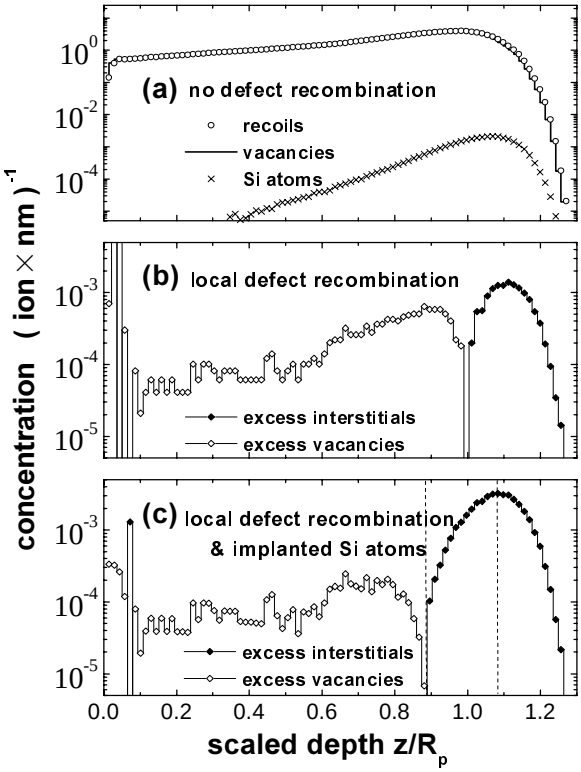

Fig. 1: TRIM simulation of 2.3 MeV Si^+ irradiation of Si ($R_p = 2.08$ μm). (a) Depth profiles of vacancies, recoils and Si ions. Vacancy and recoil profiles are nearly identical. (b) Point defects remaining after complete local vacancy-interstial recombination, which are 0.1...0.01% of the initial point defects. (c) Excess point defect profiles taking into account that implanted Si atoms contribute to the net point defect balance.

surprising agreement has been named ”+1”-model. According to this model, ion implantation induced vacancy- and interstitial-type defects annihilate completely in the initial stage of annealing leaving behind only an excess of interstitial-type defects which originate from the implanted impurity atoms. Thus, the number of interstitials found in loops equals the number of implanted ions. Small deviations from ”+1” (1 interstitial per 1 ion) have been found.

The ”+1”-model predicts for conventional ion energies (*e.g.* 50 keV B^+) the integral point defect excess for the total implanted depth. This assumption is reasonable because for such ion energies and standard annealing conditions the diffusion length of point defects is at least comparable to the width of the implantation profile, i.e. $\sqrt{D \times t_A} \gtrsim R_p$, with D – diffusion coefficient of the fastest point defect, t_A – annealing time and R_p – projected range. For MeV implantation we find $\sqrt{D \times t_A} \ll R_p$, *i.e.* a complete annihilation of interstitial- and vacancy-type defects happens locally only (being denoted as ”local +1 model” in the following). It should be emphasized that within the ”local +1 model” an excess of vacancy-type defects cannot annihilate with an excess of interstitial-type defects which is located at another depth. Therefore, for high-energy ion implantation it becomes significant that the recoil profile is slightly shifted with respect to the vacancy profile. The shift is tiny, about 1 nm, so it can not be resolved in Fig. 1a. However, due to this shift, about 0.01...0.1% of vacancies of Frenkel pairs find no interstial for recombination in the sub-R_p region (Fig. 1b). The same holds for interstitials in the R_p region.

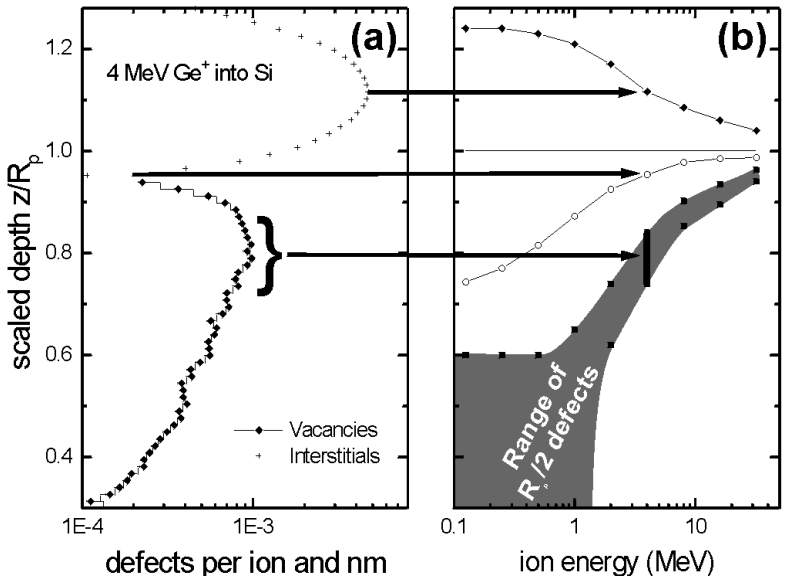

Fig. 2: (a) Presentation as in Fig. 1c, but for 4 MeV Ge^+ irradiation of Si with exchanged ordinate and abscissa. (b) The 3 characteristic depths of Fig. 2a marked by arrows are plotted as function of Ge^+ ion energy: (-O-O-) depth of complete vacancy-interstitial annihilation; (-♦-♦-) depth of maximum interstitial excess; (-■-■-) range of vacancy excess.

Including the implanted Si ions, which contribute to the number of interstitials, the boundary between the regions of vacancy- and interstitial-type defects shifts towards the surface (Fig. 1c). For a systematic study of defects of 60 keV to 32 MeV Si^+ and Ge^+ ion implantation into Si several months computing time on 400 MHz Pentium PCs have been spent. The most striking feature of the profiles of excess vacancies/interstitials is the region of complete vacancy-interstitial annihilation (Fig.1c). This region is very narrow, *i.e.* it gives a well-defined depth which is well below R_p for low ion energies and which approaches asymptotically towards R_p at higher ion energies. This characteristic depth as well as the depths of maximum interstitial

and vacancy concentration are marked by arrows in Fig. 2a for 4 MeV Ge^+ implantation into Si ($R_p = 2.02$ μm). In Fig. 2b these depths are plotted for different Ge^+ ion energies. Above 1 MeV all characteristic depths approach asymptotically the projected range R_p.

The time evolution of excess vacancies and interstitials during thermal annealing has been calculated by diffusion-reaction equations using the module for point defect-based diffusion of the one-dimensional process simulator TESIM (see Ref. [7]). The thermal formation rate of Frenkel pairs is $k = 3.43 \times 10^{-12}$ cm^3/s $\times \exp(-1.4\,\mathrm{eV}/k_BT)$, the other point defect parameters (D_I, D_I, c_I^*, c_V^*) have been taken from Ref. [7]. The fraction of vacancies/interstitials exceeding a critical concentration c_{sol} is assumed to form clusters, which re-evaporate if concentration drops during time evolution below c_{sol}. For the process simulator TESIM the TRIM profiles of excess point defects described above have been employed as initial condition. During annealing the vacancy profile changes faster than the interstitial profile due to its lower initial concentration and due to the surface sink nearby. Between the top layer of vacancy excess and a deeper layer of interstitial excess we find an intermediate region which is a sink for both, vacancies and interstitials, due to vacancy-interstitial annihilation. A defect-free gap forms there.

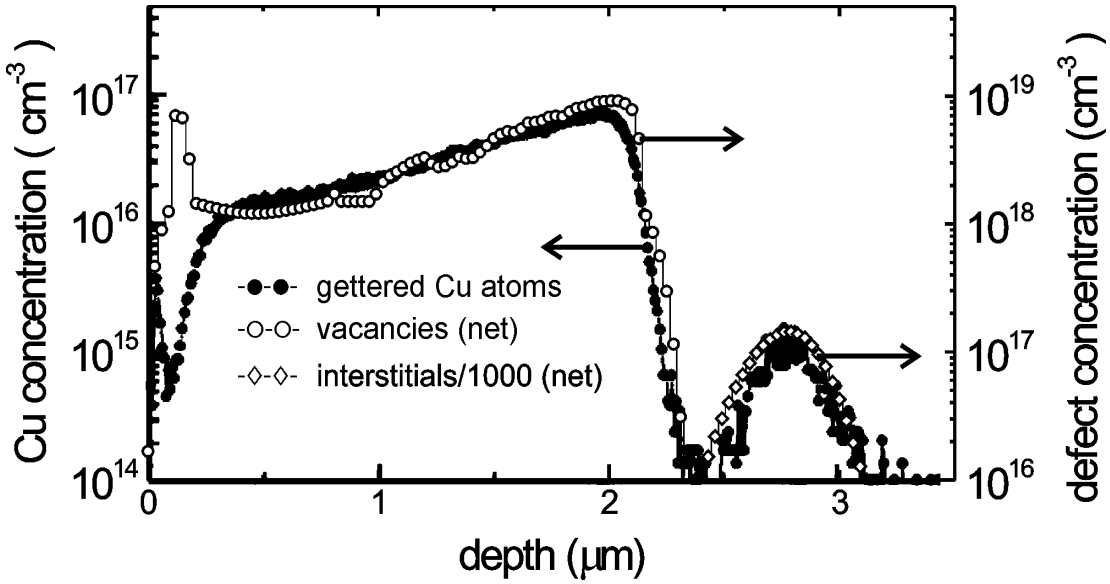

Fig. 3: Comparison of a Cu depth profile of Kögler *et al.* [6] measured by SIMS after implantation of 3.5 MeV, 5×10^{15} cm^{-2} Si^+ into Si and annealing at 900 °C for 5 s with the calculated depth profiles of vacancies and interstitials, using TRIM and diffusion-reaction simulations for the same process parameters.

In Fig. 3 a TRIM/TESIM simulation of an experiment by Kögler *et al.* [6] is shown, who studied Cu gettering in Si implanted with 5×10^{15} Si^+ cm^{-2} at 3.5 MeV for different annealing temperatures and times. For 5 s annealing at 900 °C, a SIMS profile of Cu atoms is compared with simulated profiles of vacancy and interstitial excess. The only fitted parameter for vacancies and interstitials is $c_{sol}\,(900\,^\circ\mathrm{C}) = 1.5 \times 10^{18}$ cm^{-3}, for the other quantities default parameters of TESIM have been taken. In Fig. 3, the ordinates at the left and right hand sides correspond to the measured Cu concentration and the predicted defect concentration, respectively. The excess interstitials are rescaled by 1/1000 in order to overlap in the R_p-region the predicted defect profile with the measured Cu profile. This means, corresponding to the presented model and for the particular conditions of Fig. 3, excess vacancies getter Cu 1000 times more efficiently

than excess interstitials. A comparison of both ordinates shows that about 100 excess vacancies getter one Cu atom. With the exception of a thin surface layer, the Cu profile follows exactly the vacancy profile. Although this analysis gives no direct information about the nature of the extended vacancy-type defects which getter Cu, the ratio between gettered atoms and vacancies could help to clarify this point.

The nearly perfect agreement of the shape of the experimental SIMS profile of gettered Cu atoms with the shape of the calculated point defect profile *without any rescaling of the depth scale* (see Fig. 3) is surprising in view of the well-known uncertainties in the depth scales of both SIMS measurements and TRIM calculations.The good agreement demonstrated in Fig. 3 has been found also for other annealing and implantation conditions.

The results presented here (see Figs. 2, 3) strongly support the assumption that the so-called '$R_p/2$' peak of metal gettering arises from vacancy-type defects. The time dependence of gettering in the sub-R_p region reflects the vacancy profile evolution during annealing. According to Fig. 2b, below 1 MeV Ge^+ ion energy the whole region from the surface to $0.6R_p$ is characterized by vacancy excess and a corresponding getter behavior (Fig. 3). As it is not shown here, only during longer annealing a pronounced '$R_p/2$' gettering peak forms due to two vacancy sinks, the surface and the vacancy-interstitial annihilation zone. For Ge^+ ion energies exceeding 1 MeV a sub-R_p getter peak must not be formed during annealing, it results from the TRIM profile (Fig. 2b). However, this peak is no longer located around $R_p/2,$ with increasing Ge^+ energies it approaches R_p.

Acknowledgments

The authors thank Dr. Kögler who initiated the theoretical studies. This work is part of the European Network ENDEASD.

References

[1] O. Kononchuk, R.A. Brown, Z.Radzimski, G.A. Rozgonyi, F. Gonzalez, Appl. Phys. Lett. 69 (1996) 4203
[2] A. Agarwal, K. Christensen, D. Venables, D.M. Maher, G.A. Rozgonyi, Appl. Phys. Lett. 69 (1996) 3899
[3] S. Coffa, V. Privitera, F. Priolo, S. Libertino, G. Mannino, J. Appl. Phys. 81 (1997) 1639
[4] R.A. Brown, O. Kononchuk, G.A. Rozgonyi, S. Koveshnikov, A.P. Knights, P.J. Simpson, F. Gonzalez, J. Appl. Phys. 84 (1998) 2459
[5] S.V. Koveshnikov, G.A. Rozgonyi, J. Appl. Phys. 84 (1998) 3078
[6] R. Kögler, R.A. Yankov, M. Posselt, A.B. Danilin, W. Skorupa, Nucl. Instr. Meth. B147 (1999) 96
[7] H.U. Jäger, J. Appl. Phys. 78 (1995) 176

Ion Beam Synthesis of δ-like Ge Nanocluster Bands in Thin SiO_2 Films for Memory Applications

J. von Borany, T. Gebel, K.-H. Heinig, M. Klimenkov, B. Schmidt, K.-H. Stegemann* and H.-J. Thees*
* Zentrum Mikroelektronik Dresden GmbH, Dresden, Germany

A new promising approach of scalable device structures for future microelectronics is the nanocrystal memory [1,2]. This memory is based on the effect that electrons can be reliably stored even at room temperature in small semiconductor quantum dots ($d_{nc} < 10$ nm, C ~ 10 aF) embedded in the gate oxide of a field effect transistor. The charge exchange between the clusters and the Si substrate occurs via direct tunneling, leading due to a shift in the threshold voltage of the FET with respect to the charge state within the clusters.

The main technological challenge consists in the fabrication of a band of small nanoclusters with a density of about 10^{12} cm^{-2} very close (< 5 nm) to the Si/SiO_2 interface. The nanoclusters (size: 3-5 nm) have to be arranged well separated from each other and from the Si substrate. At present, two different technologies are favoured for the fabrication of shallow nanocluster bands near the Si/SiO_2 interface. LPCVD or PVD techniques have been successfully applied to deposit self-assembled Si nanocrystal dots onto ultrathin thermally grown SiO_2 (2-3 nm), subsequently covered by an control oxide of 7-10 nm thickness [3]. The distance of the nanocrystals from the Si/SiO_2 interface is well defined by the thickness of the tunnel oxide, but unfortunately the nanocluster density is limited to about 10^{11} cm^{-2} due to preferred condensation of free Si at existing clusters formed at the early stage of deposition [4]. Alternatively, it has been shown that ion beam synthesis (IBS) is a well suited method to fabricate semiconductor nanoclusters (Si, Ge) in SiO_2 layers. The IBS process is performed by ion implantation of Si or Ge of about 10^{16} cm^{-2} (exceeding the solubility limit in the SiO_2 matrix) followed by an annealing step in order to form clusters. Following this route Normand et al. [5] applied very low energy (1-5 keV), high-fluence ($> 10^{16}$ cm^{-2}) Si implantation into 11 nm thin SiO_2 films. After annealing they found a band of clusters around the position of the implantation peak.

This contribution reports on another ion beam based process suitable for the formation of Ge nanoclusters in thin SiO_2 films. In previous experiments using SiO_2 films > 100 nm thickness it has been found, that after annealing above 900°C the Gaussian like as-implanted profile in the SiO_2 layer changes towards a Ge distribution, which is characterized by at least two separated Ge peaks in the bulk and near (or at) the Si/SiO_2 interface. Under special implantation conditions one can observe a very sharp (δ-like) nanocluster band in the oxide very close to the Si/SiO_2 interface [6]. Based on this finding experiments have been performed to investigate this effect on thin SiO_2 films ($\leq$ 50 nm) suitable for memory applications.

Thin SiO_2 films of 30 nm thickness have been prepared on (100) Si wafers by thermal oxidation. Afterwards, the wafers were implanted with ^{74}Ge ions at 12 or 20 keV to vary the position of the implantation profile with respect to the Si/SiO_2 interface The used fluence results in a Ge peak concentration of about 5 at.%. After a cleaning procedure identically prepared samples were annealed using rapid thermal processing (RTA: 950°C, 30 sec, N_2).

Transmission electron microscopy (TEM) using a Philips CM300-TEM has been performed

at cross-sectional specimens to analyse the nanocluster formation in the SiO_2 films. The detection limit of the cluster size is about 2 nm. In addition, Rutherford backscattering spectrometry (RBS) with ^4He ions of 1.7 MeV was applied to measure the Ge distribution in the SiO_2 layer. Using an incidence of 70° perpendicular to the surface a depth resolution of < 2 nm could be realized.

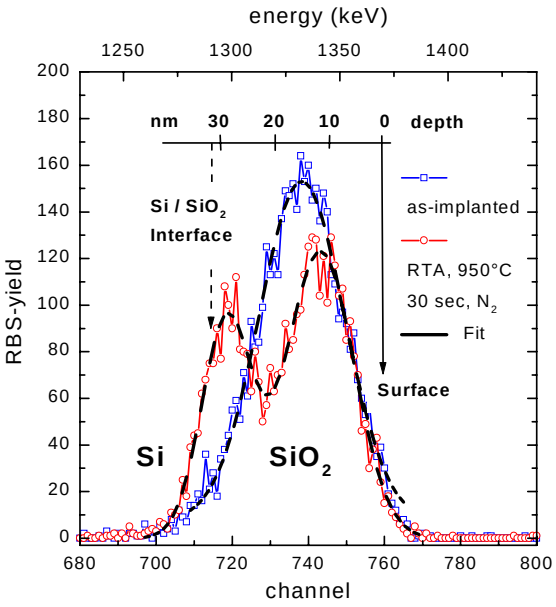

Fig. 1a: RBS-spectra showing the Ge depth distribution after implantation (^{74}Ge,20 keV,5x10^{15}cm^{-2}) in 30 nm SiO_2 films for the as-implanted state and after RTA processing (950°C, N_2, 30 sec)

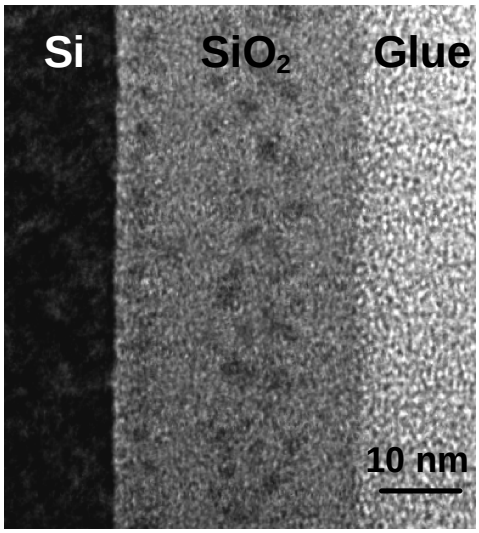

Fig. 1b: XTEM micrograph showing the two nanocluster bands in the bulk and very close to the Si/SiO_2 interface
(II: 20 keV / 5x10^{15}cm^{-2};RTA: 950°C, 30 sec)

Fig. 1a shows the Ge depth distribution for an implantation of 20 keV / 5x10^{15} cm^{-2} before and after annealing. The as-implanted profile is characterized by a single peak located at 16 nm, which corresponds to the expected value from TRIM-calculations (R_p = 18 nm). After RTA processing the Ge profile has changed to a double peak distribution with a peak at about 12 nm and a second Ge peak, which is very close to the Si/SiO_2 interface. In the TEM micrograph no nanoclusters can be detected in the as-implanted state. After RTA processing we found two different cluster bands, which are separated by a zone free of clusters (Fig. 1b). A relatively „broad“ cluster band of about 10-12 nm width is located around the peak position of the initial implantation profile, slightly shifted towards the surface. The clusters have a mean size of (3.5±1.0) nm and the cluster density can be estimated to about 8x10^{11} cm^{-2}. The second cluster band is located in a distance of only 2-3 nm from the Si/SiO_2 interface. This cluster band is very narrow (δ-like) and consists of a plane of single, clearly separated clusters parallel to the Si/SiO_2 interface. The mean size of these spherical clusters is slightly smaller (mean size: 3 nm) as compared to the bulk clusters. The cluster density within this band is about 5x10^{11} cm^{-2} (±50%). All clusters have been found to be in the amorphous state. The position of the cluster bands corresponds to the Ge distribution measured by RBS, which means that the implanted Ge is now mainly within the clusters. If the implantation is performed at 12 keV (R_p = 12 nm), no significant Ge redistribution with respect to the as-implanted profile can be observed by RBS after annealing. TEM analysis reveals the Ge nanocluster formation only as bulk clusters around the peak of the implantation profile after RTA processing. The size and density of the clusters are similar to the values mentioned above. Contrary to the

implantation at 20 keV no near-interface cluster band was found.

In the following, we will discuss a model for the evolution of the near-interface nanocluster band, which is well separated from the implantation profile. As such a band can be observed independent of the implanted species (Ge, Sn, Sb etc.) or the thickness of the SiO_2 layer (20-500 nm) [6,7], this effect is assumed to reflect intrinsic mechanisms of the ion implantation process.

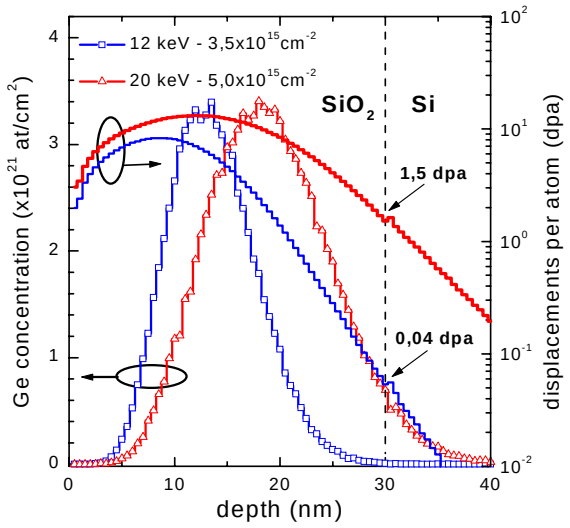

Fig. 2: Ge depth distribution (left) and number of displacements (right) of 12 and 20 keV Ge implantation into 30 nm SiO_2 films calculated by the TRIM-96 code.

The as-implanted Ge content integrated over the region of the interface nanocluster band is $\leq 5x10^{14}$ cm^{-2}, which is too small to form the near-interface nanoclusters observed in the TEM after annealing (⌀ 3 nm, $5x10^{11}$ cm^{-2}, see Fig. 1b). Therefore, diffusion of Ge from the implanted profile and the accumulation of Ge at nucleation centers in a thin layer parallel to the Si/SiO_2 interface have to be basic phenomena in the model. The TRIM calculation (see Fig. 2) shows for the 20 keV implantation an average value of 1.5 dpa at the SiO_2/Si interface. That implies, that due to collisional mixing (mainly by the recoil atoms) each atom of the SiO_2 network is displaced at least once, which means a dissociation of the SiO_2 network into the elemental components Si and O.

Whereas within the SiO_2 layer displaced Si and O recombine, the Si/SiO_2 interface acts as a strong sink mainly for oxygen due to its relatively large diffusion coefficient during irradiation. As a result the SiO_2 region close to the Si substrate becomes depleted from oxygen or, controversely, Si accumulates above the stoichiometric value. This phenomenon has been proven by STEM-EDX measurements at appropriately irradiated 500 nm thick SiO_2 layers on Si. Rate-equations studies reveal, that the maximum value of Si excess is realised in a distance of about 3-4 nm from the Si/SiO_2 interface. During subsequent thermal treatment the excess Si atoms form small precipitates on which Ge diffusing from the implanted region condenses. A corresponding kinetic 3D lattice Monte Carlo simulation starting with a Gaussian like Ge profile and taking into account the excess Si close to the SiO_2/Si interface qualitatively describes the experimental results. During the simulated annealing a near-interface band of Ge nanoclusters (containing Si) and additional Ge clusters around R_p are formed, which are separated by a zone nearly free of clusters (for details see [8]). It should be pointed out that the nanoclusters in the oxide represent a metastable state. Due to evaporation of Ge from the cluster surface or (in most cases) due to chemical reactions with residual contaminations (oxygen and/or hydrogen) within the annealing atmosphere cluster bands disappear, especially at higher temperatures ($>900°C$) and longer annealing times (>60 min) [9]. Therefore, much care has to be spent to realize reproducibly clean and dry annealing conditions.

In the case of the 12 keV implantation almost no decomposition of the SiO_2 matrix occurs close to the SiO_2/Si interface (dpa-rate < 0.1, see Fig. 2). Consequently, no near-interface Ge

nanoclusters can be expected, as the Si precipitates are a prerequisite according to the model described above.

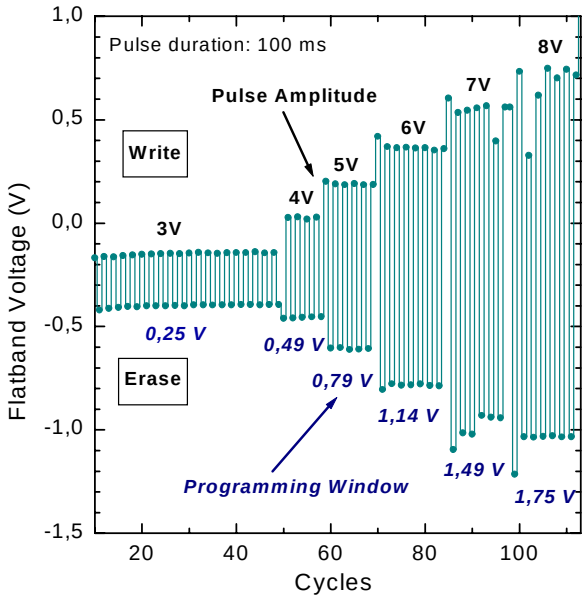

Fig.3: Shift of the flatband voltage after write/ erase cycling using different pulse amplitudes for tp = 100 ms.

MOS capacitors containing nanoclusters in the gate oxide near the Si/SiO_2 interface were used to investigate the feasibility for a memory device. Contacts with an area of $9x10^{-2}$ mm^2 were realized by patterning of n^+-doped Poly-Si (d = 300 nm). When forward biasing the gate with respect to the substrate electrons are injected towards the nanoclusters and cause a positive flatband voltage shift (Write). The charge can be removed by a programming pulse of the opposite polarity (Erase). Fig. 3 shows the results of high frequency CV-measurement. Erase and write pulses of different amplitudes were applied to the structure, while the programming time was kept constant at 100 ms. For programming pulse amplitudes between 3-8 V the flatband voltage difference after write/erase pulses (programming window) shift has been found to be between 0.25 V and 1.75 V, respectively. Note, that by using charge sensing for the read operation of a memory cell, a window of about 0.2 V may be sufficient. The mechanism of charge storage is still open. Electrons might be stored within the clusters or at cluster related deep trapping centres. Future investigations will be performed to clarify this question.

Acknowledgement

This work is supported by the Sächsisches Staatsministerium für Wissenschaft und Forschung (Grant-No.: 7531.50-03-844-98/4), which is gratefully acknowledged.

References

[1] S. Tiwari, F. Rana, K. Chan, L. Shi, H. Hanafi, Appl. Phys. Lett. 69 (1996) 1232
[2] C. Wasshuber, H. Kosina, S. Selberherr, IEEE Trans. on Electr. Dev. 45 (1998) 2365
[3] S. Tiwari, F. Rana, H. Hanafi, A. Hartstein, E.F. Cabbe, K. Chan, Appl. Phys. Lett. 68 (1996) 1377
[4] I. Kim, S. Han, H. Kim, J. Lee, B. Choi, S. Hwang, D. Ahn, H. Shin, Int. Electron Dev. Meeting, San-Francisco, IEDM-98, 111
[5] P. Normand, D. Tsoukalas, E. Kapetanakis, J.A. van den Berg, D.G. Armour, J. Stoemenos, Microelectr. Engineering 16 (1997) 79, ibid Electrochem. Lett. 1 (2) (1998) 26
[6] A. Markwitz, L. Rebohle, H. Hofmeister, W. Skorupa, NIM B147 (1999) 361
[7] A. Nakajima, T. Futatsugi, H. Nakao, T. Usuki, N. Horiguchi, N. Yokayama, J. Appl. Phys. 84 (3) (1998) 1316
[8] J. von Borany, R. Grötzschel, K.-H. Heinig, A. Markwitz, B. Schmidt, W. Skorupa, H.-J. Thees, Solid State Electr. 43 (1999) 1159
[9] K.-H. Heinig, B. Schmidt, A. Markwitz, R. Grötzschel, M. Strobel, S. Oswald, NIM B148 (1999) 969

Hydroxyapatite Nucleation on Na Ion Implanted Titanium Surfaces

M.T. Pham, W. Matz, H. Reuther, E. Richter, G. Steiner*
* Institut für Analytische Chemie, Technische Universität Dresden

Hydroxyapatite (HA) coating is the common approach to improve the biocompatibility of orthopaedic and dental titanium-based implants. Low-temperature processses are of current interest. In these processes, biologically active HA having the chemistry and structure of mineralized tissue may be formed under *in vivo* simulated conditions. One key problem is to impart Ti surfaces with the ability to nucleate HA formation from an aqueous solution. An enhanced HA nucleation can be achieved by (i) functionalized surfaces acting as molecular blueprints for site-directed nucleation, (ii) elevated supersaturation of HA at the surface, and (iii) surface topography providing confined reaction microenvironments and geometrically matched nucleating sites. Ti surfaces treated with NaOH have been shown to induce HA formation upon exposing to simulated body fluid (SBF) [1,2]. The effect is closely related to the above criteria: generation of hydroxylated surface Ti–OH groups and increased supersaturation of HA by increased surface pH resulted from Na_2TiO_3 hydrolysis, and etching-generated rugged surface morphology.

This paper presents the surface treatment involving ion implantation of Na into Ti to show that surface-incorporated Na_2TiO_3 and a microporous rugged surface topography are formed by reactions of Na with Ti, and such surfaces are reactive to induce HA nucleation upon exposing to SBF. The present experiments used plates of commercially pure Ti (10 × 10 × 1 mm^3). Standard procedures of polishing and cleaning were applied before use. Na ions were implanted at doses ranging from 8×10^{16} to 4×10^{17} ions cm^{-2}. The ion energies were set at 18 to 22 keV to deposit Na within a surface layer of (22 – 28) ± 14 nm thickness. Exposure experiments in SBF of pH 7.4 were conducted at 37 °C in polystyrene vials. The surfaces were characterized by XRD, FTIR, XPS, SEM, and light microscopy (LM).

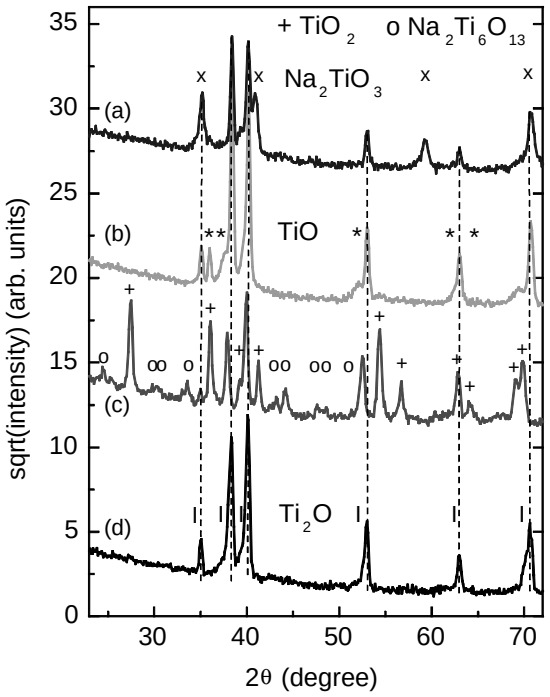

The new major phase introduced into the surface after Na implantation is Na_2TiO_3 as evidenced from the XRD analysis (Fig. 1a). The signal intensity increases with the ion dose indicating the increased concentration formed by ion implantation. The substrate Ti signal is attenuated correspondingly, confirming that the Ti surface becomes covered by the implanted layer.

Fig. 1: XRD patterns of (a) an as-implanted Ti sample, 2.4×10^{17} Na^+ cm^{-2}, showing the formation of Na_2TiO_3, (b) a sample implanted with 1.6×10^{17} Na^+ cm^{-2} followed by a heat treatment at 400 °C in air for 20 min, (c) like b with heat treatment at 700 °C producing $Na_2Ti_6O_{13}$, and (d) a preoxidized Ti surface implanted with 2.4×10^{17} Na^+ cm^{-2}. The different phases are marked by symbols. The vertical dashed lines indicate the titanium Bragg reflections of the substrate.

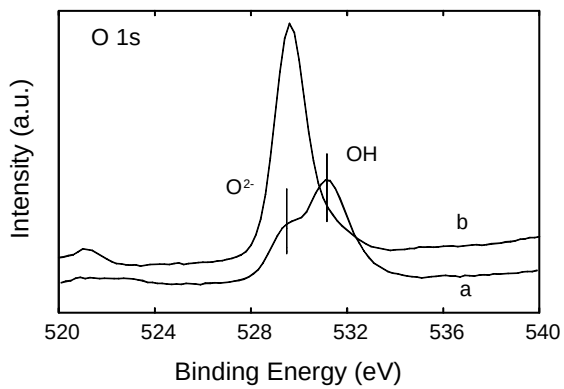

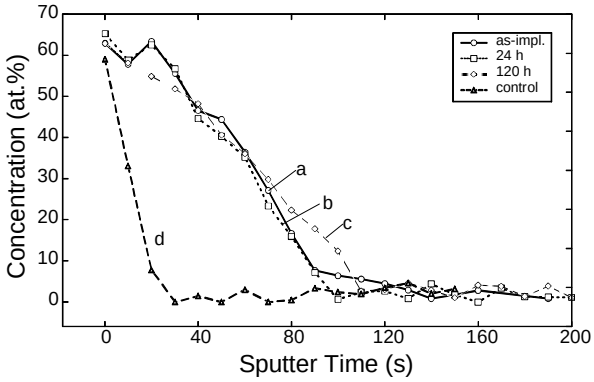

Fig. 2 (left): O 1s XPS spectra from a Ti sample implanted with 1.6×10^{17} Na^+ cm^{-2}: (a) as-implanted, (b) after heat treatment at 700 °C in air for 20 min. O 1s subpeaks reveal oxide-bound O^{2-} species at 530.0 eV and hydroxide-bound OH species at 531.3 eV. 700 °C heat treatment leads to an enhanced development of the oxide part and removal of the hydroxide part.

Fig. 3 (right): Sputter depth profiles of O determined from XPS of (a:❍) an as-implanted Ti sample (2.4×10^{17} Na^+ cm^{-2}), (b:❑) like a after 24 h incubation in a 137 mM NaCl solution at 37 °C, (c:◇) like b after 120 h incubation, and (d: Δ) a control sample without Na implantation after incubation treatment like c.

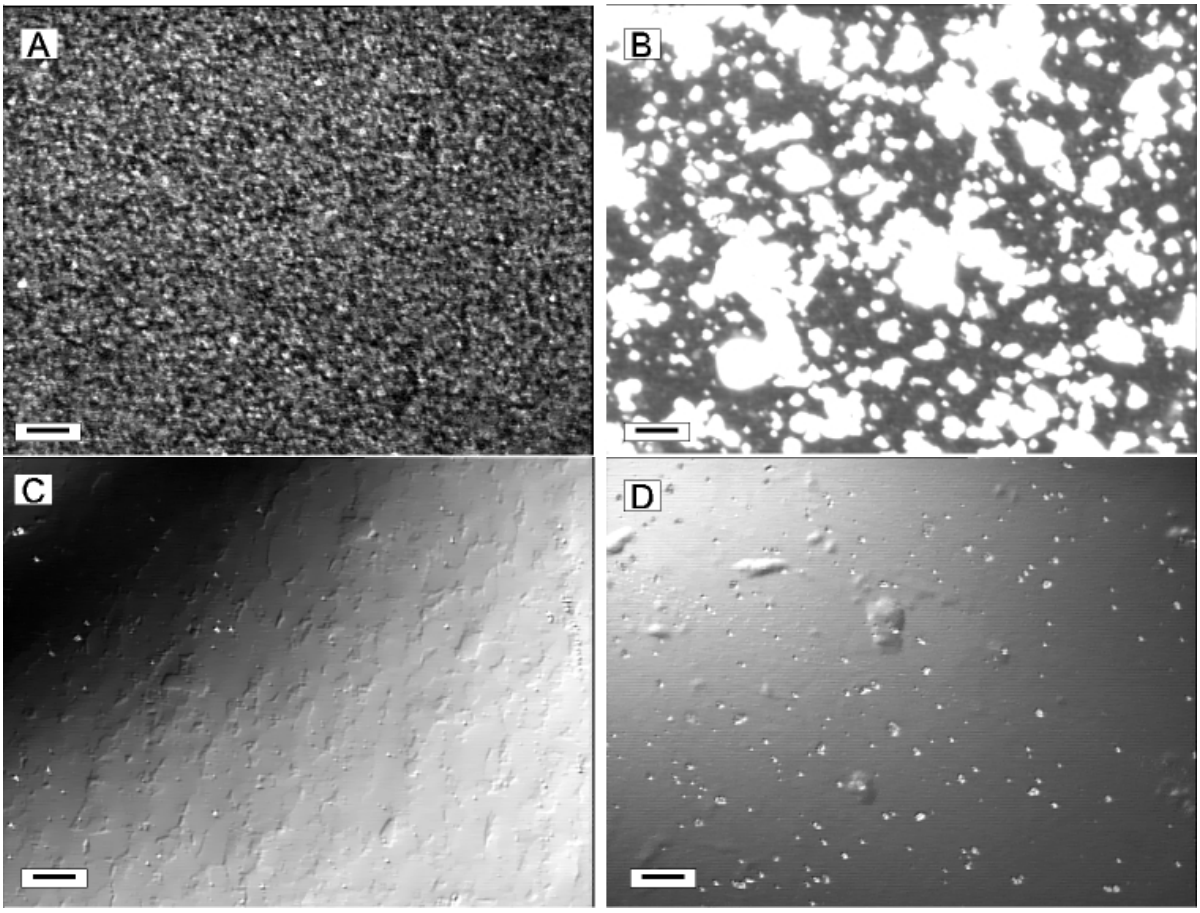

Fig. 4: Light microscopic images showing the evolution of surface morphology: (A) Ti implanted with 2.4×10^{17} Na^+ cm^{-2}, (B) sample A after 24 h incubation in SBF, (C) original Ti surface, and (D) sample C after 24 h incubation in SBF. Bright features in B and D are hydroxyapatite precipitates. Scale bars: 10 µm.

XPS measurements, Fig. 2, revealed that the surface contains oxide- and hydroxide-bound oxygen. This indicates the propencity for hydroxylating and is consistent with the presence of sodium oxide/titanate. Na_2TiO_3 is incorporated within the surface layer. The penetration of Na was seen to follow that of O, suggesting that Na ions are active oxygen-carrying species during implantation. Fig. 3 shows the depth profiles of O indicating the formed titanate layer. Heat treatment was shown to strongly modify the composition of the implanted layer. Heating to 400 °C in air for 20 min results in the formation of TiO and reduction of the Na_2TiO_3 amount (Fig. 1b). $Na_2Ti_6O_{13}$ occurs at 700 °C (Fig. 1c). These reactions can be related to the reduced power of Na and its peroxide and hyperoxide formed during the heat treatment. This is confirmed when Na was implanted into a rutile-coated (preoxidized) Ti surface showing the formation of Ti_2O, but no crystalline phase of any Na-Ti compounds (Fig. 1d).

Sodium ion implantation results in roughening the Ti surface. The roughness increases with the ion dose. Fig. 4a shows surface features produced at an ion dose of 2.4×10^{17} Na^+ cm^{-2} revealing µm-scaled porous structures homogeneously distributed over the entire surface. A rigorous reaction of Na with Ti, in addition to the ion implantation induced sputtering, can account for this large scale in roughness. The ability for HA nucleation was assessed by incubation tests in SBF. A 24 h exposure to SBF evidently revealed the enhanced deposition of calcium phosphate (Ca-P) from the solution into a Na implanted surface. Fig. 4b demonstrates this result: precipitate features covering a large part of the surface. Resolved imaging by SEM exhibited that the surface is densely seeded with precipitate nuclei. The large aggregates seen in Fig. 4b indicate the spontaneous precipitation and the rapid growth on these reactive Ca-P nuclei. The precipitates from SBF were identified by XRD and FTIR to be hydroxyapatite.

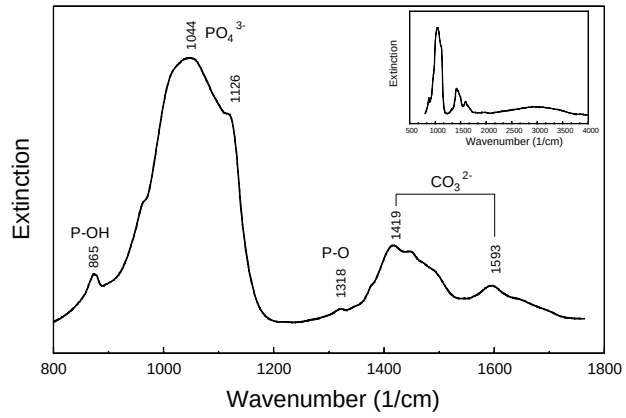

Fig. 5: IR spectra of a Na implanted Ti surface after 120 h incubation in SBF revealing characteristics of a typical carbonated hydroxyapatite. The inset shows a survey spectrum displaying the apatite OH absorption band at around 3579 cm^{-1}.

Fig. 5 shows the FTIR spectra of such precipitates formed on a Na implanted Ti surface. As shown by XRD, HA is formed while Na_2TiO_3 disappears, suggesting the active involvement of the latter in the reactions. The hydrolysis of Na_2TiO_3 produces hydroxylated surface -Ti-OH and increase in pH, two factors encouraging the HA nucleation. The morphology of a control sample is also presented for reference (Figs. 4c and d). The control surface displays only some scattered precipitates (Fig. 4d), implying that the HA nucleation on pure Ti surface is greatly inhibited.

References

[1] H.M. Kim, F. Miyaji, T. Kokubo, T. Nakamura, J. Biomed. Mater. Res. 32 (1996) 409; H.M. Kim, F. Miyaji, T. Kokubo, S. Nishiguchi, T. Nakamura, J. Biomed. Mater. Res. 45 (1999) 100

[2] H.B. Wen, J.R. de Wijn, F.Z. Cui, K. de Groot, Biomaterials 19 (1998) 215

Radiation Damage in Focused Ion Beam Synthesis of $CoSi_2$

S. Hausmann, L. Bischoff, M. Voelskow, and J. Teichert

The first buried, single-crystalline $CoSi_2$ layers were produced by White et al. using ion beam synthesis (IBS), i.e. high dose Co implantation into a heated silicon substrate followed by a two step annealing [1]. Since then a lot of investigations have been performed to increase the quality of the $CoSi_2$ layers showing a strong correlation between implantation temperature and current density of the ion beam [2]. The implantations have to be performed at elevated target temperatures to avoid amorphization of the silicon. Only if the substrate remains crystalline the formation of a single-crystalline $CoSi_2$ layer can be successful.
For patterned implantations very thick masks are required due to mask sputtering according to the high dose. Mainly SiO_2 masks with a tungsten capping layer are used. A problem in the fabrication of sub-µm $CoSi_2$ structures is the sputtering of the mask material into the implanted region [3]. Therefore, it is often difficult to decide whether the IBS of small $CoSi_2$ structures was not successful or the IBS process was disturbed by the sputtered mask material. In contrast, a focused ion beam (FIB) allows to implant high doses of cobalt into silicon without contamination by the mask material. However, the high current density associated with FIB implantation influences the crystallinity of the silicon substrate. Dwell-time effects have been found which are correlated to the crystallinity of the sample [4]. It will be shown here how the radiation damage induced by a FIB can be reduced to a level being similar to conventional ion beam implantation.
For FIB implantations the IMSA-100 system [5] was used. 70 keV Co^{2+} ions were extracted from a $Co_{36}Nd_{64}$ alloy liquid metal ion source [6], mass separated by an ExB filter and implanted into Si(111) or Si(100) wafers at a target temperatures of 400 °C. The beam spot size was about 300 nm and the current density between 0.7 A/cm^2 and 1.0 A/cm^2 corresponding to a total current of 0.5 nA to 0.7 nA. FIB implantation is a serial process and therefore the implantation area was divided into discrete pixels of 80x80 nm^2 size. The dwell-time (implantation time per pixel in one scan cycle) was varied from 1 µs to 250 µs but the implanted dose was kept fixed at about $1 \cdot 10^{17}$ cm^{-2}. The tilt angle was in all cases 0°, i.e. all implantations were performed under channeling conditions. To form $CoSi_2$ layers the samples were annealed for 60 min at 600 °C and for 30 min at 1000 °C in a nitrogen ambient. The samples were analysed using scanning electron microscopy (SEM) after CF_4 reactive ion etching (RIE) removing the Si top layer with $CoSi_2$ acting as an etch stop [7]. Further, 1.7 MeV He^+ Rutherford backscattering spectroscopy / channeling (RBS/C) combined with a special preparation technique [8] was employed. Typical sizes of the implanted area were 20x20 µm^2 for SEM investigations and 300x300 µm^2 for RBS/C analysis.
For short dwell-times (1 µs) buried, single-crystalline $CoSi_2$ layers are formed as seen by the RBS/C analysis in figure 1a. The SEM analysis shows a smooth layer (figure 2a). The resulting $CoSi_2$ layers have a χ_{min} value of 7 % (defined as integrated counts of the aligned Co peak divided by the integrated peak of the random Co peak). In addition, the Si signal shows a high degree of crystallinity. This is comparable to the results of conventional ion implantation for this ion energy [9]. In Figure 3a the random RBS spectrum is compared to a RUMP simulation [10] of a layer system consisting of 31 nm Si / 29 nm $CoSi_2$ / bulk Si. The agreement is very good, showing that the $CoSi_2$ layer has sharp interfaces.
For long dwell-times (250 µs) the layers are not single-crystalline. They are not buried as seen by RBS/C in figure 1b, and they exhibit large holes in the SEM image (figure 2b). The χ_{min} value is 72 %, and also the Si signal shows that the crystal quality is very poor. Thus, we suggest that the $CoSi_2$ layer is poly-crystalline. In Figure 3b the random RBS spectrum is

compared to a RUMP simulation of a layer system consisting of 13 nm SiO_2 / 35 nm (73 % $CoSi_2$ and 27 % Si) / bulk Si. The composition of the second layer is consistent with the structure shown by the SEM result in figure 2b which shows a 76 % coverage of $CoSi_2$. The agreement is quite good except for the low energy tail of the Co peak suggesting that there are also some $CoSi_2$ clusters below the $CoSi_2$ layer. Other Co-Si phases can be excluded since $CoSi_2$ is the only stable Co-Si phase after high temperature annealing [11].

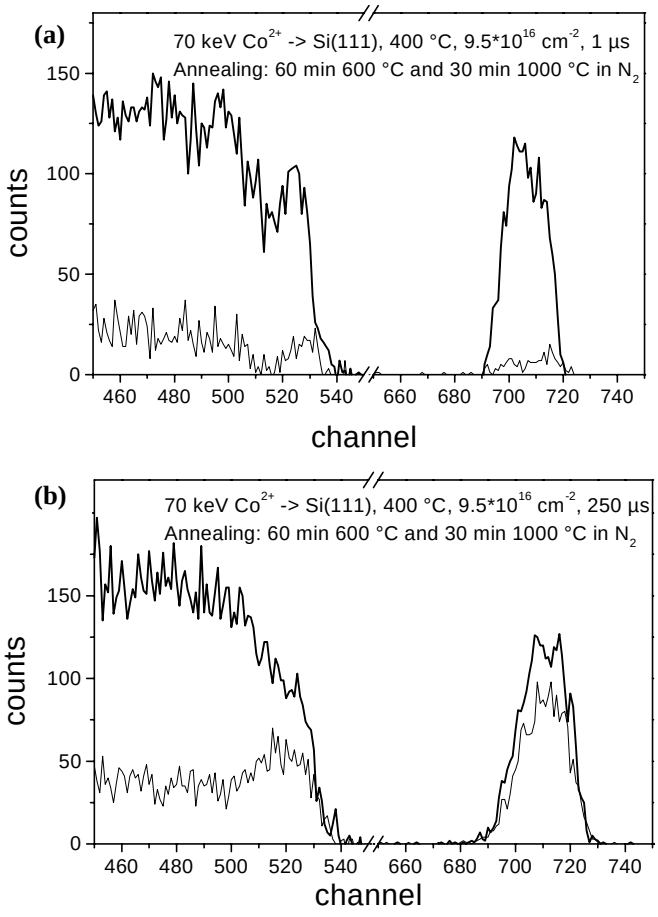

Fig. 1: 70 keV Co^{2+} implanted into Si(111) at 400 °C using a dose of $9.5 \cdot 10^{16}$ cm^{-2}. RBS/C spectra of annealed samples implanted with 1 µs dwell-time (a) or 250 µs dwell-time (b).

The different layer formation is associated with the as-implanted state of the sample [4]. For long dwell-times the silicon substrate is amorphized, whereas for short dwell-times the substrate remains partly crystalline, and in addition a part of the cobalt atoms is already incorporated into the silicon lattice [12]. This effect can already be seen for lower doses [13]. A critical dwell-time can be defined by the transition from crystalline to amorphous silicon. The critical dwell-time is correlated to the beam parameters and exhibits an exponential dependence on the target temperature [12]. In this report only the extreme cases for short (1 µs) dwell-times and long (250 µs) dwell-times will be discussed and the beam overlap at neighbouring pixels will be neglected for reasons of simplicity.

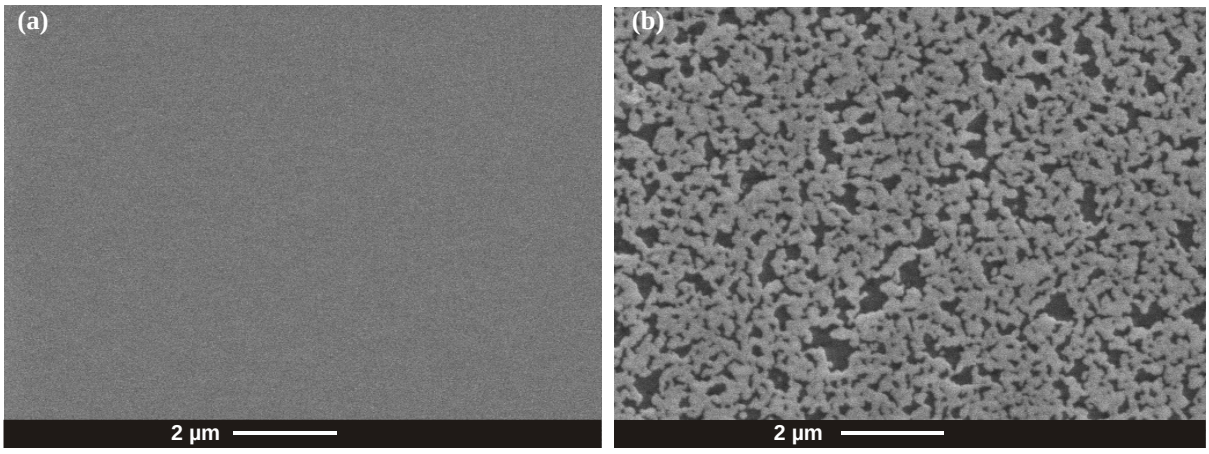

Fig. 2: 70 keV Co^{2+} implanted into Si(111) at 400 °C using a dose of $1 \cdot 10^{17}$ cm^{-2}. SEM images of annealed samples implanted with 1 µs dwell-time (a) or 250 µs dwell-time (b).

For long dwell-times the beam can be assumed to be a steady-state beam, with the current density of 1 A/cm^2 amorphizing the silicon lattice. However, $CoSi_2$ IBS requires a crystalline Si lattice and therefore the process fails. It is useful to utilise the Morehead-Crowder (MC) model [14] for the implantations using short dwell-times. In this model the impact of one ion disturbs a cylindrical region of the target. The size of the cylinder is given by the ion energy, ion mass, mass of the target atoms and target density. For a given current density it is now straightforward to calculate the mean time between two ion impacts into an area of A_{MC} = 2.4 nm^2 according to a cylinder of the MC model. In our case the mean time between two impacts into A_{MC} is about 10 µs. This means, that for a dwell-time of 1 µs mainly either one or no ion is implanted into a specific area A_{MC}. Than the other parts of the structure are implanted and only in the next scan cycle of the FIB it is possible to hit the area according to the cylinder in the MC model by an ion impact again. Therefore the current density of the FIB j_{eff} is reduced to an effective current density $j_{eff} = j_{FIB} / N_{pixel}$ by a factor of the total number of implanted pixels N_{pixel}. In our case N_{pixel} is 256^2 and this means that j_{eff} is 10 to 15 µA/cm^2 which is very close to the current densities used in conventional ion implantation for $CoSi_2$ IBS. The mean time between two ion impacts is now so long that the pause is sufficient to anneal the defects created by one ion impact. This explains why our results for short dwell-times are comparable to the broad beam results of Mantl et al. [9].

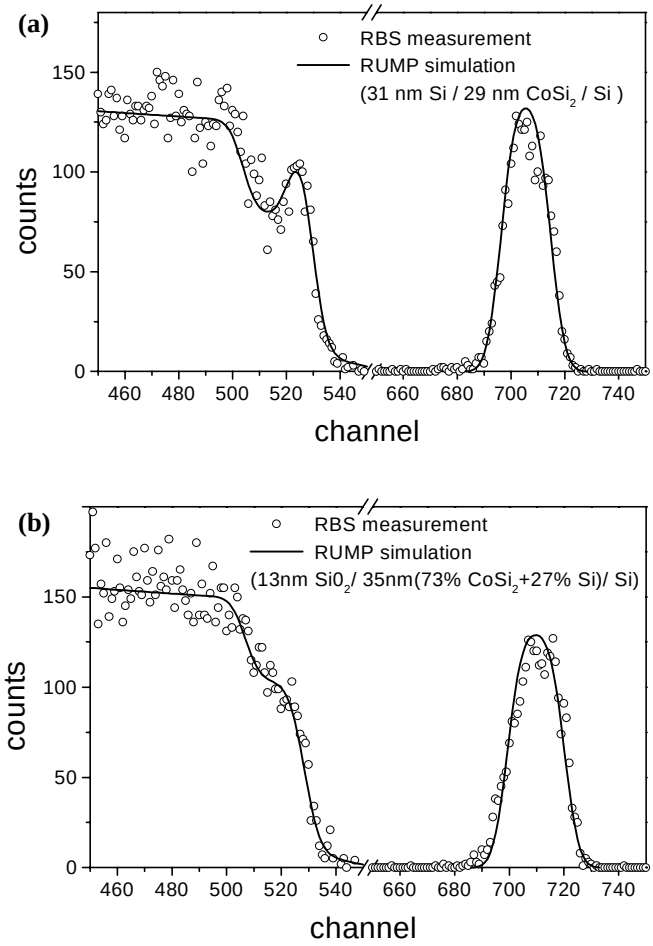

Fig. 3: Random RBS spectra (taken from figure 1) compared with RUMP simulations for 1 µs dwell-time assuming a layer system of 31 nm Si / 29 nm $CoSi_2$ / bulk Si (a) and 250 µs dwell-time for of 13 nm SiO_2 / 35 nm (73 % $CoSi_2$ + 27 % Si) / bulk Si (b).

Using this knowledge a simple recipe can be given to ensure that FIB and conventional ion beam implantation can be compared with regard to the current density. The dwell-time has to be chosen short enough that no more than one ion is implanted into an area according to the MC model during one scan cycle of the FIB. The area has to be calculated for every ion-target combination. Then, the mean time between two ion impacts becomes only a function of the current density. The effective current density can be reduced by the number of pixels implanted in one scan cycle, e.g., to the exact value used in the conventional ion implantation. If the implanted area is too small, i.e. the number of implanted pixels is too small, it is also favourable to add a pause at the end of every scan cycle.

Now, after understanding the basic radiation damage effects in FIB implantation one can start in the future to learn more about IBS for very small $CoSi_2$ structures by a contamination-free FIB. This process is rather complicated and will require further investigations. To

demonstrate the possibilities of this technique an example of a $CoSi_2$ line pattern with a width below 70 nm is shown in figure 4. The spot size of the beam was about 300 nm and only the exploitation of self-organisation processes in the IBS allow the production of a $CoSi_2$ line with a much smaller width than the beam spot size.

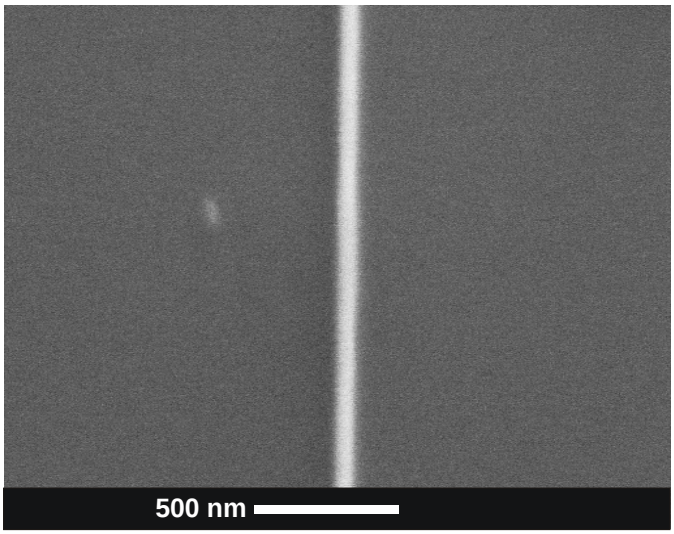

Fig. 4: SEM image of a fine $CoSi_2$ wire produced by 70 keV Co^{2+} implantation into Si(100) at 415 °C and a subsequent annealing. The beam diameter was 300 nm.

In this work single crystalline $CoSi_2$ layers have been produced by focused ion beam implantation. The cristallinity of the Si / $CoSi_2$ / bulk-Si layer system is comparable to the results achieved by conventional ion implantation. This was explained by the possibility to reduce the current density of a focused ion beam to an effective current density which is similar to that of conventional ion implantation by the application of short pixel dwell times.

The authors would like to thank the Deutsche Forschungsgemeinschaft for financial support under contract No. Te 250/1-3. They gratefully acknowledge the SEM investigation by E. Christalle and the technical assistance by I. Beatus.

References

[1] A.E. White, K.T. Short, R.C. Dynes, J.P. Garno and J.M. Gibson, Appl. Phys. Lett. 50 (1987) 95
[2] E.H.A Dekempeneer, J.J.M. Ottenheim, D.E.W. Vandenhoudt, C.W.T. Bulle-Lieuwma, and E.G.C. Lathouwers, Nucl. Instrum. Meth. B 55 (1991) 769
[3] D. Lenssen and S. Mantl, Appl. Phys. Lett. 71 (1997) 3540
[4] S. Hausmann, L. Bischoff, J. Teichert, M. Voelskow, D. Grambole, F. Herrmann, and W. Möller, Appl. Phys. Lett. 72 (1998) 2719
[5] L. Bischoff, E. Hesse, D. Janssen, K.F. Naehring, F. Nötzold, G. Schmidt, and J. Teichert, Microelectron. Eng. 13 (1991) 367
[6] E. Hesse, L. Bischoff, and J. Teichert, J. Phys. D: Appl. Phys. 27 (1994) 427
[7] N.M. Zimmerman, J.A. Liddle, A.E. White, and K.T. Short, Appl. Phys. Lett. 62 (1993) 387
[8] J. Teichert, M. Voelskow, L. Bischoff, and S. Hausmann, Vacuum 51 (1998) 261
[9] S. Mantl, R. Jebasinski, and D. Hartmann, Nucl. Instrum. Meth. B 59/60 (1991) 666
[10] L.R. Doolittle, Nucl. Instrum. Meth. B 9 (1985) 334
[11] F.M. d'Heurle and C.S. Petersson, Thin Solid Films 128 (1985) 283
[12] L. Bischoff, S. Hausmann, M. Voelskow, and J. Teichert, Nucl. Instrum. Meth. B 147 (1999) 327
[13] S. Hausmann, L. Bischoff, M. Voelskow, J. Teichert, W. Möller, and H. Fuhrmann, Nucl. Instrum. Meth. B 149 (1999) 610
[14] F.F. Morehead, Jr. and B.L. Crowder, Rad. Eff. 6 (1970) 27

The Diffusion Mechanism of Ion Nitriding of Aluminium

T. Telbizova, S. Parascandola, U. Kreissig, R. Günzel, E. Richter and W. Möller

Aluminium and its alloys find wide industrial application due to a high strength to weight ratio, good corrosion resistance, and good formability. On the other hand hardness and wear resistance are not satisfactory for numerous potential applications. Nitriding is a promising method for surface modification of Al since AlN has excellent physical and chemical properties, e.g. high hardness and thus increased wear resistance. An obstacle for successful nitriding of Al is the existence of a dense native surface oxide layer which acts as a barrier for the incorporation of nitrogen by diffusion. In this context, ion nitriding techniques which are associated with the removal of surface atoms due to sputtering are of advantage [1]. Furthermore, a thick and stoichiometric AlN layer can be formed only at sufficiently high temperatures to cause diffusion. The mechanism of diffusional transport appears to play an important role for the nitriding process and therefore it is a subject of the present research.

In this contribution the dominant diffusing element during ion nitriding of Al is identified by employing a marker layer. The depth region at which the nitriding takes place is also determined by use of an isotope exchange technique. First, after mechanical polishing and ultrasonic cleaning, a sample of pure Al (99.999%) was ion nitrided from a hot-filament ion source using a feed gas of ^{14}N [2]. A stoichiometric AlN layer of about 400 nm was formed using an ion energy of 1 keV, a total ion fluence of 2.8 x 10^{18} N/cm^2 and a substrate temperature of 500 °C. Afterwards Au was implanted at normal incidence with an ion energy of 1 MeV and a fluence of 1 x 10^{16} Au/cm^2 by a tandetron accelerator. According to SRIM calculations [3] the resulting mean projected range is about 200 nm with a straggling of 100 nm. Also, the simulated peak maximum concentration is 1 at. %. Subsequently the sample was re-installed in the ion nitriding set-up and ion nitrided with ^{15}N at an ion energy of 1 keV and a total ion fluence of 2.3 x 10^{18} N/cm^2 at 400 °C. During the second ion nitriding, a part of the sample was covered by a Si wafer.

Elemental depth profiles were obtained before and after ion nitriding with ^{15}N by means of ion beam analysis techniques. For analysis of the Au marker profile Rutherford Backscattering Spectrometry (RBS) was used with 1.7 MeV $^4He^+$ ions and a scattering angle of 170°. Nitrogen depth profiles were obtained from Elastic Recoil Detection Analysis (ERDA) using 35 MeV Cl^{7+} ions and a time-of-flight energy telescope at a scattering angle of 45° [4]. Under these conditions, the ^{14}N and ^{15}N profiles can be measured separately and simultaneously. Additionally, X-ray diffraction with Cu Kα radiation at 0.5° grazing incidence was used to determine the phases being present in the modified layer.

Fig. 1a shows the RBS spectra obtained after ^{14}N ion nitriding and Au ion implantation. A nitrogen to aluminium ratio of 1.0 is found by RUMP simulations [6]. The thickness of the AlN layer is about 400 nm, considering the density of AlN (3.26 g/cm^3). The signal of the implanted Au has the typical gaussian shape and it is situated in a 160 nm thick zone starting at a depth of 130 nm. The average Au concentration in the implanted zone is 0.65 at.%. This corresponds well to the simulated projected range and straggling. The low Au concentration is necessary to ensure that the diffusion of the Al or N atoms will not be affected by the implanted Au.

Further ion nitriding with ^{15}N allows to investigate the mechanism of diffusional transport. The implanted Au may be redistributed due to two reasons: i) the Au may migrate because of

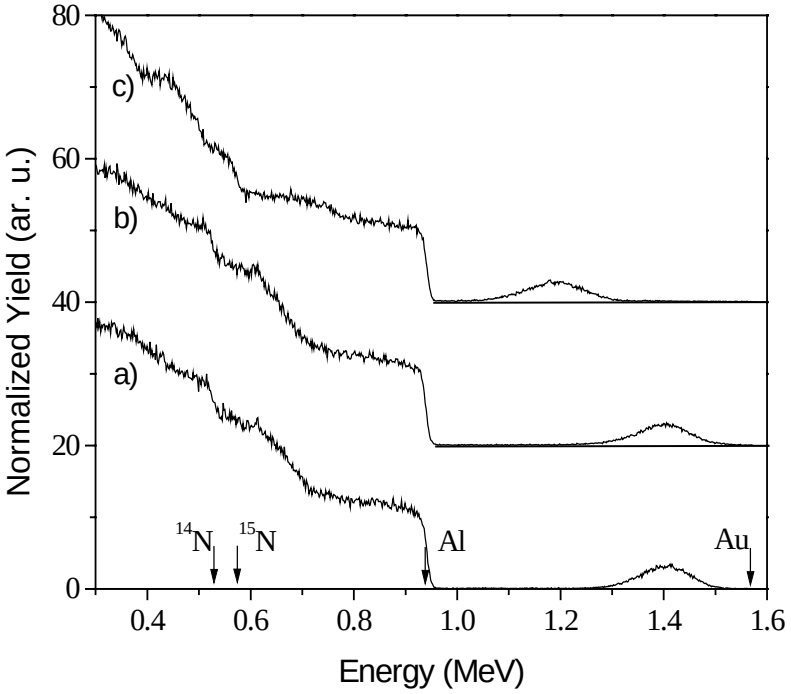

Fig. 1:
Rutherford backscattering spectra obtained after a) ^{14}N ion nitriding and Au ion implantation, b) additional heat treatment at 400 °C and c) additional ion nitriding with ^{15}N. The arrows denote the surface backscattering energies of ^{14}N, ^{15}N, Al and Au [5].

the high substrate temperature of 400 °C and ii) the Au marker layer may move due to the diffusion of Al and N. To separate these two effects, the influence of temperature alone was investigated in the capped section of the sample. If the Au profile does not shift here, the shift of the Au layer in the nitrided section can be used as an indication for the relative migration of Al and N atoms.

Fig. 1b shows the RBS spectrum measured after the heat treatment from the capped sample area. The position and the shape of the Au peak remain nearly unaffected, therefore purely thermal Au diffusion in AlN can be neglected. Also the elemental depth profiles of Al, N and O obtained after the heat treatment by ERDA are shown in Fig. 2a. The measurement confirms the formation of a 400 nm thick stoichiometric AlN surface layer. There is a well established plateau with equal atomic density of Al and N (average $(0.48 \pm 0.04) \times 10^{23}$ at/cm^3). Small amounts of oxygen are found at the surface and close to the interface between the AlN layer and the Al substrate.

The effect of diffusional transport can be seen in Fig. 1c, where the RBS spectrum after subsequent ion nitriding with ^{15}N is shown. The thickness of the AlN layer in front of the Au marker layer is significantly increased, even though the surface was eroded due to sputtering. An erosion depth of about 160 nm is estimated from the retained amount of N in comparison to the initial mean depth of the Au marker of 200 nm. According to a RUMP simulation, the Au implanted zone starts at about 380 nm from the new surface, but its width and average Au concentration remained unchanged. The observed shift must be due to diffusional transport of N or Al atoms, since the Au diffusion in AlN can be neglected. If the diffusional transport would be dominated by inward diffusion of N, the Au peak should be shifted relative to the surface in the opposite direction (due to sputtering), because the new AlN layer would grow behind the marker layer. In contrast, the observed change of the Au peak position after ^{15}N ion nitriding indicates that the AlN layer grows from the surface due to Al diffusion from the underlying bulk through the nitride formed before.

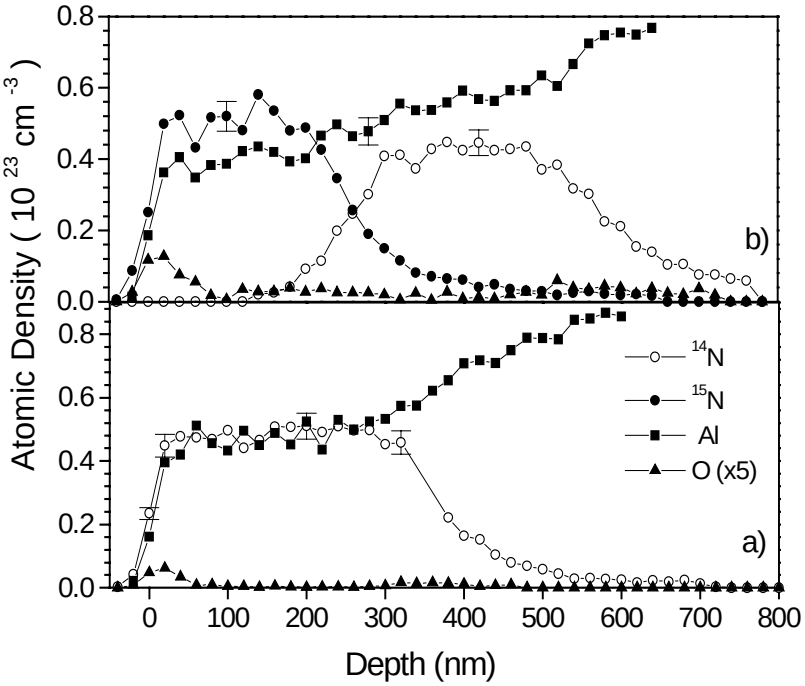

Fig. 2:
Elemental depth profiles of ^{14}N (open circles), ^{15}N (full circles), Al (squares) and O (up triangles) obtained by ERDA after a) heat treatment at 400 °C and b) subsequent ion nitriding with ^{15}N [5].

The use of ^{15}N enables to determine the depth region at which the nitriding takes place. Fig. 2b shows the elemental depth profiles of ^{14}N, ^{15}N, Al and O obtained after ion nitriding with ^{15}N. The pre-implanted ^{14}N is found only in the bulk, while the post-implanted ^{15}N is located near the surface. Considering the limited depth resolution of high-energy ion beam analysis, both nitrogen profiles are nearly rectangular and well separated. This supports a layer by layer growth of the nitride phase where the continuos nitriding takes place close to the surface. Also, the observed profile distribution confirms a mechanism dominated by diffusion of Al. An eventual substitution mechanism of ^{14}N present in the form of AlN by the added ^{15}N is unlikely from an energetic point of view. Behind the implantation range (about 2 nm) the atoms have only thermal energy (≈ 0.1 eV) which is much less than the binding enthalpy of AlN (3.3 eV) [7]. Furthermore, a N substitution would result in more overlapping elemental depth profiles of ^{14}N and ^{15}N and would shift the position of the Au marker to the surface. A mechanism of collisional mixing [8] can be excluded too, because the projected range of the implanted 1 keV nitrogen ions is much smaller than the observed changes in the modified layer.

The transport dominated by diffusion of Al is also consistent with the oxygen depth profiles. Fig. 2b shows that after ion nitriding small amounts of oxygen are present not only at the surface but also near the interfaces. These peaks can be attributed to the original surface positions, which are now buried due to Al diffusion to the surface. This effect occurs because the oxygen incorporation is stronger in the beginning of each process when the original surface oxide is thick.

Additionally, a phase analysis of the modified layer has been performed. Fig. 3 shows the XRD pattern obtained after ion nitriding with ^{14}N. The positions of the Bragg peaks show only formation of the hexagonal AlN phase. The broadening of the AlN peaks reveals that the nitride layer consists of fine grains. By applying the Scherrer's formula a grain size of about

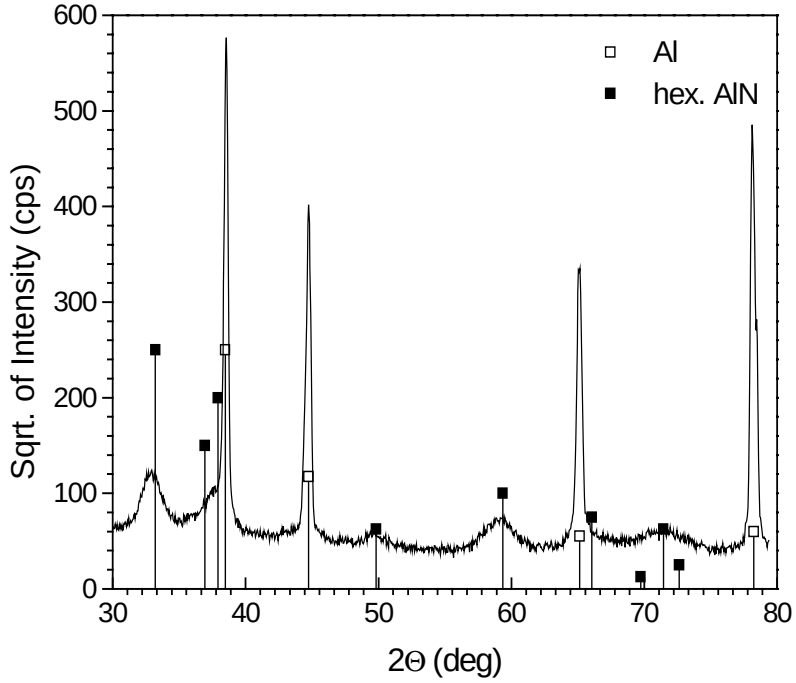

Fig. 3:
XRD pattern (0.5° grazing incidence) from the modified layer after ion nitriding with ^{14}N. The solid and open squares show PDF data for hexagonal AlN and Al, respectively [9].

5 nm is estimated. Such a size of the AlN precipitates in the nitride layer suggests that the diffusion of Al may occur via a grain boundary mechanism.

In summary, the diffusional transport during ion nitriding of aluminium is dominated by diffusion of Al. The AlN layer nucleates at the surface because of nitrogen implantation in the near surface region and Al diffusion from the underlying bulk through the already formed nitride. Determination of the activation energy for Al diffusion and the diffusion coefficient for different temperatures is a matter of further investigations.

References

[1] S. Parascandola, O. Kruse, W. Möller, Appl. Phys. Lett. 75 (1999) 1851
[2] S. Parascandola, O. Kruse, E. Richter, W. Möller, J. Vac. Sci. Technol. B 17(2) (1999) 855
[3] J.F. Ziegler, J.P. Biersack, U. Littmark, The Stopping and Range of Ions in Solids, Pergamon Press, New York 1985
[4] U. Kreissig, S. Grigull, K. Lange, P. Nitzsche, B. Schmidt, Nucl. Instr. and Meth. B 136-138 (1998) 674
[5] T. Telbizova, S. Parascandola, U. Kreissig, R. Günzel, W. Möller, Appl. Phys. Lett. (in press)
[6] L.R. Doolittle, Nucl. Instr. and Meth. B 15 (1985) 227
[7] CRC Handbook of Chemistry and Physics, 74th Edition, Ed.: D.R. Linde, CRC Press, Florida 1994, 5-1
[8] G. Terwagne, S. Lucas, Surf. and Coat. Techn. 51 (1992) 368
[9] T. Telbizova, S. Parascandola, F. Prokert, E. Richter, W. Möller, Nucl. Instr. and Meth. B (in press)

An Integrated High Voltage Modulator for Plasma Immersion Ion Implantation

R. Günzel, U. Hornauer, A.I. Rogozin* and V.T. Astrelin*
*Institute of Nuclear Physics, 630090 Novosibirsk, Russia

Plasma immersion ion implantation (PIII) is a promising technology to implant gaseous or metallic ions into different materials to modify the surface properties [1 - 4]. The sample to be implanted is immersed into a plasma and negatively biased. A positively charged sheath develops conformably around the sample. Ions are extracted from the sheath and implanted into the sample by the potential drop. Recently design parameters for PIII systems have been specified [5, 6]. Following these design considerations for implantation voltages of 40 kV, a plasma density of about 10^{16} m^{-3} is recommended. Depending on the electron temperature a stationary ion current of several A/m^2 can be extracted from the plasma sheath surrounding the biased sample. To control the thermal load of the sample during treatment a pulsed bias voltage is mandatory. Applying a negative voltage pulse to the sample, the sheath is initially expanding with supersonic velocity and reaches an equilibrium stage after a few µs. Due to this rapid sheath expansion the ion current is further increased [7 - 9]. For PIII on an industrial scale, with surface areas in the range of square meters, the peak current during the first µs will be in the range of several hundreds of amperes. Treatment voltages of up to 200 kV have been reported [10]. Hence, the equipment to produce suitable high voltage pulses is rather expensive and shares a considerable part of the total cost of PIII equipment. A new cost effective high voltage modulator is presented in this contribution.

The basic idea of the new modulator is that in case of two floating electrodes, immersed into a plasma and connected to both plates of a charged capacitor, both the electron flow to the anode as well as the ion flow to the cathode electrode will obey the Child - Langmuir law. As the mass of the electrons is small compared to the mass of ions, the resulting potential of the

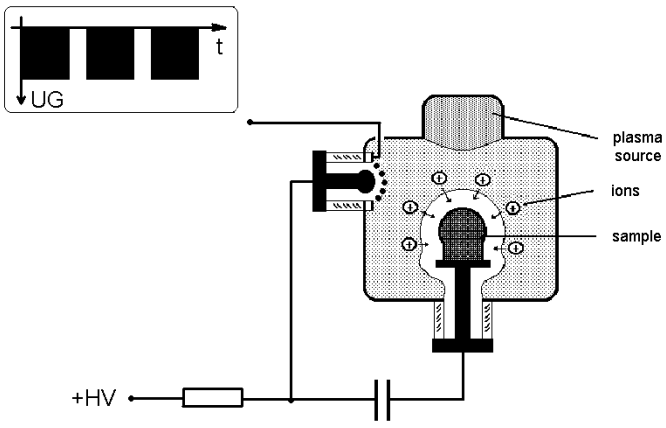

Fig. 1: Scheme of plasma immersion ion implantation with integrated high voltage modulator.

anode will be close to the plasma potential, whereas the electrode, connected to the negative plate of the capacitor (sample to be treated) will become negative compared to the plasma potential. If the anode is surrounded by a negatively biased grid (see Fig. 1), the anode becomes insulated from the plasma and the cathode (sample) is now at floating potential. In this way the sample voltage can be modulated by controlling the grid bias voltage. The modulator works under the condition that the grid voltage and the distance between two grid wires are properly arranged to control the flow of plasma electrons to the anode, and that this flow of extracted plasma electrons is large enough.

In the following, dynamical effects will be neglected and stationary currents will be estimated, assuming that anode and cathode potentials and the sheaths at cathode and chamber wall became stationary. The maximum anode current, which can be extracted from a plasma in the stationary case, can be estimated from the Bohm sheath criterion. In a cold plasma in local thermal equilibrium there exists always a stationary flow of positive ions to the wall, enclosing the plasma:

$$j_i = \exp\left(-\frac{1}{2}\right) e n_0 v_B, \quad v_B = \sqrt{\frac{kT_e}{m_i}}, \tag{1}$$

with m_i mass of the ions and n_0 the plasma density. The total ion current flowing from the plasma to the wall is

$$I_i = j_i \cdot S_w, \tag{2}$$

with the wall area S_w. To keep the plasma balanced, the same amount of electrons must flow to the wall too. A positively biased electrode increases the plasma potential, thus decreasing the electron loss to the wall. If the plasma potential is high enough, the electron loss to the wall will become negligible so that the anode saturation current, which can be extracted from a plasma in the stationary case, becomes

$$I_{es} \le \exp\left(-\frac{1}{2}\right) e n_0 v_B S_w. \tag{3}$$

Applying eq. (1) to the cathode sheath with area S_c, the ion current I_{ci} extracted to the cathode in the stationary case is [7, 8, 10]

$$I_{ci} = \exp\left(-\frac{1}{2}\right) e n_0 v_B \cdot S_c. \tag{4}$$

The energetic ions release secondary electrons with the yield γ from the cathode. Thus the modulator works, if the electron saturation current of eq. (3) exceeds the cathode current

$$I_{es} \ge I_{ci} + I_{cs}, \tag{5}$$

with the secondary electron current I_{cs}.

The area of the wall, enclosing the plasma is composed of the area of the chamber S_{ch} and the area of the cathode sheath S_c. From eqs. (3) - (5), the “modulator criterion” for the stationary case is obtained as

$$S_{ch} \ge \gamma \cdot S_c. \tag{6}$$

Basic experiments and tests of this new modulator concept have been performed using a nitrogen hot filament assisted arc plasma at different plasma densities. The cubic plasma chamber used for the tests has a volume of 15 l and an inner surface area of 0.36 m^2. As anode a steel rod of 12 mm diameter and 200 mm length is used. The anode is surrounded by a cylindrical mesh with a diameter of 45 mm and a length of 200 mm. The mesh is manufactured of stainless steel wires of 0.7 mm diameter with 1.7 mm mesh size. The anode is located parallel to a corner of the cubic chamber in a distance of 60 mm to the wall. The cathode is a disk of 50 mm diameter, located in the centre of the chamber.

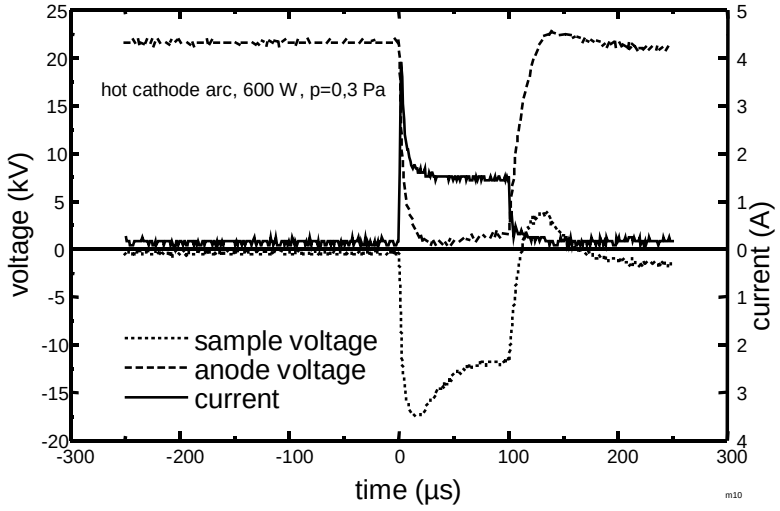

Fig. 2: Cathode voltage, anode voltage and current during the on-time of the voltage pulse.

In Fig. 2 the behaviour of anode voltage, cathode voltage and current are shown for a plasma density of about 4 x 10^{16} m^{-3} and an electron temperature of 1 eV. The grid voltage (not shown in the figure) was –145 V during the off-time of the high voltage pulse. At time 0 the grid voltage was switched off for 100 µs and than applied again. As during the on-time of the pulse the capacitor starts discharging, the cathode voltage is smaller than the maximum anode voltage of 22 kV. Further, the anode needs about +200 V to extract electrons from the plasma. During the rise time of the high voltage pulse the current has a maximum of more than 4 A, and remains at a constant value of about 1.7 A when the cathode sheath has become stationary. This stationary current is very close to the predictions of eq. (3) with an electron saturation current of 1.9 A for the given plasma parameters.

The above model was also confirmed by time-resolved measurements of the current flowing from the plasma to the wall and the change of the floating potential during the pulse. Different to the electric scheme of Fig. 1, these investigations have been performed by keeping the anode constantly at +20 kV in order to avoid dynamical effects. In agreement with the assumptions leading to eq. (3), indeed a change of the plasma floating potential from –8 V up to +60 V was measured when the grid voltage was switched off. Thus, all electrons leaving the plasma are collected by the anode.

For a given sample size, to be treated by PIII, a minimum size of the vacuum chamber is mandatory [5, 6]. According to eq. (5), this implies an automatic scaling of the modulator current, following the scaling of the chamber size with the sample size. This means that the modulator criterion (6) is fulfilled so that no principal limitation of the sample size to be treated exists. Further, the treatment voltage requires only a proper insulation between grid and anode. Thus the integrated modulator offers the possibility of high voltage and large scale PIII treatment. The costs of the modulator are small compared to modulators available up to now. Problems may arise at treatment voltages > 100 kV, as the secondary electron rate increases with increasing ion energy, resulting in an disadvantageous ratio between chamber size and sample size. However, additional studies have shown possibilities to overcome the limitations established by the modulator criterion, like local enhanced plasma densities or the use of additional electron sources.

References

[1] J. Conrad, J. Appl. Phys. 62 (1987) 777
[2] J. Tendys, I.J. Donelly, M.J. Kenny, J.T.A. Pollock, Appl. Phys. Lett. 53 (1988) 2143
[3] I.G. Brown, A. Anders, S. Anders, M.R. Dickinson, R.A. MacGill, J. Vac. Sci. Technol. B 12 (1994) 823
[4] R. Günzel, E. Wieser, E. Richter, J. Steffen, J. Vac. Sci. Technol. B 12 (1994) 927
[5] S. Mändl, J. Brutscher, R. Günzel, W. Möller, J. Vac. Sci. Technol. B 14 (1996) 2701
[6] S. Mändl, J. Brutscher, R. Günzel, W. Möller, Nucl. Instr. and Meth. B 112 (1996) 252
[7] R. Günzel, J. Brutscher, Surf. Coat. Technol. 85 (1996) 98
[8] W. En, N.W. Cheung, J. Vac. Sci. Technol. B 12 (1994) 833
[9] G.A. Collins, J. Tendys, J. Vac. Sci. Technol. B 12 (1994) 875
[10] J.N. Matossian, D.M. Goebel, Surf. Coat. Technol. 85 (1996) 86

Thin Films

A. Belov

Atomic-level and effective elastic properties of amorphous carbon films on crystalline substrates

The concept of atomic-level elastic moduli is modified for composite materials with the interatomic interaction described by an empirical bond order potential. The atomic-level elastic moduli directly incorporate the contribution due to the internal relaxation of atoms in a solid subjected to a uniform strain. An advantage of such atomic-level elastic moduli over the previously used definitions is that their average represents the effective elastic moduli rather then the Voigt bounds. This property enables for the effective elastic moduli to be calculated not only for a whole composite solid but also for each of its constituents, in particular, for an amorphous film on a crystalline substrate. It is shown that the Brenner interatomic potential used in molecular dynamics studies of the amorphous carbon film deposition satisfies the criteria necessary for the introduction of the atomic-level elastic moduli.

supported by DFG

H.-U. Jäger
*K. Albe**

Molecular-dynamics simulations of steady-state growth of ion-deposited tetrahedral amorphous carbon films

Molecular dynamics calculations were performed to simulate the ion beam deposition of diamond-like carbon films. Using the computationally efficient analytical potentials of Tersoff and Brenner we were able to simulate more than 10^3 carbon atom impacts on {111} diamond, so that steady-state film properties could be computed and analyzed. The film composition calculated with Tersoff's potential is dominated by spurious bonding sequences between three- and fourfold coordinated atoms, which lead to sp^3-contents of about 40 % in maximum, but occur as result of the overbinding inherent to this potential. Using Brenner's more refined potential, which includes overbinding corrections, unreal high dense structures with low sp^3-contents of only a few percent are achieved. The small range of the binding orbitals, represented in these potentials by the cutoff-function, is identified as reason for this shortcoming. By re-adjusting the cutoff-parameters we got an improved forcefield, which allows for the first time the simulation of steady-state growth of ta-C structures with realistic densities and sp^3-contents which are in line with experimental studies.

supported by DFG

Collaboration: *University of Illinois at Urbana-Champaign, Urbana, USA; Fraunhofer-Institut für Werkstoff- und Strahltechnik, Dresden

A. Kolitsch
S. Malhouitre

Synthesis and characterization of nitrogen containing carbon films

XPS measurements of CN_x films deposited by IBAD at temperatures ranging from RT to 1000°C and fixed ion/neutral parameters reflect a change of the main chemical state of the nitrogen bonds at growing deposition temperature. The nitrogen content of the films decreases significantly at deposition temperatures above 600°C and correlates well with two different binding energies measured by XPS. Results of nano-indentation techniques concerning hardness and elastic modulus also agree with these measured structural information about the incorporated nitrogen and with the analysed nitrogen content at different deposition temperatures. Additional EELS investigations at the same films show only weak changes of the carbon plasmon peak position and the sp^2/sp^3 ratio in the films with increasing deposition temperature in correlation to the nitrogen content.

supported by EC (TMR-Project)

Collaboration: University of Stockholm, Sweden; University of Linköping, Sweden; University of Newcastle, UK; Universite Paris-Sud, France and CNRS, France

S. Malhouitre
A. Kolitsch

Synthesis and characterization of Si_3N_4 and $Si_xC_yN_z$ films deposited by IBAD

$-$Si_3N_4$ and $-$C_3N_4$ have the same crystallographic structure. Deposition of silicon nitride by IBAD have been studied to grow on these films the predicted carbon nitride phase. The stoichiometry of the deposited nitride film was controlled by the silicon/nitrogen transport ratio of the IBAD process. The measured infrared spectra are typical of Si_3N_4 films. The nitrogen ion energy (300-1200 eV) and temperature of the substrates (RT-700°C) have no influence on the structure of the films. Grazing incidence XRD performed on films made at various temperatures shows that the films are composed with nanocrystalline grains. $Si_xC_yN_z$ films were deposited by IBAD with an additional carbon evaporation and with C/Si arrival ratios varying between 0.5 and 2. The resulting films present a C/Si atomic ratio between 0.4 and 0.95. XPS shows that the nitrogen atoms are mainly linked to silicon atoms, and the carbon atoms are mainly linked to carbon atoms. Few Si-C and C-N bonds are also present.

supported by EC (TMR-Project)

Collaboration: University of Stockholm, Sweden; University of Linköping, Sweden; University of Newcastle, UK; Universite Paris-Sud, France; CNRS, France

*F. Piazza**
*Y. Arnal***
*A. Lacoste***
*G. Relihan****
*M. Kildemo****
D. Grambole
F. Herrmann
*A. Golanski**

Investigation of the properties of hydrogenated amorphous DLC thin films fabricated by ECR plasma deposition

An uniformly distributed multipolar ECR microwave plasma at 2.45 GHz was used to deposit ta-C:H (DLC) films on silicon substrates at RT. The influence of the process parameter (acetylene initial pressure and the substrate bias) on the growth rate, structure and hydrogen content of the DLC films has been investigated using SE and NRA, respectively. For the latter the resonance at 6.385 MeV of the nuclear reaction $^1H(^{15}N,\alpha)^{12}C$ was used. The DLC deposition rate and the hydrogen content increase significantly with increasing acetylene pressure from 0.6 to 1.1 mTorr. Against the variation of the substrate bias within the range from –30 V to –190 V (at a acetylene pressure of 0.6 mTorr) has no measurable impact on both.

Collaboration: *CNRS, Laboratoire PHASE, Strasbourg, France; ** CNRS, Laboratoire LEMD, Grenoble, France; ***National Microelectronics Research Centre, University College, Cork, Ireland

E. Wieser
*J. Schreiber**
*C. Wenzel***
W. Matz
H. Reuther

Modification of Ta-based thin film barriers by ion implantation of nitrogen and oxygen

For copper metallization schemes of microelectronic devices tantalum is a promising candidate for the necessary diffusion barrier. Ta-based thin film have been treated by ion implantation of nitrogen and oxygen to decrease the density of diffusion enhancing defects and to improve the barrier stability. The implantation changes the composition and the microstructure of the films. Above a threshold dose of $1x10^{17}$ N^+/cm^2 and $3x10^{17}$ O^+/cm^2, respectively, in 100 nm Ta the original Ta structure is destroyed. Oxygen implantation leads to amorphization. In the high dose N^+-implanted samples ($3x10^{17}$ N^+/cm^2 into 100 nm Ta) nitride formation is detected. These changes of the micro-structure have to increase the barrier stability considerably. The layers amorphized by oxygen implantation remain amorphous also after annealing at 650°C/1h. PIII has been successfully tested to modify very thin Ta films (15 nm).

Collaboration: * FhG Institut für Zerstörungsfreie Prüfverfahren Dresden (EADQ), ** TU Dresden, Institut für Halbleiter- und Mikrosystemtechnik

J. Noetzel
*D.C. Meyer**
A. Mücklich
F. Prokert

Amorphization of Fe/Al

Due to some contrary results on the non-equilibrium behaviour of Fe-Al, Fe/Al multilayers with an overall composition of 55-85 at.% Al were fully ion-beam mixed by 150 keV Fe ions (10^{16} cm^{-2}). The resulting homogeneous, non-equilibrium Fe-Al alloys were investigated by XRD, TEM, EXAFS and Mössbauer spectroscopy. It was shown that the alloys with 55-70 at.% Al are of bcc-crystalline structure, while around 75 at.% Al the bcc lattice becomes distorted towards an Fe_2Al_5-like structure. The alloys with 80 and 85 at.% Al are amorphous. Mössbauer and EXAFS measurements show that during the transition from the crystalline to the amorphous state the short-range order remains essentially unchanged. Especially, no additional Al atoms were incorporated into the first two neighboring shells of the Fe atoms. It is concluded that the amorphization is due to the formation of Al-Al pairs away from Fe. Within the existence range of the amorphous state, additional Al can again enter the first two neighboring shells of Fe, leading to a less distorted short-range order with increasing Al concentration.

supported by DFG

Collaboration: * Institut für Kristallographie, TU Dresden

J. Noetzel
*U. Rößler**
*A. Handstein**
F. Prokert
E. Wieser

Ion-beam mixing of laser-deposited Co/Cu multilayers

Aim of this work was to investigate the possibility to prepare a metastable solid solution of Co in Cu by means of ion-beam mixing of laser-deposited Co/Cu multilayers. For this purpose, various laser-deposited Co/Cu multilayers were irradiated with 150 keV Cu^+ ions. The fluence was between $1x10^{15}$ and $5x10^{15}$ cm^{-2}. The as-deposited state is characterized by morphologically rough interfaces as described below (Prokert, et al.). Low-angle XRR shows that mixing with $5x10^{15}$ cm^{-2} leads to a complete degradation of the multilayer structure. High-angle XRD reveals that radiation enhanced grain growth occurs, leading also to a change in the texture. However, a super-paramagnetic behaviour is observed, indicating that no solid solution but a granular system of Co clusters in a Cu matrix was formed. The results prove that the positive heat of mixing of the Co/Cu system reverses any ballistic mixing introduced by the energetic ions. Still, the ion-beam mixing of Co/Cu layers could offer a way to control the cluster size in the achieved granular system.

supported by DFG

Collaboration: * Institut für Festkörper- und Werkstoffforschung, Dresden

F. Prokert
J. Noetzel
E. Wieser
N. Schell
W. Matz
*A. Gorbunov**
*A. Tselev**

Diffuse X-ray scattering on Co-Cu multilayers (ML) near absorption edges

Two types of MLs, prepared by crossed beam pulse laser deposition with different layer thickness of Co- and Cu-layers on a Si-substrate, $Si/SiO_2/n$ x[Co(k nm)/Cu(k nm)] with (n, k) = (8, 4) or (4, 8), were investigated using synchrotron radiation near the absorption edges (Co: 7.71 keV; Cu: 8.96 keV) at ROBL. From the distribution of the diffuse scattered intensity a characterization of the roughness of the surface and interfaces could be given by simulations based on Sinha's representation of the height-height correlation function. The correlation length *x* and the Hurst parameter *h* have been determined and the roughness correlation between the layers could be quantified. The results are nearly the same for both types of MLs. In the 'as-deposited' state the roughness is dominated by a high morphological jaggyness, represented by a high fractal dimension (D=3-h) of about 2.75. After annealing (500°C, 2h) this 'short-scale roughness' is reduced (D=2.5). However, the correlation length, which is a lateral measure for the biggest morphologicial feature determining the roughness value, is drastically shorte-

supported by DFG

ned. This is accompanied by a reduction of the roughness conformity. Both effects are ascribed to thermal grain growth.

Collaboration: *TU Dresden, Inst. f. Werkstoffwissenschaft

*J. Jagielski**
W. Matz
*A. Turos**
H. Reuther

Hardening of chromium nitride covers on steel by ion implantation

In order to improve mechanical surface properties steel was coated with 1.5 µm chromium nitride of the composition $CrN_{0.4}$. After nitrogen irradiation of the layer a significant wear reduction was found; the wear trace depth reduces from 4.5 µm to 0.5 µm. In order to understand the structural reasons of this behaviour a XRD study of samples implanted with (5, 10, 20)x10^{16} N/cm^2 was performed. It was found that most of the $CrN_{0.4}$ layer remains amorphous. Only near the surface crystalline phases are formed. The first occuring phase is Cr_2N at 5x10^{16} N/cm^2 . With increasing fluence CrN is formed, remaining the only phase at 2x10^{17} N/cm^2. The width of the diffraction peaks is quite broad indicating very small crystallites. A quantitative estimation was not possible because of the huge background from the remaining amorphous material. AES depth profiles support that the composition change due to irradiation is limited to the top 15% of the layer.

Collaboration: *Institute of Electronic Materials Technology, Warsaw, Poland

G. Brauer
W. Anwand
E.-M. Nicht
*J. Kuriplach**
*I.. Prochazka**
*F. Becvar**
*A. Osipowicz***
*P.G. Coleman****

Characterization of RF-sputtered platinum films by positron annihilation spectroscopy

Pt films on Al substrates and bulk Pt samples have been investigated by conventional PAS as well as by SPIS. A variety of state-of-the-art theoretical calculations have been performed. Only the atomic superposition technique in connection with an approaching scheme introduced by Boronski and Nieminen led to positron lifetimes in Pt which are in good agreement with experimental results. We suggest that the positron lifetimes in vacancy + dislocation, monovacancy and divacancy are 168 ps, 174 ps and 206 ps, respectively. The lifetime for perfect Pt was found to be 99 ps. The research shows that a re-interpretation of earlier defect studies of bulk Pt by PAS is required in order to achieve a satisfactory agreement with the present experimental findings and theory. Pt films on Al substrates were found to contain open-volume defects, most probably of the size of a monovacancy. However, in the as-received film the defect concentration decreases with depth, compared to an uniform distribution in the annealed film, but is generally much larger than in the annealed film.

Collaboration: *Charles University Prague, Czech Republic, **Fachhochschule Fulda, ***University of Bath, UK

Semiconductors

*A. Ster**
M. Posselt,
*A. Hallen***

Atomistic simulations of ion implantation into different polytypes of SiC

A new version of the Crystal-TRIM code was developed which allows the determination of ion range and energy deposition profiles in 3C-, 2H-, 4H-, and 6H-SiC. The models employed to describe the electronic energy loss of the incident ions and their enhanced dechanneling due to the damage buildup with growing dose are similar to those used in the simulation of implantation into Si by the standard Crystal-TRIM. The program was applied to reproduce experimental range distributions for 1.44 MeV B^+, 1.5 MeV Al^+, and 3 MeV Ga^+ implantations into (0001) 6H-SiC at nearly normal incidence and doses between 10^{12} and 10^{15} cm^{-2}. The consideration of such channeling implantation profiles allows a reliable test of the models used for electronic energy loss and damage buildup and of the values chosen for the model parameters. A satisfactory agreement between the results of computer simulations and the measured data could be achieved. In contrast to the modeling of ion implantation into Si, in the case of SiC the parameter describing the damage buildup does not so strongly depend on the ion mass. This is interpreted by the difference between the defect accumulation processes occuring in Si and SiC during ion bombardment.

Collaboration: *MTA-KFKI, Research Institute for Technical and Materials Science, Budapest, Hungary; **Royal Institute of Technology, Kista-Stockholm, Sweden

*V. Belko**
M. Posselt
E. Chagarov

Elementary processes of ion-beam-induced defect formation in SiC

Classical molecular dynamics simulations were performed in order to study elementary processes of defect formation during the introduction of dopants into SiC by ion implantation. A modified Tersoff potential is employed which describes the repulsion at short interatomic distances more precisely. For the 3C-, 4H-, and 6H-polytypes of SiC the threshold energies for atomic displacements and defect formation were determined for primary-knockon-atoms (PKAs) with directions of motion parallel and antiparallel to [0001]. In contrast to 3C-SiC, in 4H- and 6H-SiC the number of nonequivalent Si- and C-PKAs in each direction is greater than one due to the more complex structure of these polytypes. In dependence on the PKA chosen the threshold energy for defect formation varies from 20 to 70 eV. The point defect configurations formed by PKAs with near-threshold energies were identified. Some of the interstitial types found in 4H- and 6H-SiC have not been reported so far.

supported by DAAD and SMWK

Collaboration: *Belorussian State University, Minsk, Belarus

E. Chagarov
M. Posselt

Improvement of the repulsive part of the classical interatomic potential for SiC

Investigations of ion-beam-induced defect formation by classical molecular dynamics simulations are determined decisively by the quality of the interatomic potentials employed. In order to describe correctly the ballistic and athermal processes occuring during ion bombardment of SiC the Tersoff potential was modified. At small interatomic distances its pair part was replaced by the well-tested ZBL potential. An exponential function was used to connect that potential with the two-body part of the Tersoff potential in the region between some ten and zero eV. The resulting pair potential and its first derivative are continuous and monotonic over the whole range where the modifications were introduced. The consideration of repulsive interactions in Si-Si, Si-C, and C-C dimers by ab-initio DFT calculations using the code

Dmol yielded energies which agree satisfactorily with the values of the improved pair potential. The second modification of the Tersoff potential for SiC concerns its three-body part. Its contribution to the total potential was reduced for small interatomic separations at which the interaction between two atoms should be independent of their coordinations to the other neighbour atoms. This was realized in such a manner that the total potential and its derivative remain continuous and monotonic in the region where the reduction of the three-body part is performed.

V. Heera
W. Skorupa
*B. Pécz**
*L. Dobos**

Ion beam synthesis of carbon phases in silicon carbide

Silicon carbide (SiC) is the only equilibrium phase in the binary system of Si and C. Additional carbon introduced in this system should form pure carbon phases, because all of the tetrahedral (sp^3) Si-C bonds are saturated in the SiC crystal. A high dose of $1x10^{18}cm^{-2}$, 60 keV carbon ions was implanted into single crystalline 6H-SiC at elevated temperatures (300-900°C). According to a SRIM calculation the composition of the compound is about $Si_{0.20}C_{0.80}$ in the carbon maximum at the depth of 130 nm. The formation of carbon phases in the crystalline SiC lattice was investigated by XTEM. An amorphous phase was produced at 300°C. Precipitates of graphite were obtained at 600°C, whereas at 900°C small diamond grains were formed. These grains are in perfect epitaxial relation with the surrounding SiC lattice.

supported by DFG

Collaboration: *Research Institute for Technical Physics and Materials Science, Budapest, Hungary

A. Höfgen
V. Heera
A. Mücklich
F. Eichhorn
W. Skorupa

Ion beam induced nanocrystallization of silicon carbide

Ion-beam-induced crystallization (IBIC) was used to produce nanocrystals in the preamorphized region of a 6H-SiC bulk crystal. The precipitation was stimulated by high dose implantation with Al and Si at temperatures between 300°C and 700°C. The morphology and size of the nanocrystals in dependence on the implantation parameters were investigated by XTEM and XRD under grazing incidence. Above a certain threshold dose, randomly oriented grains of 3C-SiC with almost spherical shape and mean diameters ranging from 4 to 25 nm are formed. The recrystallization is completed within a very narrow time window. Therefore the nucleation process could not be observed directly in our experiments. From the extrapolation of the kinetics of the secondary grain growth to zero time the window of suitable parameters for the observation of nucleation and primary grain growth was estimated. A critical temperature (T_C #300°C) as well as an incubation time (t_I $300 s below 700°C) for the beginning of the recrystallization were found.

supported by DFG

F. Eichhorn
N. Schell
W. Matz
R. Kögler

SiC crystallite formation by ion implantation into Si: structural studies by synchrotron XRD

Implantation of C ions with an energy of 45 or 195 keV, respectively, into Si results in an elastic distortion of the Si host lattice and in a formation of crystalline SiC particles or their prestages depending on fluence and temperature of implantation. Synchrotron XRD at ROBL was used to reveal phase formation, the associated lattice strain changes, and the orientation correlations. Fluences below $5x10^{15}$ C^+/cm^2 induce only strain in the Si lattice. After implantation up to $4x10^{17}$ C^+/cm^2 at a temperature of 500°C prestages of Si-C and an altered state of Si lattice deformation are found. By implantation of $4x10^{17}$ ions/cm^2 at 800°C or at 500°C with a subsequent thermal treatment particles of the 3C-SiC phase grow and the Si lattice strain relaxes. The SiC

crystallites are aligned to the Si matrix, that the cubic crystallographic axes of matrix and particles coincide with a spread of 2.5° to 5°. In material implanted at 800 °C a small but detectable part of SiC particles is anisotropically oriented. Implantation at higher temperature is more effective in formation of an aligned crystallite distribution than a subsequent annealing even at higher temperatures.

*E. Theodossiu**
M. Klimenkov
W. Matz
*H. Baumann**

Characterization of crystallinity of SiC-surface layers formed by ion beam synthesis

Carbon implantations into silicon were carried out in order to form thin SiC-surface layers. The samples were implanted with 40 keV ^{13}C ions and an understoichiometric fluence of $3.8x10^{17}$ ions/cm^2. Subsequent thermal treatment was performed under high vacuum conditions at different temperatures between 900°C and 1050°C using a 20 kV electron beam. The isotope ^{13}C offers the advantage to measure the carbon redistribution caused by the thermal treatment process using the narrow resonant nuclear reaction $^{13}C(p,\gamma)^{14}N$. The crystallinity of the SiC-surface layers are studied by XRD and TEM analysis. In contrast to earlier findings the SiC-surface layer of about 70 nm thickness contains not only 3C-SiC but also a low amount of 6H-SiC grains is formed. The XRD findings of 6H-SiC were proved by HRTEM. The fast Fourier transform technique shows that the 6H-SiC modification preferably coexists with the 3C-SiC modification in the near interface region.
Collaboration: *Institut für Kernphysik, J.W. Goethe-Universität, Frankfurt/Main, Germany

D. Panknin
H. Wirth
W. Skorupa

Electrical effects in high dose nitrogen implanted 6H-SiC

N^+-ions were implanted at 400°C into 6H-SiC EPI layers to form a buried (100 nm) 500 nm thick layer with plateau concentrations between $5x10^{17}$ cm^{-3} and $5x10^{20}$ cm^{-3}. The wafers were furnace annealed between 1450°C and 1650°C or alternatively at 2000°C, 20 ms using flash lamps. The electrical properties were measured by Hall effect between RT and 650°C. For furnace annealing the carrier concentration increases with increasing N concentration and increasing annealing temperature. The highest observed value (measured at RT) amounts to $1.5x10^{21}$ cm^{-3}. The mobility decreases with growing plateau concentration and annealing temperature. Applying flash lamp annealing, which leads in the case of Al implantation to higher carrier concentration, no enhancement of the carrier concentration was found. The analysis of temperature dependent Hall effect measurements shows that during the short annealing time only the nitrogen on the low energetic hexagonal site of the SiC lattice gets electrically activated.

supported by
DaimlerCrysler AG

A. Peeva
*P.F.P. Fichtner**
*M. Behar**
*J.R.A. Kaschny**
R. Koegler
W. Skorupa

Copper gettering at half the projected ion range induced by low energy channeling He implantation into silicon

He ions were implanted at 40 keV in channeling <100> Si direction to a fluence $8x10^{15}$ He/cm^2 at both RT and 350°C. The samples were contaminated with Cu by implanting the Si wafer with 20 keV, $1x10^{12}$ Cu/cm^2 in the rear side and submitted to 800°C thermal treatment for 600 s. Cu gettering was observed for He^+ implantation at 350 ºC only at the projected ion range region (R_p). For the same implantation performed at RT, Cu gettering appears at two different regions, at R_p and around $R_p/2$. The corresponding XTEM image displays the existence of a well defined buried layer around R_p containing cavities and dislocation loops. This layer is located in the vicinity

where the Cu is trapped at the R_p region. It is important to note that in this study the second gettering region at $R_p/2$ is induced by a light ion implanted at low energies into channeling direction. The gettering behaviour is similar to that observed for MeV implantation of heavier ions. However, in the present case much less energy was deposited at that region, and still the $R_p/2$ effect of the same order of magnitude as the gettering at R_p was detected. The absence of Cu gettering at $R_p/2$ for the 350ºC implantation is ascribed to the damage annealing that occurs during the implantation process.
Collaboration: * UFRGS, Porto Alegre, Brasil

R. Kögler
A. Peeva
*P. Werner**
W. Skorupa

Equalization of the V/I ratio at $R_P/2$ of high-energy ion-implanted Silicon
The vacancy to interstitial (V/I) ratio of high-energy ion-implanted Si is known to be a function of depth, x. At the projected ion range, $x=R_P$, it is $V/I<1$ and around $x=R_P/2$ $V/I>1$ is valid. Because of this disparity residual point defects or defect clusters may remain after annealing at temperatures up to 1000ºC. Such defects act as gettering centres for impurities in Si. In our study the V/I ratio of ion-implanted Si is equalized by a series of additional implants of Si^+ ions into the V-rich domains leading to self-interstitials. In this way a complete local recombination of all radiation induced Frenkel pairs during annealing should be possible. The implantation of self-interstitials just equalizing the excess of vacancies (predicted by TRIM calculations) does not result in their disappearance by recombination. Instead, the additionally introduced interstitials form small dislocation loops beside those formed at R_P. This means that either the excess of vacancies at $R_P/2$ is lower than predicted or the recombination of Frenkel pairs is remarkably incomplete.
Collaboration:* MPI für Mikrostrukturphysik, Halle

Nanoclusters

K.-H. Heinig

Analytical theory of nanocluster evolution under ion irradiation: Inverse Ostwald ripening
The spatial displacement probability of an individual atom of a solid due to collision cascades was determined assuming isotropic ion beam mixing. Integrating over the atomic displacement probabilities of a half-space, for an interface the spatial mixing probability of phase A into phase B has been obtained. The same mixing probability has been simulated by TRIM and fitted with the analytical function. The fit shows (i) that the analytical function allows a perfect description of the displacement distribution for forward as well as backward scattering, and (ii) that ion beam mixing can deviate from isotropy by more than 50%. The steady-state concentration of dissolved phase-A impurities in phase B under ion irradiation was found from the solution of the diffusion equation for a detailed interface balance including ion-beam induced detachment events. Below a critical temperature, the steady-state solubility is substantially higher than the Arrhenius-like thermal equilibrium solubility. Performing the same but now much more complex analysis for nanoclusters of phase A embedded in a matrix B, the well-known Gibbs-Thomson-like R_C/R radius dependence of equilibrium solubility could be proven to be valid under ion irradiation too (R_C-capillary length). The crucial new feature is an ion beam induced reduction of R_C, where even negative values become possible. Negative R_C mean that steady-state solubility around large nanocluster is higher than around smaller ones,

where the Cu is trapped at the R_p region. It is important to note that in this study the second gettering region at $R_p/2$ is induced by a light ion implanted at low energies into channeling direction. The gettering behaviour is similar to that observed for MeV implantation of heavier ions. However, in the present case much less energy was deposited at that region, and still the $R_p/2$ effect of the same order of magnitude as the gettering at R_p was detected. The absence of Cu gettering at $R_p/2$ for the 350ºC implantation is ascribed to the damage annealing that occurs during the implantation process.
Collaboration: * UFRGS, Porto Alegre, Brasil

R. Kögler
A. Peeva
*P. Werner**
W. Skorupa

Equalization of the V/I ratio at $R_P/2$ of high-energy ion-implanted Silicon
The vacancy to interstitial (V/I) ratio of high-energy ion-implanted Si is known to be a function of depth, x. At the projected ion range, $x=R_P$, it is $V/I<1$ and around $x=R_P/2$ $V/I>1$ is valid. Because of this disparity residual point defects or defect clusters may remain after annealing at temperatures up to 1000ºC. Such defects act as gettering centres for impurities in Si. In our study the V/I ratio of ion-implanted Si is equalized by a series of additional implants of Si^+ ions into the V-rich domains leading to self-interstitials. In this way a complete local recombination of all radiation induced Frenkel pairs during annealing should be possible. The implantation of self-interstitials just equalizing the excess of vacancies (predicted by TRIM calculations) does not result in their disappearance by recombination. Instead, the additionally introduced interstitials form small dislocation loops beside those formed at R_P. This means that either the excess of vacancies at $R_P/2$ is lower than predicted or the recombination of Frenkel pairs is remarkably incomplete.
Collaboration:* MPI für Mikrostrukturphysik, Halle

Nanoclusters

K.-H. Heinig

Analytical theory of nanocluster evolution under ion irradiation: Inverse Ostwald ripening
The spatial displacement probability of an individual atom of a solid due to collision cascades was determined assuming isotropic ion beam mixing. Integrating over the atomic displacement probabilities of a half-space, for an interface the spatial mixing probability of phase A into phase B has been obtained. The same mixing probability has been simulated by TRIM and fitted with the analytical function. The fit shows (i) that the analytical function allows a perfect description of the displacement distribution for forward as well as backward scattering, and (ii) that ion beam mixing can deviate from isotropy by more than 50%. The steady-state concentration of dissolved phase-A impurities in phase B under ion irradiation was found from the solution of the diffusion equation for a detailed interface balance including ion-beam induced detachment events. Below a critical temperature, the steady-state solubility is substantially higher than the Arrhenius-like thermal equilibrium solubility. Performing the same but now much more complex analysis for nanoclusters of phase A embedded in a matrix B, the well-known Gibbs-Thomson-like R_C/R radius dependence of equilibrium solubility could be proven to be valid under ion irradiation too (R_C-capillary length). The crucial new feature is an ion beam induced reduction of R_C, where even negative values become possible. Negative R_C mean that steady-state solubility around large nanocluster is higher than around smaller ones,

which is opposite to thermal equilibrium behaviour. Therefore, the resulting nanocluster evolution, which is called inverse Ostwald ripening, results in a very different nanocluster size distribution. A narrowing of broad size distributions becomes feasible.

*G. Rizza**
M. Strobel
K.-H. Heinig
*H. Bernas**

Ion irradiation-induced formation of nanocluster shells around gold inclusions in SiO_2: Experiments and simulations

Ion irradiation of sub-µm size gold inclusions in SiO_2 leads to the formation of nanometer-size Au clusters in their immediate surroundings. The size, density and radial distributions of the nanoclu-sters have been determined by TEM. Kinetic 3D Monte Carlo simulations account for the experimental results: In the system driven by the ion beam - under appropriate irradiation and temperature conditions - the dependence of the steady-state solubility on precipitate size may be opposite to that expected from the equilibrium Gibbs-Thomson relation. Thus, the high steady-state solubility surrounding the large gold inclusions allows nucleation of small gold nanoclusters. Other than under thermal equilibrium conditions, under ion irradiation small nanocluster survive in the immediate neighbourhood of less curved interfaces, they can even grow there.

Collaboration: *CSNSM, IN2P3, Orsay, France

B. Schmidt
K.-H. Heinig
*S. Oswald**
R. Grötzschel

Oxidation states of Ge in SiO_2 during precipitation and ripening

The change of the depth profile and chemical bond character of Ge in Ge^+ ion implanted SiO_2 layers (d_{ox} = 500 nm) during annealing in an O_2 atmosphere has been studied by RBS, XTEM and XPS. The Ge depth profiles in as-implanted and annealed samples as measured by XPS in combination with sputter etching are in agreement with profiles measured by RBS. Near the SiO_2/Si interface XPS enables a better depth resolution than RBS. Thus, other than RBS, XPS could proof that the fraction of implanted Ge, which moves during annealing to the SiO_2/Si interface region, resides on the Si side of this interface. Additionally, the high and low contrast nanoclusters in Ge implanted samples, which have been found recently in XTEM images, could be identified by XPS, in combination with data evaluation by factor analysis, to consist mainly of elemental Ge and GeO_2, respectively. For the interpretation of the XPS spectra the influence of ion beam mixing on nanoclusters during sputtering must be taken into account.

Collaboration:* Institut für Festkörper- und Werkstofforschung, Dresden

T. Müller
B. Schmidt
K.-H. Heinig
A. Mücklich

Shape evolution of oxidized V-grooves on (100) Si during high-dose Ge^+ implantation

The shape evolution of V-grooves on (100) Si has been studied both after thermal oxydation and subsequent high dose ion implantation by XTEM. The V-grooves covered with 200 nm SiO_2 have been fabricated by anisotropic etching with 30% KOH at 80 °C followed by oxydation at 1000 °C in dry oxygen. For the investigation of the change of the SiO_2 covered V-groove due to sputtering, re-deposition and swelling the grooves were implanted with 70 keV Ge^+ ions to a dose of $1x10^{17}$ cm^{-2}. The implanted Ge accumulates at the bottom of the grooves. Additionally, some SiO_2 sputtered from the groove walls is redeposited at the bottom smoothing out the corner at the bottom. Both features support the formation of quantum wires in the bottom region due to precipitation and Ostwald ripening during appropriate subsequent annealing steps.

H. Seifarth
M. Klimenkov
B. Schmidt

Sputtered semiconductor nanocluster *-layers within a SiO_2 matrix

-layers of Si nanocrystals embedded in the SiO_2 gate insulator of a field effect transistor in a (2-5) nm distance from the SiO_2/Si interface exhibit superior charge storage properties and may be favoured for future nonvolatile memory devices. A (2-5) nm SiO_2 / (5-10) nm SiO_x / 30 nm SiO_2 layer stack was deposited on a n-Si (100) substrate in a single process by reactive rf-magnetron-sputtering from a Si target and controlling the setpoint to adjust the composition parameter x = 2 in SiO_2 layers and x = (1.5-1.75) in the SiO_x layer. The as deposited SiO_x layer with $x < 2$ is amorphous with a random bonding mixture of Si-Si_nO_{4-n} tetrahedra, which distribution depends on x and n (n = 1...4). During subsequent annealing at T = 1000°C in N_2 atmosphere, the exceeding Si of the SiO_x layer forms a Si nanocrystal "-layer" embedded in SiO_2. The mean diameter and the mean distance of the Si nanocrystals within the *-layer depend on the Si excess in the SiO_x layer, the annealing regime and the mechanical stress within the layer stack during annealing. The lattice structure of Si nanocrystals has been observed by HRTEM. CV-measurements on MOS-structures with the insulator layer stack described above show a distinct shift of the CV-curve after negative and positive voltage stress indicating charge storage in the nanocrystal containing SiO_2 layer.

H. Seifarth
B. Schmidt
T. Müller
A. Mücklich

Stacked Ge nanocrystal layers in SiO_2

Multilayer structures consisting of stacked layers of Ge nanocrystals separated by SiO_2 have been produced by alternating rf-magnetron sputtering from a elemental Ge target and a quartz target respectively onto thermal grown SiO_2 and subsequent annealing. In the sputtered samples, the number of periods was up to 4 and the a-Ge thickness was 2 nm while that of the SiO_2 was 20 nm. The recrystallization was performed by annealing at 600-900°C for 30 min in N_2 atmosphere. HRTEM investigations show that isolated Ge nanocrystals forms along the Ge layers. The mean nanocrystal diameter in each Ge layer after 900°C annealing increases in direction from the SiO_2 surface to the SiO_2/Si interface from 6 nm in the last deposited Ge layer up to 40 nm in the first deposited Ge layer. For ripening of isolated nanoclusters within one layer the maximum Ge layer thickness was 2 nm. At higher layer thicknesses continuous polycrystalline Ge layers have been observed.

T. Gebel
T. Müller
*E. Boer**
*H. A. Atwater**

Charging experiments on Ge nanoclusters in SiO_2 films using AFM

Charging of semiconductor nanoclusters with an AFM is considered to be a well suited method to study their electrical properties. Selected SiO_2 films of 20-100 nm thickness have been investigated which show in the XTEM a band of small nanoclusters (2-3 nm size) very close to the Si/SiO_2 interface. To realize a very narrow distance of the AFM tip to these clusters oxide etching by buffered HF down to the cluster region or selective anisotropic Si etching from the backside using KOH/H_2O solution until the oxide layer has been applied. Charging was carried out by applying –10V to the AFM tip and contacting the surface with this tip for 10 s. Subsequently the area was scanned in non-contact mode. The stored charge leads to an additional coulomb force to the tip, which suggests an increased height of the charged area. Charged spots of relatively large size (1..2 μm) have been observed, which disappear with typical retention times between several minutes and 2 hours. The quality of the AFM-tip and surface adsorbates play a key role for

the reproducibility of the results.
Collaboration: * California Institute of Technology, Pasadena (CA), USA

T. Gebel
J. von Borany
W. Skorupa
*H.-J. Thees**
*M. Wittmaack**
*K.-H. Stegemann**

Thin gate oxides with Ge and Si nanoclusters for memory applications

Thin thermally grown SiO_2 films of 20 and 30 nm thickness on n-type (100) Si wafers have been alternatively implanted with Ge^+ (12 - 20 keV) and Si^+ (6 - 12 keV) ions to doses of 1 .. 9 x10^{15} cm^{-2}. After rapid thermal annealing at 950°C, 30 s under N_2 atmosphere a poly-Si layer (300 nm) was deposited by LPCVD, doped with P^+ ions and patterned to form the gate of a MOS capacitor. Additional thermal treatment steps were carried out to simulate the thermal budget during memory fabrication. The charge storage effects have been studied by high frequency CV-measurements of the MOS capacitors. For Ge implanted layers, samples containing bulk and additional interface Ge clusters near the Si/SiO_2 interface show a larger programming window but worse retention characteristics than samples with bulk clusters only. This implies, that electrons stored in the cluster band near the interface are released faster by direct tunneling. For lower programming fields (up to 4 $MVcm^{-1}$) the achieved programming window for Ge based structures is higher than that for comparable Si implanted SiO_2 films. At programming fields of 6.25 $MVcm^{-1}$ the programming windows are nearly of the same size. SiO_2 films containing Si clusters show excellent retention characteristics. Even after long term treatment (72 h) at 225°C a programming window of more than 2 V was observed.

supported by SMWK and SMWA

Collaboration: * Zentrum für Mikroelektronik Dresden GmbH

T. Gebel
J. von Borany
L. Rebohle
W. Skorupa
*D. Borchert**

Monolithically integrated optical coupler in silicon technology

Optical interconnects are very promising to overcome limitations in conventional interconnection technologies in microelectronics which are caused by capacitive and inductive effects at higher frequencies and due to electromagnetic interferences. A monolithically integrated optical coupler consisting of an emitter based on ion beam synthesized Ge nanoclusters in a SiO_2 layer and a pin-photodiode for light detection was designed. As transparent metal layers for contacts within the emitter-diode-stack indium-tin-oxide has been applied. The galvanic separation was realized by a 500 nm SiO_2 layer deposited by magnetron sputtering. The light detection element consists of a pin- layer of 680 nm thickness which was deposited by plasma based processes involving in-situ doping. The sensitivity of the photodiode at a wavelength of 400 nm is about 0.2 A/W and the dark current is in the range of some pA. The minimum operating current for electroluminescence excitationis 2x$10^{-7}$$Acm^{-2}$. Measurements show a linear dependence between the excitation current and the photocurrent over more than three orders of magnitude.

Collaboration: * Fern-Universität Hagen, Fakultät für Elektrotechnik

Biotechnological Materials

*N. Huang**
R. Günzel
M. T. Pham
E. Richter

Surface modification of titanium biomaterials by oxygen ion implantation using PIII

Titanium is a popularly applied biomaterial. The natural formed titanium oxide layer on the surface is commonly considered to play an important role for the biocompatibility, but this layer is only several nm in thickness and obeys several defects. It can not effectively prevent the release of metal ions into the biological environment.

Pure titanium was modified by oxygen PIII at the a temperature of 450°C. The implanted doses were varied from $5x10^{17}$ to $1x10^{19}$ ions/cm^2. Rutile type titanium dioxide layers were obtained. Ti ion release in simulated body solution examined by atom absorption spectrum revealed that after PIII treatment the dissolution of Ti ions was decreased up to two orders of magnitude. The surface wear resistance was also improved significantly. It was found that the surface morphology of titanium oxide layers affect the Ti release rate in a large extent.

Collaboration: *Biomaterials and Surface Engineering Laboratory, Department of Materials Engineering, Southwest Jiaotong University, Chengdu, China

Others

H. Tyrroff
*H. Preuße**
*G. Zschornack**

EDX-studies of highly charged neon ions colliding with a Si <100> surface

Highly charged ions approaching a solid state target can capture electrons from the surface and form transient 'hollow atoms'. Varying the ion velocity the X-ray spectra are expected to comprise information about the decay mechanism of the formed hollow atoms. Using a Si(Li) detector we have measured and analysed the X-ray spectra emitted by Ne^{8+} and Ne^{9+} ions with kinetic energies in the range from 50 eV up to 5 keV in the vicinity of a <100> Si target. At the lower end of the kinetic energy scale the center of the emitted neon $K_{"}$ and $K_{\$}$ lines is shifted towards higher values by about 25 eV. Higher lying levels are depopulated now and influence the central potential screening. Furthermore, the observed X-ray fluorescence yields increase by about one order of magnitude if the ions are slowed down. The $K_{"}$ yield of Ne^{9+} exceeds $2x10^3$ quants/ion and is 100 times higher then the corresponding Ne^{8+} yield. This results reflect the influence of the effective ion charge state of actual orbital populations on radiation yields characteristic for this interaction process.

Collaboration: *Technische Universität Dresden, Institut für Kern- und Teilchenphysik

T. Hauschild
*M. Jentschel**
K.-H. Heinig
*H.-G. Börner**

Study of interatomic potentials in zinc sulfide

At the high-flux reactor in Grenoble the former Crystal-GRID experiments with ZnS crystals having their <111> and <110> orientations aligned with respect to the axis of the GAMS spectrometer were completed by the third principle crystal orientation, the <100> alignment. Fitting molecular dynamics simulations to this set of measurements a more precise nuclear lifetime of (49±1 fs) has been determined for the 3221 keV level of ^{33}S, which is consistent with the previously reported value (40±12 fs). Due to bad

Biotechnological Materials

*N. Huang**
R. Günzel
M. T. Pham
E. Richter

Surface modification of titanium biomaterials by oxygen ion implantation using PIII

Titanium is a popularly applied biomaterial. The natural formed titanium oxide layer on the surface is commonly considered to play an important role for the biocompatibility, but this layer is only several nm in thickness and obeys several defects. It can not effectively prevent the release of metal ions into the biological environment.

Pure titanium was modified by oxygen PIII at the a temperature of 450°C. The implanted doses were varied from $5x10^{17}$ to $1x10^{19}$ ions/cm^2. Rutile type titanium dioxide layers were obtained. Ti ion release in simulated body solution examined by atom absorption spectrum revealed that after PIII treatment the dissolution of Ti ions was decreased up to two orders of magnitude. The surface wear resistance was also improved significantly. It was found that the surface morphology of titanium oxide layers affect the Ti release rate in a large extent.

Collaboration: *Biomaterials and Surface Engineering Laboratory, Department of Materials Engineering, Southwest Jiaotong University, Chengdu, China

Others

H. Tyrroff
*H. Preuße**
*G. Zschornack**

EDX-studies of highly charged neon ions colliding with a Si <100> surface

Highly charged ions approaching a solid state target can capture electrons from the surface and form transient 'hollow atoms'. Varying the ion velocity the X-ray spectra are expected to comprise information about the decay mechanism of the formed hollow atoms. Using a Si(Li) detector we have measured and analysed the X-ray spectra emitted by Ne^{8+} and Ne^{9+} ions with kinetic energies in the range from 50 eV up to 5 keV in the vicinity of a <100> Si target. At the lower end of the kinetic energy scale the center of the emitted neon $K_{"}$ and $K_{\$}$ lines is shifted towards higher values by about 25 eV. Higher lying levels are depopulated now and influence the central potential screening. Furthermore, the observed X-ray fluorescence yields increase by about one order of magnitude if the ions are slowed down. The $K_{"}$ yield of Ne^{9+} exceeds $2x10^3$ quants/ion and is 100 times higher then the corresponding Ne^{8+} yield. This results reflect the influence of the effective ion charge state of actual orbital populations on radiation yields characteristic for this interaction process.

Collaboration: *Technische Universität Dresden, Institut für Kern- und Teilchenphysik

T. Hauschild
*M. Jentschel**
K.-H. Heinig
*H.-G. Börner**

Study of interatomic potentials in zinc sulfide

At the high-flux reactor in Grenoble the former Crystal-GRID experiments with ZnS crystals having their <111> and <110> orientations aligned with respect to the axis of the GAMS spectrometer were completed by the third principle crystal orientation, the <100> alignment. Fitting molecular dynamics simulations to this set of measurements a more precise nuclear lifetime of (49±1 fs) has been determined for the 3221 keV level of ^{33}S, which is consistent with the previously reported value (40±12 fs). Due to bad

statistics, the spectra of independent measurements differ substantially from each other. The improved statistics due to multiple measurements allowed to find more accurate results for both, the interatomic potential for the Zn–S interaction and the deexitation lifetime of the 3221 keV level of ^{33}S. In the studied energy range of 10 to 500 eV, the new Zn–S potential found by Crystal-GRID differs significantly from the screened Coulomb potentials, generally used in computer simulations.
Collaboration: *ILL Grenoble, France

H. Reuther
M. Betzl

Annealing behaviour of magnesium and aluminum implanted with iron ions

Mg and Al are the two metallic construction materials with the lowest weight however they are hardly applicable in pure state. Therefore alloying with different elements is commonly used in order to enlarge their application possibilities. We investigated the alloying process by implantation with iron ions. The implantation energy was 200 keV while the ion doses ranged over several decades up to $9x10^{17}$ cm^{-2}. Thus, highly disordered alloyed layers with up to 90 at.% iron can be obtained. The samples were annealed in vacuum at subsequently increasing temperatures up to 600°C for Al and up to 400°C for Mg. Possible ordering and redistribution processes during annealing were studied by CEMS, AES depth profiling, and XRD. In the case of the Fe-Mg system (insoluble with each other) "-iron is precipitated in small clusters after annealing. In the case of the Fe-Al system, only small redistribution processes occur up to 400°C while at 500°C different iron aluminides are formed. The final state for all samples after annealing at 600°C is a mixture of $Al_{13}Fe_4$ and Al_6Fe.

F. Berberich
W. Matz
E. Richter
N. Schell
U. Kreißig

Structural mechanisms of the mechanical degradation of nitrided Ti-Al-V alloys: in-situ diffraction study during annealing

Enhanced hardness of the technical alloy Ti-6Al-4V can be achieved by N^+-implantation. Samples implanted with fluences $(1\text{-}6)x10^{17}$ N^+/cm^2 at 80 keV show an hardness increase by a factor of 2.5 to 3.5. XRD studies reveal the formation of small TiN crystallites near the surface. But, loss of hardness is observed after annealing up to 700°C. The structural modifications leading to this degradation were studied by *in-situ* XRD-experiments with synchrotron radiation at ROBL. Additional sample characterisation was performed by SEM, ERDA and Vickers hardness tests. The hardness reduction due to annealing is caused by a continuous phase transformation from TiN to Ti_2N in consequence of the diffusion of nitrogen as found in ERDA results. XRD revealed additionally rearrangements in the "-Ti and $-Ti phase of the alloy.

Ion Beam Analysis

C. Neelmeijer
M. Mäder
*U. Pietsch**
*H. Ulbricht**
*H.M. Walcha**

PIXE minor element analysis of "Böttger Stoneware"

Non-destructive material analysis is of growing interest for museums in order to support attributions of art objects by objective natural scientific proofs. Regarding artifacts made of Böttger stoneware relative concentrations of both main and minor elements are suggested as characteristic "fingerprints" for indication of the authenticity. This is because preparation of the basic mass is a part of Böttger's "arcanum" and the incorporation of minor/trace elements depends mainly on the provenience of the basic material. Reliable PIXE "fingerprints" require sufficient statistics for minor and trace element signals as well. At the external beam set-up this demand was recently satisfied by the implementation of a second Si(Li) detector of large efficiency: Minor/trace elements ($25 < Z < 41$) are currently analysed by detector No. 2 (80 mm^2 area, 1 mm Acrylic absorber) in air whereas characteristic X-rays of the main elements ($13 < Z < 27$) are simultaneously measured by detector No. 1. The gain of efficiency for detector No. 2, compared to detector No. 1, is a factor of $g = 7.4$ for the given high-Z region. To combine this double PIXE arrangement with simultaneous PIGE and RBS measurements an upgraded exit pipe was successfully implemented.

Collaboration: *Staatliche Kunstsammlungen Dresden, Porzellansammlung im Zwinger; J. Paul Getty Museum Los Angeles, USA; Bartol Research Institute, University of Delaware, USA

M. Mäder
C. Neelmeijer
*M. Schreiner**

Non-destructive composition analysis of glass artefacts for precaution

Glass corrosion caused by environmental attacks is a serious problem especially for valuable historic glass objects. This is because the glasses may lose their transparency and stability. The alterations proceeding on the glass surface include ion exchange processes where network modifiers are replaced by hydrogen bearing species to form a hydrated silica-rich surface layer. In order to characterise the condition of a glass object showing no visible alteration or corrosion damage, three ion beam based techniques (PIXE, PIGE, RBS) have been combined in simultaneous measurements using the external proton beam. Combining PIXE and PIGE the yield of X- and (-radiation of the element Si was studied to indicate thin leached layers. More extended regions can be characterised by external RBS. For getting the composition of the glass bulk the PIXE spectra were treated using the GUPIX code taking into account the experimental findings about the corrosion layer. The developed procedure allows evaluation of initial corrosion on historical glass objects and the identification of glass materials which are sensitive to atmospheric corrosion processes. The analytical results may offer suggestions for storage sensitive glass objects under safe conditions, e.g. special environmental surroundings.

supported by BMBF

Collaboration: *Institut für Farbenchemie, Akademie der Bildenden Künste Wien, Österreich; Bundesanstalt für Materialforschung und –prüfung Berlin; Fraunhofer-Institut für Silicatforschung Bronnbach

U. Kreissig
*P. Skeldon**

ERDA of lithium ion mobility in anodic alumina films formed on an Al-Li alloy

Li is one of the important strengthening elements of commercial, precipitation-hardened aluminium alloys, which are normally subjected to surface treatment prior to application. The pre-treatment commonly develop amorphous alumina films, sometimes hydrated, on the alloy surface; e.g. by

anodizing. The Li mobility in the barrier anodic film formed on an Al-3at% Li alloy in ammonium pentaborate electrolyte has been determined from measurements of the film composition by ERDA. The results reveal a reduced amount of Li in the film compared with that in the alloy. The level of reduction indicates that Li migrate outward about 7 times faster than Al^{3+} ions. The Li species are lost to the electrolyte on reaching the film/electrolyte interface, leading to a slight loss in the efficiency of film growth. In contrast, loss of aluminium species to the electrolyte is negligible, as revealed by the distribution of boron in the outer ~ 40% of the film thickness. The determination of the hydrogen profiles indicates insignificant amounts of hydrogen in the film.

supported by BMBF

Collaboration: *Corrosion and Protection Centre, University of Manchester, Institute of Science and Technology, Manchester, U.K.

*B. Groß**
*J. Engeldinger**
D. Grambole
F. Herrmann
*R. Hempelmann**

Investigation of dissociative water vapour absorption in $BaZr_{0.85}Y_{0.15}O_{2.925}/H_2O$ by means of the ^{15}N nuclear reaction analysis

Thin films of the perovskite type proton conducting ceramic $BaZr_{0.85}Y_{0.15}O_{2.925}$ were prepared using a sol-gel process by multiple dip-coating on silicon single crystal wafers. The crystallite sizes of the films can be calculated to a value of about 40 nm. In addition we prepared powder bulk samples, applying the conventional carbonate route. Both, the films and powder samples were charged with hydrogen by dissociative water vapour absorption at definite values of water vapour partial pressures and charging temperatures. The absorbed hydrogen content reaches values between 2 mol.% and 10 mol.%, and was determined ex-situ at RT using the resonant nuclear reaction $^1H(^{15}N,\alpha)^{12}C$. From the resulting water vapour partial pressure/compositions isotherms the absorption enthalpies, for regular (H_0) and trap proton sites (H_t), and the absorption entropy ΔS were calculated using a two state model, based on Fermi-Dirac statistics. By this mathematical procedure each lattice oxygen ion (O^{2-}) can be occupied only by one proton (forming OH^-), i.e. double or triple bonding (forming H_2O or H_3O^+) is forbidden.

supported by BMBF

Collaboration: *Institut für Physikalische Chemie, Universität des Saarlandes, Saarbrücken

*B. Lenkeit**
D. Grambole
F. Herrmann
*R. Hezel**

Impact of the hydrogen content on the thermal stability of SiN films

In photovoltaics, amorphous hydrogenated silicon nitride (SiN) films are used simultaneously for surface passivation and as antireflection coating. The SiN films have to withstand a short annealing step in the range of 650-950°C after metal contact printing without degradation of the surface passivation quality. For this reason the influence of several parameters of PECVD on the thermal stability of the surface passivation of SiN films is investigated. The surface passivation quality is measured by the contactless light-biased microwave-detected photoconductance decay (MW-PCD) technique on symmetrical SiN/p-Si/SiN structures, while the composition of the SiN films is indirectly determined by ellipsometric measurements. A direct correlation is observed between thermal stability and H content by the resonant nuclear reaction $^1H(^{15}N,\alpha)^{12}C$. The SiN films featuring a relatively low hydrogen content of about 10 - 12 at% show an excellently thermally stable surface passivation (refractive index between 2.0 and 2.2, i.e. N/Si ratio of about 0.9 to 1.2). In contrast, SiN films with a relatively high H content after deposition ($\$$ 15 at%) degrade much faster, so that they are not suited as surface passi-

vation for Si solar cells any more.
Collaboration: * Institut für Solarenergieforschung Hameln/Emmerthal (ISFH)

A. Markwitz[*]
D. Grambole
F. Herrmann
*B. Trompetter**
*T. Dioses***
*R. W. Gauldie**,***

Reliable micro-measurement of Sr is the key to cracking the life-history code in the fish otolith

The fish otolith (consisting of aragonite [=calcium carbonate] crystal) grows continuously during fish's life and is not continuously re-metabolised like bone. Consequently, the otolith has long been regarded as a potential store of information about the life history of an individual fish which is encoded in the composition of trace elements. The code has been difficult to crack. However, recent developments have shown that Sr is one of the few stable trace elements in the otolith which summarises the effects of variables that affect the growth rate of the otolith crystal. Therefore, reliable micro-PIXE measurements of the Sr content at spatial resolutions of 10 µm or less have been performed, which represents about 4-6 days of otolith growth in most species of fish. A beam resolution of 2 µm for line scans and of 6 µm for mapping (300 µm x 300 µm) have been applied. These micro-measurements were linked to macro-measurements of 2D maps of the entire surface of sections of otoliths up to 5 mm square at beam resolutions of 25 µm.
Collaboration: *Institute of Geological and Nuclear Sciences, Lower Hutt, New Zealand; **Instituto del Mar del Peru, Callao, Peru; ***Hawaii Institute of Geophysics and Planetology, School of Ocean, Earth Sciences and Technology, Honolulu, USA

D. Grambole
C. Neelmeijer
*K. Noll**
F. Herrmann

^{19}F(p,p'()^{19}F and ^{18}O(p,()^{19}F g-ray interference studied on liquids by external PIGE

In earlier PIGE investigations of meteorites at the Rossendorf nuclear microprobe a detection limit for fluorine of 3.5 wt.-ppm was obtained by using a planar Ge detector with a high sensitivity for the 110 keV (-rays of the nuclear reaction ^{19}F(p,p'()^{19}F. However, in oxygen-rich materials there is an interference effect for the 110 keV and 197 keV (-ray lines of the nuclear reactions ^{18}O(p,()^{19}F and ^{19}F(p,p'()^{19}F. In order to study this effect qualitatively, thick liquid targets were examined by PIGE using the external proton beam of 3.4 MeV energy. Several grades of dilutions were prepared from 76.3 % ^{18}O enriched H_2O and from 1000 ppm F standard NaF solution. From this, a data base was obtained in order to extrapolate the 110 keV and 197 keV (-ray yields of the ^{18}O(p,()^{19}F reaction for a target of water containing 0,2 % ^{18}O. As a main result it was obtained that, for fluorine in oxygen-rich materials, the reaction ^{19}F(p,p'()^{19}F allows minimum detection limits of (1.06±0.12) at.ppm and (1.85±0.20) at.ppm for the 110 keV and 197 keV (-line, respectively.
Collaboration: *Universität Bern, Fakultät für Chemie and Biochemie, Bern, Schweiz

*G. Müller**
*J. Böhmert**
D. Grambole
F. Herrmann

Correlation between segregations and toughness parameters of a reactor pressure vessel steel

Material inhomogeneities (segregations), depending of their depth in a thick-wall block, lead to large variations of toughness parameters. The composition of such segregations in a ASTM A533 B cl 1 reactor pressure vessel steel was investigated by PIXE using the Rossendorf nuclear microprobe. Spectra and line scans were measured in points on and beside and over a segregation, respectively. In the segregation an increased content of Mg (+23 %), Cr (+15%), Mo (+30%) and Ni (+16%) was found. It was detected a gradient of

the evolution of microstructure and segregations in dependence of the depth. The changes of the composition correlate with micro-hardness variation.
Collaboration: *Forschungszentrum Rossendorf, Institut für Sicherheitsforschung

*T. Som**
D. Grambole
F. Herrmann
B. Schmidt
R. Grötzschel
W. Möller

Study of the diffusion behaviour of implanted hydrogen in Si (100)
Hydrogen has been found to interact with defects in semiconductors and is capable of changing their electrical properties. Therefore mobility and release of hydrogen is an interesting subject. We have implanted 20 keV H ions of a fluence of $1x10^{16}$ ions/cm² in p-Si (100). The implanted samples were annealed both isothermally and isochronally in the temperature range of 300-700°C in an Ar atmosphere. The H depth profiles were obtained by ERDA measurements using $^{12}C^{3+}$ ions of 8 MeV. The total H content in the Si sample has been observed to decrease steadily up to a certain annealing time for all annealing temperatures and after there almost getting saturated. This trend is clear above the annealing temperature of 300°C, while after the samples being annealed at 700°C, no implanted H was observed anymore indicating complete desorption of H from the sample. Annealing temperature versus total implanted hydrogen concentration data have been evaluated by exponential fitting, which give rise to the time constants for H desorption. These constants have been plotted as a function of inverse temperature to obtain the activation energy for H desorption to be ~ 0.2 eV. This result has been attributed to the formation of relatively immobile H_2 molecules under high H concentration in these samples.
Collaboration: *Nuclear Science Centre, New Delhi, India

M. Friedrich
W. Pilz
*R. Hellborg**
*R. Vesanen**
*N. Bekris***
*R.-D. Penzhorn***

Tritium detection by accelerator mass spectrometry (AMS)
The activities on AMS have been continued for tritium depth profiling of high-level samples from JET Culham/UK and in the frame of the European Large-Scale Facility for low-level tritium-marked biomedical samples. The biomedical investigations require a reduction of the background at the 3 MV Tandetron. Therefore, a separate air-insulated 100 kV tandem accelerator was constructed to remove the high-level measurements from the 3 MV Tande-tron. After stopping of the depth profiling measurements of the JET samples at the Tandetron and cleaning of the injector region the background was reduced by about 3 orders of magnitude. The first low-level AMS measurements were directed on the improvement of the sample preparation technique. The planned high-level depth profile measurements at the 100 kV tandem accelerator require a special operating permission from the supervising authorities. The according activities are in progress.
supported by
FZ Karlsruhe
Collaboration: *University of Lund/Sweden; **Forschungszentrum Karlsruhe

*F. Schrempel**
*Y.-S. Kim**
D. Grambole
F. Herrmann
*W. Witthuhn**

Realisation of a microlens structure by an ion microbeam
A new technique basing on the Deep Ion Beam Lithography has been developed, which allows the production of microlenses in an arbitrary shape. The realisation of the technique could be very useful for the forthcoming application in optical computer technology. A collimated proton beam with dia-meters of some micrometers penetrates the resist up to a sharply limited depth. By tilting and rotating the resist the microbeam describes a hemisphere, if the tilting axis and the rotating axis intersect in the point where the ion beam hits the resist surface. The shape of the structures can be modified by changing the distances between these axes relative to each other. The irradiated regions can be solved without affecting the non-irradiated

regions. First experiments were carried out at PMMA resist with 3 MeV protons focused to 10 µm for 0°...90° tilt angles at steps of 1° and rotating the sample at each irradiation. Du to the limited position accuracy of the used goniometer for rotation and tilting the beam spot at each tilt angle was not precisely enough for the microlens production. Therefore, the quality of the formed structures remains below the required accuracy, but the experiments show the feasibility of the method. The roughness of the structures produced was smaller than 10 nm and complies with the requirements for the application in microoptical devices.

Collaboration: *Friedrich-Schiller-Universität Jena, Institut für Festkörperphysik

Focused Ion Beam

J. Teichert,
L. Bischoff
*J. Martin**
*R. Wannemacher**
*W. Sigle***
*B. Köhler****

Local colour centres in synthetic diamond produced by FIB and high-energy electron irradiation

Localised colour centres were produced by electron and ion beam irradiation of synthetic diamonds of type Ib (substitutional nitrogen impurities). Irradiations were carried out with 400 keV electron beams and with focused ion beams of Ge (70 keV), Co (35 keV), and Ga (30 keV). In a subsequent annealing process the colour centres were formed by vacancy defect migration to the substitutional nitrogen atoms. Light emission mainly appears at 575 nm and 637 nm, corresponding to the neutral and negative charged nitrogen vacancy complex. The point defect production with electron beams requires sufficient high electron energies. Consequently the large penetration depth and the lateral straggling of the electrons prevents a sharp localisation of light emitting areas. Point light sources of nanometer dimension could be formed by means of focused ion implantation and proper annealing conditions. Light emitting lines and point arrays were produced. Local photo luminescence and crystal damage were measured by confocal microscopy and Raman spectroscopy, respectively. Diamond cantilever tips were irradiated on their tops with the focused ion beam. The point light sources formed in this way can be used for a new type of optical near field microscope.

Collaboration: *Technische Universität Chemnitz, Institut für Physik; **Max-Planck-Institut für Metallphysik, Stuttgart; *** Fraunhofer-Institut für zerstörungsfreie Prüfverfahren, Außenstelle EADQ, Dresden

regions. First experiments were carried out at PMMA resist with 3 MeV protons focused to 10 µm for 0°...90° tilt angles at steps of 1° and rotating the sample at each irradiation. Du to the limited position accuracy of the used goniometer for rotation and tilting the beam spot at each tilt angle was not precisely enough for the microlens production. Therefore, the quality of the formed structures remains below the required accuracy, but the experiments show the feasibility of the method. The roughness of the structures produced was smaller than 10 nm and complies with the requirements for the application in microoptical devices.
Collaboration: *Friedrich-Schiller-Universität Jena, Institut für Festkörperphysik

Focused Ion Beam

J. Teichert,
L. Bischoff
*J. Martin**
*R. Wannemacher**
*W. Sigle***
*B. Köhler****

Local colour centres in synthetic diamond produced by FIB and high-energy electron irradiation
Localised colour centres were produced by electron and ion beam irradiation of synthetic diamonds of type Ib (substitutional nitrogen impurities). Irradiations were carried out with 400 keV electron beams and with focused ion beams of Ge (70 keV), Co (35 keV), and Ga (30 keV). In a subsequent annealing process the colour centres were formed by vacancy defect migration to the substitutional nitrogen atoms. Light emission mainly appears at 575 nm and 637 nm, corresponding to the neutral and negative charged nitrogen vacancy complex. The point defect production with electron beams requires sufficient high electron energies. Consequently the large penetration depth and the lateral straggling of the electrons prevents a sharp localisation of light emitting areas. Point light sources of nanometer dimension could be formed by means of focused ion implantation and proper annealing conditions. Light emitting lines and point arrays were produced. Local photo luminescence and crystal damage were measured by confocal microscopy and Raman spectroscopy, respectively. Diamond cantilever tips were irradiated on their tops with the focused ion beam. The point light sources formed in this way can be used for a new type of optical near field microscope.
Collaboration: *Technische Universität Chemnitz, Institut für Physik; **Max-Planck-Institut für Metallphysik, Stuttgart; *** Fraunhofer-Institut für zerstörungsfreie Prüfverfahren, Außenstelle EADQ, Dresden

L. Bischoff
J. Teichert
*H. Tritschler**

Micro-tools of tungsten carbide fabricated by focused ion beam milling
Tungsten carbide (WC) embedded in a Co matrix (7.5%) is a very promising material for micro-tools like drills or milling cutters. Due to the small structure size and the extreme hardness of WC(Co) traditional mechanical techniques are not possible to apply. Focused ion beam milling initiate an alternative for processing this material. On WC wires with a diameter of 50 µm two edges were fabricated by sputtering a 10 x 20 μm^2 area on each side of the wire. A sharp edge is only formed on the bottom side so that the wire has to be rotated to precise 180 degrees between the two steps. 35 keV Co (0.6 nA) and Au (1.5 nA) as well as a 70 keV Nd (0.5nA) FIBs using the system IMSA-100 were successful tested to perform the erosion of the material. In spite of the grain structure of WC(Co) smooth surfaces and sharp edges with radii in the nm-scale could be achieved. For the heavy ion species the processing time for one tool was in the range of 4 hours. A proper scanning regime where the beam hits the target always under a small angle

can further reduce the processing time. A special sample holder for accurate rotating of the tool during processing is under construction.
Collaboration: *Universität Karlsruhe (TH), Lehrstuhl und Institut für Werkzeugmaschinen und Betriebstechnik

Ch. Akhmadaliev
L. Bischoff
J. Teichert
*B. Köhler**

Investigation of the ion acoustic effect using focused ion beams

Acoustic waves in solids induced by the irradiation with an intensity modulated focused ion beam are investigated. The aim of this study is the development of an ion acoustic microscope which would allow to image surface as well as subsurface structures with high lateral resolution. First experiments were performed with a 35 keV Ga^+ FIB with a current of about 3 nA and a spot size of about 300 nm. The ion beam was pulsed with a variable frequency up to 200 kHz. The acoustic waves were detected using a piezoelectric transducer with an integrated pre-amplifier. The in-phase signal from the transducer synchronised with the chopping mode was measured by a look-in amplifier. Scanning the ion beam across a sample, it was shown that the measured amplitude and phase signals reflect the lateral material distribution of the sample. A model of this process was developed based on a two-dimensional approach of the wave generation and propagation in the material. For the fast data transfer in the experiment a new computer controlled scanning and imaging system was implemented to the IMSA-100 FIB equipment.

supported by
DFG

Collaboration: *Frauenhofer-Institut für zerstörungsfreie Prüfverfahren, Einrichtung für Akustische Diagnostik und Qualitätssicherung, Dresden

L. Bischoff
B. Schmidt
J. Teichert

Fabrication of fast diodes with very low capacity using focused ion beam implantation

The high lateral resolution of a focused ion beam offers the opportunity to irradiate very small areas. In this way, n-type (100)-silicon substrates can be implanted with Ga ions acting as an acceptor and Co ions which form metallic $CoSi_2$ leading to p^+n- and Schottky-junctions, respectively. The implantation was performed with a stationary beam (spot size of about 200 nm) through a SiO_2-layer (90 nm) leading to an active area to less than 0.01 μm^2 or alternatively with a scanning area of 1x1 μm^2 (dose: 5 -7.5x10^{17} cm^{-2}). The expected capacity of the diodes is in the range of fF to aF. In addition the oxide acts as an insulating layer for the conducting paths. The patterning of the diode Al contacts was performed by photolithography. The diodes were investigated with respect to their IU-characteristics depending on the process parameters like implantation dose and annealing temperature. The Ga implanted „point-diodes“ (irradiated with 240 pA for 0.5 s) as well as the 1 x 1 μm^2„square-diodes“ show a typical diode behaviour with a reverse current of about 1 pA at –1 V bias.

J. Teichert
L. Trojok
L. Bischoff
*B. Köhler**
H. Lichte

FIB preparation of samples for high resolution TEM investigations

FIB micromachining becomes a promising technique for TEM specimen preparation. For HR TEM investigations of silicon bulk material thin lamellas were fabricated using the dual-beam equipment FIB 4400 (Orsay Physics). Sputtering and polishing of the lamella with the 30 keV Ga FIB with different currents leads to a surface damaging due to implantation and amorphization of a thin surface layer of about 10-20 nm. This effect aggravates resolution and contrast in HRTEM investigations. To decrease the damage at the surface the beam energy was reduced to 15 keV for polishing

First TEM results show an improvement of the image quality. For the application of the FIB to the localised TEM sample preparation from the whole wafer a special lift-out micro-manipulator was designed and is now under construction.

supported by SMWK

Collaboration: *Frauenhofer-Institut für zerstörungsfreie Prüfverfahren, Einrichtung für Akustische Diagnostik und Qualitätssicherung, Dresden; **Technische Universität Dresden, Institut für Angewandte Physik und Didaktik der Physik

S. Hausmann
J. Teichert
L. Bischoff
M. Voelskow

Dose rate dependence of irradiation damage in silicon

The influence of the dose rate on the damage creation in silicon has been investigated by means of high current density FIB implantation. 70 keV Co and Ge ions with a current density of about 1 A/cm^2 have been implanted into silicon at target temperatures in the range from room temperature to 420°C. The effective dose rate was varied between 10^{13} ions /cm^{2}s and about 10^{19} ions/cm^{2}s applying different pixel dwell times from 1 µs to 250 µs. The damage has been investigated using RBS/C, SEM, micro-Raman spectroscopy and reflectivity measurements. It is found that at short dwell times at an implantation temperature of about 400°C the silicon remains crystalline after Co as well as Ge ion bombardment also in the limit of high doses while at long dwell times the silicon sample becomes amorphous. These studies of damage accumulation and dynamic annealing reveal that the characteristic time of defect annealing lies in the range from 1 µs to 10 ms depending on the defect type and the process temperature.

supported by DFG

M. Posselt
J. Teichert
L. Bischoff
S. Hausmann

Dose rate and temperature dependence of Ge range profiles in Si obtained by channeling implantation

A strong influence of dose rate and temperature on the dependence of the shape of Ge depth profiles in Si on the ion dose was found using the FIB equipment. 70 keV channeling implantations of Ge into (100)Si were performed at two different effective dose rates (3.5×10^{17} and 10^{10} cm^{-2}s^{-1}) and temperatures (300 and 520 K). The variation of the pixel dwell time was employed to obtain identical total doses between 10^{12} and 6×10^{14} cm^{-2} at different effective dose rates. The depth distributions of Ge were determined by SIMS. The dose dependence of the shape of these profiles is most pronounced at the high dose rate and the low target temperature. The dose rate and temperature effects found can be explained in the framework of an extended phenomenological model of defect accumulation. Crystal-TRIM atomistic computer simulations employing this damage buildup model reproduce the measured depth profiles very well.

Equipment

M. Friedrich
W. Bürger
S. Turuc

Operation and development of the electrostatic accelerators

At the 2 MV VdG a Wennerlunds charging belt has been in operation since 700 hours at a maximum field strength of 1.7 MV/m. The primary electric equipment for the accelerator and for the control system has been comprehensively reconstructed.

The 5 MV tandem has been applied mainly for ion beam analysis. The stripper canal with 6 mm inner diameter was replaced by a canal with 9 mm inner diameter to increase the beam transmission especially for high energy implantation applications. At the Cs sputter ion source all power supplies on 20 kV ion source potential were modernised.

The 3 MV Tandetron has been applied mainly for high-energy implantation and ion beam analysis. Within the dual beamline facility (see separate short contribution) the beamline from the 3 MV Tandetron to the Browne-Buechner-Spectrometer was put into routine operation. A soft-start device for the driver inside the pressure vessel was installed to prevent breaks of the isolating rod between the driver and the generator inside the terminal. Because of a strong lithium contamination inside the injector vacuum chamber a liquid-nitrogen cooled trap was installed between the lithium charge-exchange canal and the high-vacuum pump.

H. Tyrroff
W. Bürger
W. Gläser
F. Herbrand
W. Neumann
B. Richter

The Rossendorf Dual Beam Facility

Multi Beam Facilities open novel approaches to ion beam modification and analysis. The Rossendorf Dual Beam Facility allows to cross the 500 kV Ion Implanter beam and the 3 MV Tandetron Accelerator beam at two target stations. At the double implantation station two different ion species can be implanted simultaneously. This station includes beam sweeping, ion dose and target temperature control during irradiation. At the analysis station both beams are used either for Rutherford Backscattering or for Elastic Recoil Analysis. This station includes a secondary particle Browne-Buechner magnetic spectrometer which can be positioned in front resp. behind the target. The whole facility is ionoptically optimized in respect of beam profil and/or transmission, and it is operated by a PC / PLC network based on the Siemens WinCC code and the Siemens Simatic S7 system. Tests proved well focused beams and high transmission to both target stations for an energy range of 100 keVamu to 100 MeVamu.

Collaboration: Danfysik, National Electrostatic Corporation

R.Grötzschel
F. Herrmann
*R. Jainsch**
Ch. Klein
O. Kruse

A dual-beam facility for in situ high resolution RBS/C and ERDA

A new UHV scattering chamber with an UHV goniometer was installed at one of the beam crossing points of the 3 MV Tandetron and the 500 kV implanter. The beams are crossing at the target plane under an angle of 71° which allows simultaneous irradiation of samples. The UHV goniometer was designed for channeling experiments both in backscattering and transmission geometry. It consists of an X-Y-table (50 mm range each), which is mounted on an high-precision 3-axes rotational stage. A variety of sample holders can be transferred to the goniometer with a load lock system. All axes are driven by stepping motors wich allows the full PC control of the goniometer movements. A modular VisualBasic software package enables automatic crystal orientation, mechanical scanning or batch mode measurement, respectively. RBS and ERDA spectra can be measured both with bakeable Si detectors and with a magnet spectrometer of Browne-Buechner type. This

spectrometer with an radius of 650 mm is arranged with the medium plane in vertical direction. Using a 60 mm long PSD as focal plane detector we achieved with 3 MeV Li ions an energy resolution) E/E of $1.3*10^{-3}$. All the IBA data acquisition is accomplished with commercially available PC-based multichannel dataprocessors, which also can be controlled via Ethernet. Two low-rate e-beam evaporators are used for in-situ deposition of monolayers and thin films. A sputter gun for sample cleaning, a residual gas analyser and a RHEED system are among the auxillary equipment.

supported by BMBF

Collaboration: *FZR, Zentralabteilung Forschungs- und Informationstechnik

J. Teichert
J. von Borany

New low-energy ion implantation chamber

For shallow pn-junction, nanocluster or near surface silicide layer formation low-energy ion implantation becomes more important in microelectronics. Instead of a special low-energy implanter, a more flexible and low cost alternative especially for R&D applications is the use of a medium-energy implanter together with a target camber where the ions are decelerated electrostatically. Such an equipment has been developed for the beamline 2 of the high-current implanter DANFYSIK 1090. In former systems with a simple electrode arrangement the dose inhomogeneity for larger samples was a strong disadvantage. The designed electrostatic lens system in the new system bases on a novel ion optical concept in which the geometrical aberrations are compensated. This guarantees high dose uniformity over large implantation areas at low energy. Implantation can be carried out in the energy range 2 – 30 keV with an dose inhomogeneity < 5% for 125 mm wafers. Accepting smaller implantation areas or higher inhomogeneity, implantation energies down to 200 eV can be used. The energy of 30 keV of the implanter beam allows an optimum operation at high ion current.

Publications

Anwand, W., Brauer, G., Coleman, P.G., Yankov, R.A., Skorupa, W.,
Characterization of vacancy-type defects in Al^+ and N^+ co-implanted SiC by slow positron implantation spectroscopy,
Appl. Surf. Sci. 149 (1999) 140

Anwand, W., Brauer, G., Coleman, P.G., Voelskow, M., Skorupa, W.,
Characterization of defects in ion implanted SiC by slow positron implantation spectroscopy and Rutherford backscattering,
Appl. Surf. Sci. 149 (1999) 148

Assmann, W., Huber, H., Karamian, S.A., Grüner, F., Mieskes, H.D., Andersen, J.U., Posselt, M., Schmidt, B.,
Transverse cooling or heating of channeled ions by electron capture and loss,
Phys. Rev. Lett. 83 (1999) 1759

Barradas, N. P., Jeynes, C., Webb, R. P., Kreissig, U., Grötzschel, R.,
Unambiguous automatic evaluation of multiple Ion Beam Analysis data with Simulated Annealing,
Nucl. Instr. Meth. B149 (1999) 233

Behrisch, R., von der Linden, W., von Toussaint, U., Grambole, D.,
Surface layer destruction during ion beam analysis,
Nucl. Instr. Meth. B155 (1999) 440

Beling, C.D., Fung, S., Li Ming, Gong, M., Panda, B.K.,
A theoretical search for possible high efficiency semiconductor based field assisted positron moderators,
Appl. Surf. Sc. 149 (1999) 253

Belov, A.Yu., Scholz, R., Scheerschmidt, K.,
Dissociation of screw dislocations in (001) low-angle twist boundaries: a source of the 30° partial dislocations in silicon,
Phil. Mag. Lett. 79 (1999) 531

Belov, A.Yu., Scheerschmidt, K.,
Atomic structures of screw dislocation intersections at (001) low-angle twist and shear boundaries in silicon,
Phil. Mag. Lett. 79 (1999) 107

Belov, A.Yu., Scheerschmidt, K., Gösele, U.,
Extended point defect structures at intersections of screw dislocations in Si: a molecular dynamics study,
Phys. Stat. Sol. (a). 171 (1999) 159

Biederman, H., Stundzia, V., Slavinska, D., Zalman, J., Pesicka, J., Vanecek, M., Zemek, J., Fukarek, W.,
Composite germanium/C:H films prepared by unbalanced magnetron sputtering,
Thin Solid Films 351 (1999) 151

Biederman, H., Zalman, J., Slavinska, D., Pesicka, J., Fukarek, W., Kvasnica, S., Olcaytug, F.,
Composite Germanium/hard plasma polymer (C:H) films,
Conf. Proc. ISPC-14, Prague (1999) 1797

Bischoff, L., Hausmann, S., Voelskow, M., Teichert, J.,
Dwell-time dependence of the defect accumulation in focused ion beam synthesis of $CoSi_2$,
Nucl. Instr. Meth. B147 (1999) 327

Borany, J. von, Grötzschel, R., Heinig, K.-H., Markwitz, A., Schmidt, B., Skorupa, W., Thees, H.-J.,
The formation of narrow nanocluster bands in Ge implanted SiO_2 layers,
Solid State Electronics 43 (1999) 1159

Borany, J. von, Heinig, K.-H., Grötzschel, R., Klimenkov, M., Strobel, M., Stegemann, K.-H., Thees, H.-J.,
Ion beam synthesis of narrow Ge nanocluster bands in thin SiO_2 films,
Microelectronic Engineering 48 (1999) 231

Borany, J.v., Heinig, K.-H., Skorupa, W.,
Ion beam synthesis of semiconductor nanoclusters for opto- and microelectronics,
in: Advances in Solid State Physics 39, ed. B. Kramer, Vieweg Verlag Braunschweig, 1999, pp. 171

Borodin, V.A., Heinig, K.-H., Schmidt, B.,
Modeling of Ge nanocluster evolution in ion implanted SiO_2 layers,
Nucl. Instr. Meth. B147 (1999) 286

Brauer, G., Ley, R., Schneider, H., Arnold, W.,
Concept of an intense positron source at the new superconducting LINAC 'ELBE',
in: Proc. 15th Int. Conf. Appl. Accelerators in Research and Industry (CAARI'98), Denton/TX 1998, eds. J.L. Duggan, I.L. Morgan, AIP Conf. Proc. 475, New York/NY, 1999, pp. 369

Deak, L., Bayreuther, G., Bottyan, L., Gerdau, E., Korecki, J., Kornilov, E. I., Lauter, H.J., Leupold, O., Nagy, D.L., Petrenko, A.V., Pasyuk-Lauter, V.V., Reuther, H., Richter, E., Röhloberger, R., Szilagy, E.,
Pure nuclear Bragg reflection of a periodic $^{56}Fe/^{57}Fe$ multilayer,
J. Appl. Phys. 85 (1999) 1

Deshkovskaya, A., Richter, E.,
Einfluß der Ionenimplantation auf die Festigkeit von Quarzglas,
Z. Perspektivische Materialien 6 (1999) 85

Dobler, M., Reuther, H.,
CEMS study of iron disilicide formation by iron ion implantation into silicon,
Nucl. Instr. Meth. B155 (1999) 468

Eichhorn, F., Schell, N., Matz, W., Kögler, R.,
Strain and SiC particle formation in silicon implanted with carbon ions of medium fluence studied by synchrotron x-ray diffraction,
J. Appl. Phys. 86 (1999) 4184

Feudel, T., Strecker, N., Krause, U., Schmidt, Br., Posselt, M.,
Monte Carlo ion-implantation simulation for deep ULSI transistors,
in: Proc. 1999 Semiconductor TCAD Workshop, Hsinchu, Taiwan, May 1999, vol. 2, p. 7.1

Fichtner, P.F.P., Kaschny, J.R., Behar, M., Yankov, R.A., Mücklich, A., Skorupa, W.,
The effects of annealing temperature on the formation of helium filled structures in silicon,
Nucl. Instr. Meth. B148 (1999) 329

Fontaine, F.,
Calculation of the hole concentration in boron-doped diamond,
J. Appl. Phys. 85 (1999) 1409

Fukarek, W., Kaschny, J.R.,
Cavities in helium implanted and annealed silicon characterized by spectroscopic ellipsometry,
J. Appl.Phys. 86 (1999) 4160

Funke, H., Reich, T., Bernhard, G., Brendler, V., Claussner, J., Hüttig, G., Matz, W., Neumann, W., Oehme, W.,
The radiochemistry experimental station at the Rossendorf beamline,
in: Speciation, Techniques and Facilities for Radioactive Materials at Synchrotron Light Source, Grenoble, France, Oct. 4 - 6, 1998, Workshop Proc., Paris: OECD/NEA, 1999, pp. 181-187

Gong, M., Fung, S., Beling, C.D., Brauer, G., Wirth, H., Skorupa, W.,
Gallium implantation induced deep levels in n-type 6H-SiC,
J. Appl. Phys. 85 (1999) 105

Gong, M., Beling, C.D., Fung, S., Brauer, G., Wirth, H., Skorupa, W., You, Z.-P.,
Aluminium and electron-irradiation induced deep levels in n-type and p-type 6H-SiC,
in: Defect and Impurity Engineered Semiconductors II, Mat. Res. Soc. Symp. Proc. Vol. 510, eds. S. Ashok, J. Chevallier, K. Sumino, S. Sopori, W. Goetz ,Mat. Res. Soc., Warrendale/PA, 1999, pp. 455

Gorbunov, A., Brand, K., Geisler, H., Noetzel, J., Wehner, B., Tselev, A., Kharlamov, V., Mai, H., Thomas, J., Lichte, H., Pompe, W., Trushin, J., Wieser, E., Worch, H.,
Non-conventional transition layer formation during PLD of nm-period multilayers,
in: International Workshop on Nondestructive Testing and Computer Simulations in Materials Science and Engineering", Alexander I. Melker, Editor, Proc.SPIE Vol. 3687, (1999) 244

Grambole, D., Herrmann, F., Behrisch, R., Hauffe, W.,
Hydrogen and deuterium depth profiling in divertor tiles of a fusion experiment by micro-ERDA,
Nucl. Instr. Meth. B158 (1999) 647

Grigull, S., Behrisch, R., Parascandola, S.,
Nitrogen implantation into carbon: retention, release and target-erosion processes,
J. Nucl. Mat. 275 (1999) 158

Groß, B., Marion, St., Lind, K., Grambole, D., Herrmann, F., Hempelmann, R.,
Proton conducting $Ba_3Ca_{1.18}Nb_{1.82}O_{8.73}$ -H_2O: pressure - compositions isotherms in terms of Fermi-Dirac-statistics, concentration and fuel-cell measurements, and impedance spectroscopy,
Solid State Ionics 125 (1999) 107

Große, M., Nitzsche, P., Böhmert, J., Brauer, G.,
Investigation of the development of irradiation-induced precipitates in VVER-440 type reactor pressure vessel steels and weld metals after irradiation and annealing,
in: Effects of radiation on materials: 18th Int. Symp., Hyannis/MA 1996, eds. R.K. Nanstad, M.L. Hamilton, F.A. Garner, A.S. Kumar, ASTM STP 1325, West Conshohocken/PA, 1999, pp. 346

Gueorguiev, Y.M., Kögler, R., Peeva, A., Panknin, D., Mücklich, A., Yankov, R.A., Skorupa, W.,
Impurity gettering by high-energy ion implantation in silicon beyond the projected range,
Appl. Phys. Lett. 75 (1999) 3467

Günzel, R., Betzl, M., Alphonsa, I., Ganguly, B., John, P., I., Mukherjee, S.,
Plasma-source ion implantation compared with glow-discharge plasma nitriding of stainless steel,
Surf. Coat. Technol. 112 (1999) 307

Günzel, R.,
An integrated high voltage modulator for plasma immersion ion implantation,
J. Vac. Sci. Technol. B17 (1999) 895

Günzel, R., Richter, E., Uglov, V., V., Khodasevich, A., K., Kuleshov, A., K., Fedotova, J., A., Rusalsky, D., P.,
Plasma immersion ion implantation for improvement of mechanical properties of AISI M2 steel,
J. Vac. Sci. Technol. B17 (1999) 836

Günzel, R., Mändl, S., Richter, E., Liu, A., Tang, B., Y., Chu, P., K.,
Corrosion protection of titanium by deposition of niobium thin films,
Surf. Coat. Technol. 112 (1999) 1107

Hausmann, S., Bischoff, L., Voelskow, M., Teichert, J., Möller, W., Fuhrmann, H.,
Dwell-time effects in focused ion beam synthesis of cobalt disilicide: reflectivity measurements,
Nucl. Instr. Meth. B148 (1999) 610

Hausmann, S., Bischoff, L., Teichert, J., Voelskow, M., Möller, W.,
Single-crystalline $CoSi_2$ layer formation by focused ion beam synthesis,
Jpn. J. Appl. Phys. 38 (1999) 7148

Heera, V., Stoemenos, J., Koegler, R., Voelskow, M., Skorupa, W.,
Crystallization and surface erosion of SiC by ion irradiation at elevated temperatures,
J. Appl. Phys. 85 (1999) 1378

Heera, V., Stoemenos, J., Koegler, R., Voelskow, M., Skorupa, W.,
Crystallization and surface erosion of SiC by ion irradiation at 500°C,
Mat. Sci. Eng. B61-62 (1999) 358

Heinig, K.H., Schmidt, B., Markwitz, A., Grötzschel, R., Strobel, M., Oswald, S.,
Precipitation, ripening and chemical effects during annealing of Ge^+ implanted SiO_2 layers,
Nucl. Instr. Meth. B148 (1999) 969

Heinig, K.-H., Jäger, H.-U.,
Simulations for impurity gettering in silicon by ion implantation induced defects,
in: Proc. First ENDEASD (European Network on Defect Engineering of Advanced Semiconductor Devices) Workshop, C. Claeys, (ed.), Santorini, Greece, April 1999, p. 294

Höfgen, A., Heera, V., Eichhorn, F., Skorupa, W., Möller, W.,
Annealing and recrystallization of amorphous silicon carbide produced by ion implantation,
Mat. Sci. Eng. B61-62 (1999) 353

Hornauer, U., Richter, E., Wieser, E., Möller, W., Schumacher, G., Lang, C., Schütze, M.,
Improvement of the high temperature oxidation resistance of Ti50Al via ion implantation,
Nucl. Instr. Meth. B148 (1999) 858

Jagielski, J., Kopcewicz, M., Turos, A., Eichhorn, F.,
Structural analysis of Si/Fe and Mo/Fe ion-beam mixed layers,
Nucl. Instr. Meth. B148 (1999) 886

Jiang, W., Grötzschel, R., Pilz, W., Schmidt, B., Möller, W.,
Random and channeling stopping powers and charge-state distributions in silicon for 0.2-1.2 MeV/u positive heavy ions,
Phys. Rev. B59 (1999) 226

Knapp, W., Bischoff, L., Teichert, J.,
Electron emission characteristics of solidified gold alloy liquid metal ion sources,
Appl. Surf. Sci. 146 (1999) 134

Kögler, R., Eichhorn, F., Mücklich, A., Danilin, A.B., Skorupa, W.,
Distribution of gettering centres at a buried amorphous layer in silicon,
Nucl. Instr. Meth. B148 (1999) 334

Kögler, R., Peeva, A., Anwand, W., Brauer, G., Skorupa, W., Werner, P., Gösele, U.,
Experimental evidence for interstitial defects away of the projected ion range of high energy ion implanted and annealed silicon,
Appl. Phys. Lett. 75 (1999) 1279

Kögler, R., Yankov, R.A., Posselt, M., Danilin, A.B., Skorupa, W.,
Defects remaining in MeV-ion-implanted and annealed silicon away from the peak of the nuclear energy deposition profile,
Nucl. Instr. Meth. B147 (1999) 96

Kolitsch, A., Wang, X., Manova, D., Fukarek, W., Oswald, S., Möller, W.,
Effects of titanium and aluminum incorporations on the structure of boron nitride films,
Diamond Rel. Mat. 8 (1999) 386

Krieger, K., Maier, H., Grambole, D., Schleussner, D., Franzen, P., and the ASDEX UPGRADE TEAM,
Hydrogen isotope inventories in plasma facing components of ASDEX Upgrade,
IAEA-F1-CN-69/FTP/34

Kulikov D.V., Pezoldt J., Rybin P.V., Skorupa W., Trushin Yu.V.,Yankov R.A.,
Theoretical and experimental studies of (AlN)(1-x)(SiC)(x) layer structures formed by N+ and Al+ co-implantation in 6H-SiC,
SPIE Proc. 3687 (1999) 312

Kuriplach, J., Sob, M., Brauer, G., Nicht, E.-M., Coleman, P.G., Wagner, N.,
Positron affinity in semiconductors: theoretical and experimental studies,
Phys. Rev. B59 (1999) 1948

Mändl, S., Günzel, R., Richter, E., Möller, W.,
Nitrogen and boron implantation into austenitic stainless steel,
J. Vac. Sci. Technol. B17 (1999) 832

Mändl, S., Richter, E., Günzel, R., Möller, W.,
Nitrogen plasma immersion ion implantation into high speed steel,
Nucl. Instr. Meth. B148 (1999) 846

Markwitz, A., Grötzschel, R., Heinig, K.-H., Rebohle, L., Skorupa, W.,
Microstructural investigation of Sn nanoclusters in double-energy implanted and annealed SiO_2 layers with cross-sectional TEM,
Nucl. Instr. Meth. B152 (1999) 319

Markwitz, A., Rebohle, L., Hofmeister, H., Skorupa, W.,
Homogeneously size distributed Ge nanoclusters embedded in SiO_2 layers produced by ion beam physics,
Nucl. Instr. Meth. B147 (1999) 361

Martin, J., Wannemacher, R., Teichert, J., Bischoff, L., Köhler, B.,
Generation and detection of fluorescent color centers in diamond with submicron resolution,
Appl. Phys. Lett. 75 (1999) 3096

Maser, K., Mohr, U., Leihkauf, R., Ecker, K., Beck, U., Grambole, D., Grötzschel, R., Herrmann, F., Krauser, J., Weidinger, A.,
Hydrogen migration in wet-thermally grown silicon dioxide layers due to high dose ^{15}N ion beam irradiation,
Microel. Eng. 48 (1999) 139

Matz, W.,
Introduction to x-ray diffraction at synchrotron light sources,
in: Speciation, Techniques and Facilities for Radioactive Materials at Synchrotron Light Source, Grenoble, France, Oct. 4 - 6, 1998, Workshop Proc., Paris: OECD/NEA, 1999, pp. 39-48

Matz, W., Schell, N., Bernhard, G., Prokert, F., Reich, T., Claußner, J., Oehme, W., Schlenk, R., Dienel, S., Funke, H., Eichhorn, F., Betzl, M., Pröhl, D., Strauch, U., Hüttig, G., Krug, H., Neumann, W., Brendler, V., Reichel, P., Denecke, M.A., Nitsche, H.,
ROBL - a CRG beamline for radiochemistry and materials research at the ESRF,
J. Synchr. Rad. 6 (1999) 1076

Misiuk, A., Surma, B., Rebohle, L., Jun, J., Antonova, I.V., Tyschenko, I.E., Romano-Rodriguez, A., Lopez, M.,
Luminescence properties of oxygen-containing silicon annealed at enhanced argon pressure,
phys. stat. sol. (b) 211 (1999) 233

Moebius, A., Frenzel, C., Thielsch, R., Rosenbaum, R., Adkins, C. J., Schreiber, M., Bauer, H.-D., Grötzschel, R., Hoffmann, V., Krieg, T., Matz, N., Vinzelberg, H., Witcomb, M.,
The metal-insulator transition in amorphous Si1-xNix:So, was Mott right after all?,
in: Proc. 24th Int. Conf. on the Physics of Semiconductors, Jerusalem/Israel, 2.-7.8.98, World Scientific, Singapore, CDII.D.4 (1999)

Moebius, A., Frenzel, C., Thielsch, R., Rosenbaum, R., Adkins, C. J., Schreiber, M., Bauer, H.-D., Grötzschel, R., Hoffmann, V., Krieg, T., Matz, N., Vinzelberg, H., Witcomb, M.,
Metal-insulator transition in amorphous Si1-xNix:Evidence for Mott's minimum metallic conductivity,
Physical Review B60 (1999) 14209

Möller, W., Parascandola, S., Kruse, O., Günzel, R., Richter, E.,
Plasma-immersion ion implantation for diffusive treatment,
Surf. Coat. Technol. 116-119 (1999) 1

Mrotchek, I., Günzel, R., Matz, W., Möller, W., Anishchik, V.,
Implantation of boron ions into hard metals,
Nucleonika 44 (1999) 217

Nancheva, N., Docheva, P., Anwand, W., Brauer, G., Coleman, P.G.,
Magnetron sputtered SnO_x films on tin probed by slow positron implantation spectroscopy,
Acta Phys. Polonica A95 (1999) 623

Narojczyk, J., Piekoszewski, J., Richter, E., Werner, Z.,
Wear properties of tin coated cutting tools implanted with nitrogen ions,
Nukleonika 41 (1999) 225

Noetzel, J., Brand, K., Geisler, H., Gorbunov, A., Tselev, A., Wieser, E., Möller, W.,
Structural investigations on laser deposited Fe/Al multilayers,
Appl. Phys. A68 (1999) 497

Noetzel, J., Handstein, A., Mücklich, A., Prokert, F., Reuther, H., Thomas, J., Wieser, E., Möller, W.,
Co/Cu solid solution prepared by ion implantation,
J. of Magnetism and Magnetic Materials 205 (1999) 177

Oswald, S., Wirth, H.,
Core-level shifts at B-and Al-doped 6H-SiC studied by XPS,
Surf. Interf. Anal. 27 (1999) 136

Panda, B.K., Brauer, G.,
Positron affinities and deformation potentials in cubic semiconductors,
Acta Phys. Polonica A 95 (1999) 641

Panknin, D., Wirth, H., Mücklich, A., Skorupa, W.,
Correlation of electrical and microstructural properties after high dose aluminium implantation into 6H-SiC,
Mat. Sci. Eng. B 56 (1999) 351

Parascandola, S., Kruse, O., Richter, E., Möller, W.,
Time - and depth-resolved characterization of the near surface composition during the ion nitriding process,
J. Vac. Sci. Technol. B17 (1999) 855

Parascandola, S., Kruse, O., Möller, W.,
The interplay of sputtering and oxidation during plasma diffusion treatment,
Appl. Phys. Lett. 75 (1999) 1851

Peeva, A., Kögler, R., Brauer, G., Skorupa, W., Werner, P.,
Metallic impurity gettering to defects remaining in the $R_P/2$ region of MeV-ion implanted and annealed silicon,
Proc. 1st ENDEASD (European Network on Defect Engineering of Advanced Semiconductor Devices)-Workshop, ed. C. Claeys, IMEC Leuven, Santorini, Greece, April 1999, p. 269

Pezoldt, J., Yankov, R.A., Mücklich, A., Fukarek, W., Voelskow, M., Reuther, H., Skorupa, W.,
A novel $(SiC)_{1-x}(AlN)_x$ compound synthesized using ion beams,
Nucl. Instr. Meth. B147 (1999) 273

Pezoldt, J., Yankov, R.A., Werninghaus, T., Zahn, D.R.T., Fukarek, W., Teichert, G., Luebbe, M., Skorupa, W.,
Structural and compositional characterization of 6H-SiC implanted with N^+ and Al^+ ions using optical methods,
Diamond Rel. Mat. 8 (1999) 346

Piekoszewski, J., Werner, Z., Wieser, E., Langner, J., Grötzschel, R., Reuther, H., Jagielski, J.,
Formation of surface Pd-Ti alloys using pulsed plasma beams,
Nukleonika 44 (1999) 225

Piekoszewski, J., Wieser, E., Grötzschel, R., Reuther, H., Werner, Z., Langner, J.,
Pulsed plasma beam mixing of Ti and Mo into Al_2O_3 substrates,
Nucl. Instr. Meth. B148 (1999) 32

Posselt, M.,
Prediction of the morphology of the as-implanted damage in silicon using a novel combination of BCA and MD simulations,
in: Proc. First ENDEASD (European Network on Defect Engineering of Advanced Semiconductor Devices) Workshop, C. Claeys (ed.), Santorini, Greece, April 1999, p. 308

Posselt, M.,
A novel method to investigate ion-beam-induced defect evolution in Si,
in: Process Physics and Modeling in Semiconductor Technology, C.S. Murthy, G.R. Srinivasan, and S.T. Dunham (eds.), The Electrochemical Society, Inc., Proceedings Series, Pennington, NJ, USA, (1999) PV 99-2, p. 58

Rebohle, L., von Borany, J., Skorupa, W., Tyschenko, I.E., Fröb, H.,
Photoluminescence and electroluminescence investigations at Ge-rich SiO_2 layers,
J. of Luminesc. 80 (1999) 275

Rebohle, L., Tyschenko, I.E., von Borany, J., Skorupa, W., Fröb, H.,
Strong violet light emission from Ge^+-implanted SiO_2 layers,
SPIE Proc. 3630 (1999) 155

Romanov, S.I., Dvurechenskii, A.V., Yakovlev, Yu.I., Grötzschel, R., Kreissig, U., Kirienko, V.V., Obodnikov, V.I., Gutakovskii, A.,
Characterization of porous silicon layers containing a buried oxid layer,
NATO ASI Series 3 , ed. P. Hemment , 1999

Rybin, P.V., Kulikov, D.V., Trushin, Y.V., Yankov, R.A., Ecke, G., Fukarek, W., Skorupa, W., Pezoldt, J.,
Modelling high-temperature co-implantation of N^+ and Al^+ ions in silicon carbide: the effect of stress on the implant and damage distributions,
Nucl. Instr. Meth. B147 (1999) 279

Sass, J., Mazur, K., Gladki, A., Turos, A., Eichhorn, F.,
Reciprocal space mapping and reflectivity investigations of epi-ready InP substrate,
Phys. Stat. Sol. (a) 171 (1999) 395

Schumacher, G., Lang, C., Schütze, M., Hornauer, U., Richter, E., Wieser, E., Möller, W.,
Improvement of the oxidation resistance of γ- titanium aluminides by microalloying with chlorine using ion implantation,
Mat. Corr. 50 (1999) 162

Schumacher, G., Dettenwanger, F., Schütze, M., Hornauer, U., Richter, E., Wieser, E., Möller, W.,
Microalloying effects in the oxidation of TiAl materials,
Intermetallics 7 (1999) 1113

Sendezera, E.J., Davidson, A.T., Fischer, C.G., Connell, S.H., Sellschop, J.P.F., Anwand, W., Brauer, G., Nicht, E.-M.,
Characterisation of Al^+-implanted LiF by a monoenergetic positron beam,
Appl. Surf. Sci. 149 (1999) 125

Serre, C., Romano-Rodriguez, A., Perez-Rodriguez, A., Morante, J.R., Fonseca, L., Acero, M.C., Kögler, R., Skorupa, W.,
Beta-SiC on SiO_2 formed by ion implantation and bonding for micromechanical applications,
Sensors and Actuators A74 (1999) 169

Serre, C., Perez-Rodriguez, A., Romano-Rodriguez, A., Morante, J.R., Fonseca, L., Acero, M.C., Esteve, J., Kögler, R., Skorupa, W.,
Bonding and etch-back of ion beam synthesized beta-SiC for SiCOI formation,
In "Perspectives, Science and Technologies for Novel Silicon on Insulator Devices", Proc. NATO Advanced Research Workshops, P.L.F. Hemment (Editor), Kluwer Academic Publ. B.V., Dordrecht, The Netherlands, 1999, p. 342

Smirnov, V.K., Kibalov, D.S., Krivelevich, S.A., Lepshin, P.A., Potapov, E.V., Yankov, R.A., Skorupa, W., Makarov, V.V., Danilin, A.B.,
Wave-ordered structures formed on SOI wafers by reactive ion beams,
Nucl. Instr. Meth. B147 (1999) 310

Stoemenos, J., Pécz, B., Heera, V.,
Epitaxial aluminium carbide formation in 6H-SiC by high-dose Al^+ implantation,
Appl. Phys. Lett. 74 (1999) 2602

Strobel, M., Heinig, K.-H., Möller, W., Meldrum, A., Zhou, D.S., White, C.W., Zuhr, R.A.,
Ion beam synthesis of gold nanoclusters in SiO_2: Computer simulations versus experiments,
Nucl. Instr. Meth. B147 (1999) 343

Strobel, M., Heinig, K.-H., Möller, W.,
Can core/shell nanocrystals be formed by sequential ion implantation? Predictions from kinetic lattice Monte Carlo simulations,
Nucl. Instr. Meth. B148 (1999) 104

Teichert, G., Schleicher, L., Knedlik, Ch., Voelskow, M., Skorupa, W., Yankov, R.A., Pezoldt, J.,
Thermal wave analysis: a tool for non-invasive testing ion beam synthesis of wide band gap materials,
Mat. Res. Soc. Symp. Proc. 540 (1999) 103

Thiele, E., Hecker, M., Schell, N.,
Change of internal strains in ultrafine-grained nickel due to cyclic plastic deformation,
Mat. Sci. Forum 321-324 (1999) 598

Thompson,G.E., Skeldon, P.,Wood, G.C., Zhou, X., Kreissig, U.,Wieser, E., Habazaki, H., Shimizu, K.,
Elastic Recoil Detection Analysis (ERDA), RBS and TEM study of barrier film formation on Al-4.5at.%Mg-0.05at.%Cu alloy,
Surf. Interf. Anal. 27 (1999) 57

Turos, A., Gawlik, G., Jagielski, J., Stonert, A., Matz, W., Grötzschel, R.,
Ion beam mixing of the ZrO_2/Fe system,
Nucl. Instr. Meth. B148 (1999) 778

Tyschenko, I.E., Volodin, V. A., Rebohle, L., Voelskow, M., Skorupa, W.,
Photoljumineszenzia pljonok Si_3N_4 implantyrovanych ionami Ge^+ i Ar^+,
Fisika i technika poluprovodnikov 33 (1999) 559

Tyschenko, I.E., Rebohle, L., Yankov, R.A., Skorupa, W., Misiuk, A., Kachurin, G.A.,
The effect of annealing under hydrostatic pressure on the visible photoluminescence from Si^+-ion implanted SiO_2 films,
J. of Luminesc. 80 (1999) 229

Ueda, M., Berni, L.A., Gomes, G.F., Beloto, A.F., Abramof, E., Reuther, H.,
Application of a DC glow discharge source with cotrolled plasma potential in plasma immersion ion implantation,
J. Appl. Phys. 86 (1999) 4821

Uglov, V.V., Khodasevich, V.V., Kuleshov, A.K., Fedotova, J.A., Rusalsky, D.P., Günzel, R., Richter, E.,
Plasma immersion ion implantation for improvement of mechanical porperties of AISI M2 steel,
J. Vac. Sci. Technol. B17 (1999) 836

Uglov, V.V., Kholmetskii, A.L., Kuleshov, A.K., Fedotova, J.A., Rusalsky, D.P., Kohodasevich, V.V., Rübenbauer, K., Richter, E., Günzel, R., Parascandola, S.,
CEMS-investigations of AISI M2 steel after nitrogen plasma immersion ion implantation,
Nucl. Instr. Meth. B148 (1999) 841

Waidmann, S., Bartsch, K., Endler, I., Fontaine, F., Arnold, B., Knupfer, M., Leonhardt, A., Fink, J.,
Electron energy-loss spectroscopy in transmission of undoped and doped diamond films,
Carbon 37 (1999) 823

Walter, T., Dörr, K., Müller, K.-H., Holzapfel, B., Eckert, D.,Wolf, M., Schläfer, D., Schultz, L., Grötzschel, R.,
Low-field magnetoresistance of $La_{0.7}Sr_{0.3}MnO_3$ thin films with gradually changed texture,
Appl. Phys. Lett. 74 (1999) 2218

Weber, R., Skorupa, W.,
Precipitation kinetics in formation of SiO_2 layers: The role of spatial correlation functions,
Proc. of the 9. Int. Symp. On Silicon-on-Insulator Technology and Devices, P.L.F.Hemment,
S.Cristoloveanu, T.W.Houston, K.Izumi, H.Hovel (eds.) Electrochem. Soc. Proc. 99-3 (1999) 149

Wieser, E., Tsyganov, I., Matz, W., Reuther, H., Oswald, S., Pham, T., Richter, E.,
Modification of titanium by ion implantation of calcium and/or phosphorus,
Surf. Coat. Technol. 111 (1999) 103

Wirth, H., Panknin, D., Skorupa, W., Niemann, E.,
Efficient p-type doping of 6H-SiC: Flash lamp annealing after aluminium implantation,
Appl. Phys. Lett. 74 (1999) 979

Yankov, R.A., Skorupa, W.,
„Comment on ´Gettering of Cu by He-induced cavities in SIMOX materials`"
Nucl. Instr. Meth. B149 (1999) 445

Zaitsev, M.A., Denisenko, A.V., Kosaca, G., Job, R., Fahrner, W.R., Melnikov, V.S., Varichenko, S.,
Buchard, B., Borany, J. von, Werner, M.,
Electronic devices on ion implanted diamond (Review),
J. of Wide Bandgap Materials 7 (1999) 4

Zuhr, R.A., Budai, J.D., Datskos, P.G., Meldrum, A., Thomas, K.A., Warmack, R.J., White, C.W.,
Feldman, L.C., Strobel, M., Heinig, K.-H.,
Nanostructured arrays formed by finely focused ion beams,
Mat. Res. Soc. Symp. Proc. 536 (1999) 251

Conference Contributions

Abramof, E., Beloto, A.F., Ueda, M., Gomes, G.F., Berni, L.A., Reuther, H.,
Analysis of X-ray rocking curves in (001) silicon crystals implanted with nitrogen by plasma immersion ion implantation,
IBA-14/ECAART-6, Dresden, Germany, July 26 - 30, 1999

Antons, A., Klinkhammer, F., Kappius, L., Heinig, K.H., Trinkaus, H., Mantl, S.,
Strukturierung von epitaktischen $CoSi_2$/Si-Heterostrukturen durch lokale Oxidation,
DPG-Frühjahrstagung des AK Festkörperphysik, Münster, March 22-26, 1999

Assmann, W., Huber, H., Karamian, S.A., Andersen, J.U., Posselt, M.,
Transverse cooling or heating of channeled ions by electron capture and loss,
8th Int. Conf. on Atomic Collisions in Solids (ICACS18), Odense, Denmark, August 3-8, 1999

Barradas, N.P., Khan, R.U.A., Anguita, J.V., Silva, S.R.P., Kreissig, U., Grötzschel, R.,
Growth and characterization of amorphous carbon films doped with nitrogen,
IBA-14/ECAART-6, Dresden, Germany, July 26-30, 1999

Barradas, N.P., Parascandola, S., Sealy, B.J., Grötzschel, R., Kreissig, U.,
Simultaneous and consistent analysis of NRA, RBS, and ERDA data with the IBA Datafurnace,
IBA-14/ECAART-6, Dresden, Germany, July 26 - 30, 1999

Belko, V., Chagarov, E., Posselt, M.,
Classical MD simulations of atomic displacements in 4H-, 6H-, and 3C-SiC,
E-MRS 1999 Spring Meeting, Strasbourg, France, June 1-4, 1999

Weber, R., Skorupa, W.,
Precipitation kinetics in formation of SiO_2 layers: The role of spatial correlation functions,
Proc. of the 9. Int. Symp. On Silicon-on-Insulator Technology and Devices, P.L.F.Hemment,
S.Cristoloveanu, T.W.Houston, K.Izumi, H.Hovel (eds.) Electrochem. Soc. Proc. 99-3 (1999) 149

Wieser, E., Tsyganov, I., Matz, W., Reuther, H., Oswald, S., Pham, T., Richter, E.,
Modification of titanium by ion implantation of calcium and/or phosphorus,
Surf. Coat. Technol. 111 (1999) 103

Wirth, H., Panknin, D., Skorupa, W., Niemann, E.,
Efficient p-type doping of 6H-SiC: Flash lamp annealing after aluminium implantation,
Appl. Phys. Lett. 74 (1999) 979

Yankov, R.A., Skorupa, W.,
„Comment on ´Gettering of Cu by He-induced cavities in SIMOX materials`"
Nucl. Instr. Meth. B149 (1999) 445

Zaitsev, M.A., Denisenko, A.V., Kosaca, G., Job, R., Fahrner, W.R., Melnikov, V.S., Varichenko, S.,
Buchard, B., Borany, J. von, Werner, M.,
Electronic devices on ion implanted diamond (Review),
J. of Wide Bandgap Materials 7 (1999) 4

Zuhr, R.A., Budai, J.D., Datskos, P.G., Meldrum, A., Thomas, K.A., Warmack, R.J., White, C.W.,
Feldman, L.C., Strobel, M., Heinig, K.-H.,
Nanostructured arrays formed by finely focused ion beams,
Mat. Res. Soc. Symp. Proc. 536 (1999) 251

Conference Contributions

Abramof, E., Beloto, A.F., Ueda, M., Gomes, G.F., Berni, L.A., Reuther, H.,
Analysis of X-ray rocking curves in (001) silicon crystals implanted with nitrogen by plasma immersion ion implantation,
IBA-14/ECAART-6, Dresden, Germany, July 26 - 30, 1999

Antons, A., Klinkhammer, F., Kappius, L., Heinig, K.H., Trinkaus, H., Mantl, S.,
Strukturierung von epitaktischen $CoSi_2$/Si-Heterostrukturen durch lokale Oxidation,
DPG-Frühjahrstagung des AK Festkörperphysik, Münster, March 22-26, 1999

Assmann, W., Huber, H., Karamian, S.A., Andersen, J.U., Posselt, M.,
Transverse cooling or heating of channeled ions by electron capture and loss,
8th Int. Conf. on Atomic Collisions in Solids (ICACS18), Odense, Denmark, August 3-8, 1999

Barradas, N.P., Khan, R.U.A., Anguita, J.V., Silva, S.R.P., Kreissig, U., Grötzschel, R.,
Growth and characterization of amorphous carbon films doped with nitrogen,
IBA-14/ECAART-6, Dresden, Germany, July 26-30, 1999

Barradas, N.P., Parascandola, S., Sealy, B.J., Grötzschel, R., Kreissig, U.,
Simultaneous and consistent analysis of NRA, RBS, and ERDA data with the IBA Datafurnace,
IBA-14/ECAART-6, Dresden, Germany, July 26 - 30, 1999

Belko, V., Chagarov, E., Posselt, M.,
Classical MD simulations of atomic displacements in 4H-, 6H-, and 3C-SiC,
E-MRS 1999 Spring Meeting, Strasbourg, France, June 1-4, 1999

Belov, A.Yu.,
Dissociation of screw dislocation in Si (001) low-angle twist boundaries: Atomistic simulation and experiment. - Multiscale phenomena in plasticity: from experiments to phenomenology, modelling and materials engineering,
NATO ASI Conference, Ouranopolis, Greece, September 8-19, 1999

Berberich, F., Matz, W., Richter, E., Schell, N., Kreißig, U., Möller,W.,
Structural mechanisms of the mechanical degradation of Ti-Al-V alloys: in situ study during annealing
SMMIB'99, Beijing, P.R. China, Sept. 19 - 24, 1999,
Symp. 25 Jahre Strukturforschung, Munich, Germany, Nov. 12 - 13, 1999

Bischoff, L., Teichert, J., Ganetsos Th., Mair, G.L.R.,
Temperature dependence of the electric characteristics of liquid metal alloy ion sources,
12th Int. Vacuum Microelectronics Conf., IVMC `99, Darmstadt, Germany, July 6-9, 1999

Bischoff, L., Teichert, J., Hausmann, S., Ganetsos Th., Mair, G.L.R.,
Investigation and optimization of the emission parameters of alloy liquid metal ion sources,
IBA-14/ECAART-6, Dresden, Germany, July 26-30, 1999

Bischoff, L., Ganetsos, T., Teichert, J., Mair, G. L. R.,
Temperature dependence of emission spectra of liquid metal alloy ion sources,
ICACS-18, Int. Conf. on Atomic Collisions in Solids, Odense, Denmark, August 3-8, 1999

Bischoff, L., Ganetsos, T., Teichert, J., Mair, G. L. R.,
$Si_{1-x}Ge_x$ microstructures by maskless ion implantation,
ICACS-18, Int. Conf. on Atomic Collisions in Solids, Odense, Denmark, August 3-8, 1999

Bischoff, L., Teichert, J., Hausmann, S., Ganetsos, T., Mair, G. L. R.,
Temperature and energy spread investigations of alloy LMIS,
Int. Conf. Micro- and Nano-Engineering 99, Rome, Italy, September 21- 23, 1999

Borany, J. von,
Ionenstrahlsynthese von Halbleiter-Nanoclustern für neue mikro- und optoelektronische Anwendungen (Hauptvortrag),
DPG-Frühjahrtagung, Münster, Germany, March 22 – 26, 1999

Borany, J. von, Heinig, K.H., Grötzschel, R., Klimenkov, M., Strobel, M., Stegemann, K.-H., Thees, H.-J.,
Ion beam synthesis of narrow Ge nanocluster bands in thin SiO_2-Layers,
Infos 99, Kloster Banz, Germany, June 16 - 19, 1999

Borany, J.von, Heinig, K.H., Skorupa, W., (invited)
Ionenstrahlsynthese von Halbleiter-Nanoclustern für neue mikro- und optoelektronische Anwendungen,
DPG-Frühjahrstagung des AK Festkörperphysik, Münster, March 22-26, 1999

Borany, J. von, Rebohle, L., Skorupa, W., Heinig, K.-H., (invited)
Blue light emission from ion beam synthesized semiconductor nanoclusters in SiO_2 films,
25th Annual Conf. of the IEEE Industrial Electronics Society, IECON 99, San Jose, USA,
Nov. 29 - Dec. 4, 1999

Brauer, G., (invited)
Plans for the assembly, construction and use of an intense positron source at ELBE,
Workshop "Positron source at TESLA Test Facility", DESY/Hamburg, Sept. 1 – 3, 1999

Brauer, G., Anwand, W., Yankov, R.A., Skorupa, W., Coleman, P.G.,
Vacancy-type defects in 6H-SiC caused by Al^+ and N^+ co-implantation and their annealing behaviour,
1999 Centennial Meeting, American Physical Society, Atlanta/GA, March 20-26, 1999

Conrad, D., Scheerschmidt, K., Belov, A., Timpel, D.,
Enhanced semiempirical potentials in molecular dynamics simulations of wafer bonding,
E-MRS 1999 Spring Meeting, Strasbourg, France, June 1-4, 1999

Deshkovskaya, A.A., Shuchukarev, A.V., Richter, E.,
On a chemical nature of fluorine implantation-induced centres in quartz glass,
Radiation effects in insulators, Jena, Germany, July 18 – 23, 1999

Dobler, M., Reuther, H., Mücklich, A.,
Ion beam induced epitaxial crystallization of iron disilicides studied by conversion electron Mössbauer spectroscopy,
Int. Conf. Applications Mössbauer Effect, Garmisch-Partenkirchen, Aug. 29 - Sept. 3, 1999

Eichhorn, F., Matz, W., Prokert, F., Betzl, M., Reichel, P., Schell, N.,
Thin layer studies at the material research goniometer of the ROBL-CRG beamline (ESRF Grenoble),
4th Autumn School on ”X-ray scattering from surfaces and thin layers” Smolenice, Slovakia,
Sept. 22 - 25, 1999

Feudel, T., Strecker, N., Krause, U., Schmidt, Br., Posselt, M.,
Monte Carlo ion-implantation simulation for deep ULSI transistors,
1999 Semiconductor TCAD Workshop, Hsinchu, Taiwan, May 4-6, 1999

Fichtner, P.F.P., Peeva, A., Behar, M., Kaschny, J., Koegler, R., Skorupa, W.,
He induced cavity formation in silicon upon high temperature implantation,
IBA-14/ECAART-6, Dresden, Germany, July 26-30, 1999

Fitting, H.J., Barfels, T., Trukhin, A.N., Schmidt, B.,
Cathodoluminescence of silica, SiO_2:Ge, and GeO_2,
IXth Int. Conf. on the Physics of Non-Crystalline Solids, Tucson, USA, Oct. 17-21, 1999

Fitz, C., Fukarek, W., Kolitsch, A., Möller, W.,
Investigation on stress evolution in boron nitride Films,
SMMIB, Beijing, China, Sept 19-24, 1999

Fitz, C., Fukarek, W., Kolitsch, A., Möller, W.,
An instrument for in-situ stress measurement in thin films during growth,
SMMIB, Beijing, China, 19-24 Sept, 1999

Fontaine, F.,
Holes in boron-doped diamond: comparison between experiment and an improved model,
10th Europ. Conf. on Diamond, Diamond-like Materials, Carbon Nanotubes, Nitrides and Silicon Carbide, Prague, CZ, Sept. 12-17, 1999

Friedrich, M., Pilz, W., Sun, G., Behrisch, R., García-Rosales, C., Bekris, N., Penzhorn, R.-D.,
Tritium depth profiling in carbon by accelerator mass spectrometry,
IBA-14/ECAART-6, Dresden, Germany, July 26-30, 1999

Friedrich, M., Pilz, W., Sun, G., Behrisch, R., García-Rosales, C., Bekris, N., Penzhorn, R.-D.,
Tritium depth profiling in carbon samples from fusion experiments,
AMS-8, Vienna, Sept. 6-10, 1999

Fukarek, W.,
Optische real-time-, in-situ-Diagnostik bei der Dünnschichtabscheidung,
DPG Frühjahrstagung, Münster, Germany, March 22-26, 1999

Fukarek, W.,
In-situ measurement of stress during deposition of boron nitride films,
5th Europ. Conf. on Residual Stresses, Delft-Noordwijkerhout, Sept. 28-30, 1999

Fukarek, W., Fitz, C., Möller, W.,
In situ Messung mechanischer Spannungen in dünnen Schichten während der Abscheidung,
DPG Frühjahrstagung, Münster, Germany, March 22-26, 1999

Fukarek, W., Fitz, C., Kolitsch, A., Möller, W.,
Investigation on growth of BN films by simultaneous in situ stress measurement and ellipsometry,
10th Europ. Conf. on Diamond, Diamond-Like Materials, Carbon Nanotubes, Nitrides and Silicon Carbide, Prague, CZ, Sept. 12-17, 1999

Ganetsos, T., Bischoff, L., Teichert, J., Mair, G.L.R.,
A study of Liquid Metal Alloy Ion Sources for the production of ions of interest in the microelectronics industry,
EuroFE '99, Toledo, Spain, November 15 – 19, 1999

Gebel, T., Panknin, D., Riehn, R., Parascandola, S., Skorupa, W.,
Application and improvement of the spreading resistance method for p-type 6H-SiC,
8th Int. Conf. on Silicon Carbide and Related Materials (ICSCRM 99), Research Triangle Park, NC, USA, Oct. 10-15, 1999

Gebel, T., Borany, J.von., Skorupa, W., Möller, W., Thees, H.-J., Wittmaack, M., Stegemann, K.-H.,
Non-volatile memory effects of ion-beam synthesized Ge and Si nanoclusters: Electrical properties vs. microstructure,
MRS Fall Meeting, Boston, USA, Nov.29 - Dec.3, 1999

Gorbunov, A., Tselev, A., Brand, K., Gawlitza, P., Geisler, H., Meyer, D.C., Noetzel, J., Mai, H., Paufler, P., Pompe, W., Wieser, E.,
Thin film multilayers and mixtures synthesized by PLD,
5th. Int. Conf. on Laser Ablation, Göttingen, Germany, July 19-23, 1999

Grambole, D., Neelmeijer, C., Noll, K., Herrmann, F.,
$^{19}F(p,p'\gamma)^{19}F$ and $^{18}O(p,\gamma)^{19}F$ γ-ray interference studied on liquids by external PIGE,
IBA-14/ECAART-6, Dresden, Germany, July 26-30, 1999

Grötzschel, R., Herrmann, F., Jainsch, R., Klein, C., Kruse, O., Tyrroff, H.,
The Rossendorf Dual-beam facility for RBS/channeling and ERDA,
IBA-14/ECAART-6, Dresden, Germany, July 26-30, 1999

Günzel, R., Richter, E., Möller, W., Brusky, U., Spies, H.-J., Rammelt, U., Plieht, W.,
Randaufsticken von Edelstahl ohne Korrosionsverluste,
50. Berg- und Hüttenmännischer Tag, Freiberg, Germany, June 16 – 18, 1999

Günzel, R., Hornauer, U., Rogozin, A., I., Astrelin, V., T.,
Basic investigations of an integrated modulator for plasma immersion ion implantation,
PBII Workshop, Kyoto, Japan, Dec. 13 - 16, 1999

Hauschild, T., Heinig, K.-H., Jentschel, M., Börner, H.,
Potential investigation for ZnS using Crystal-GRID high-precision gamma-spectroscopy and MD computer simulations,
DPG-Frühjahrstagung, Münster, Germany, March 22-26, 1999

Hauschild, T., Jentschel, M., Heinig, K.-H., Börner, H. G., Möller, W.,
Crystal-GRID: Investigation of interatomic solid state potentials,
HERCULES (Higher European Research Course for Users of Large Experimental Systems),
Grenoble, France, March, 1999

Hauschild, T., Heinig, K.-H., Jentschel, M., Börner, H.G., Möller, W.,
Crystal-GRID: Study of orientation-dependent slowing-down in single-crystalline ZnS,
IBA-14/ECAART-6, Dresden, Germany, July 26-30, 1999

Hauschild, T., Heinig, K.-H., Jentschel, M., Börner, H.G., Möller, W.,
Crystal-GRID: Study of orientation-dependent slowing-down in single-crystalline ZnS,
8th Int. Conf. on Atomic Collisions in Solids (ICACS18), Odense, Denmark, August 3-8, 1999

Hausmann, S., Teichert, J., Bischoff, L., Voelskow, M., Möller, W., Hobert, H., Fuhrmann, H.,
Strahlenschäden in Silicium durch fokussierte Ionenstrahlen,
DPG-Frühjahrstagung, Münster, Germany, March 22-26, 1999

Hausmann, S., Teichert, J., Bischoff, L., Voelskow, M., Möller, W.,
Radiation damage in focused ion beam implantation,
Int. Microprocesses and Nanotechnology Conf., Yokohama, Japan, July 6-8, 1999

Hecker, M., Tietjen, D., Schell, N., Prokert, F.,
Untersuchungen mittels Röntgenreflektometrie und -beugung an Co/Cu/NiFe-Vielfachschichten,
10. Tagung Festkörperanalytik, Wien, Austria, July 5 - 7, 1999

Heinig, K.-H. (invited),
Ion beam induced nanocrystals - an introduction to nanocrystal session,
Gordon Research Conference on Materials Processes Far From Equilibrium, Plymouth, NH, USA,
July 11-16, 1999

Heinig, K.-H., Borany, J. v., Schmidt, B., Klimenkov, M.,
Formation of semiconductor quantum dots in thin SiO_2 layers by ion beam synthesis,
MRS 1999 Fall Meeting, Boston, USA, Nov.29 - Dec.3, 1999

Heinig, K.-H., Jäger, H.-U.,
Simulations for impurity gettering in silicon by ion implantation induced defects,
First ENDEASD (European Network on Defect Engineering of Advanced Semiconductor Devices)
Workshop, Santorini, Greece, April 21-22, 1999

Heinig, K.-H, Jäger, H.-U.,
Modeling of impurity gettering in silicon by ion implantation induced defects,
E-MRS Spring Meeting, Strasbourg, France, June 1-4, 1999

Heinig, K.-H., Jäger, H.-U.,
Computer simulation of defect evolution during high-energy ion implantation and subsequent annealing,
IUMRS-ICAM99 Conference, Beijing, China, June 13-18, 1999

Heinig, K.-H., Ruault, M.O., Strobel, M., Bernas, H.,
Nanocrystal formation by ion beam synthesis: *in-beam* TEM observation and modeling,
E-MRS Spring Meeting, Strasbourg, France, June 1-4, 1999

Heinig, K.-H., Schmidt, B., Markwitz, M., Strobel, M., Borany, J.v., Klimenkov, M.,
Formation of d-layers of Ge nanocrystals in SiO_2,
E-MRS Spring Meeting, Strasbourg, France, June 1-4, 1999

Heinig, K.-H., Strobel, M.,
Multiscale modeling of nucleation and growth of nanocrystals,
IUMRS-ICAM99 Conference, Beijing, China, June 13-18, 1999

Hempel, A., Hasegawa, M., Brauer, G., Plazaola, F., Saneyasu, M.,
Positron lifetime and micro-Vickers hardness measurements on neutron irradiated Fe-Cu model alloys,
Annual Meeting of the South African Institute of Physics (SAIP99), Port Elizabeth, July 6 – 9, 1999

Hempel, A., Hasegawa, M., Brauer, G., Plazaola, F., Saneyasu, M., Tang, Z.,
Effects of neutron irradiation on positron lifetime and micro-Vickers hardness of Fe-Cu model alloys and reactor pressure vessel steel,
9th Int. Conf. on Environmental Degradation of Materials in Nuclear Power Systems-Water Reactors,
Newport Beach /CA, Aug. 1-5, 1999

Höfgen, A., Heera,V., Mücklich, A., Eichhorn, F., Skorupa, W.,
Ion beam induced crystal grain nucleation in amorphous silicon carbide,
IBA-14/ECAART-6, Dresden, Germany, July 26-30, 1999

Höfgen, A., Heera, V., Mücklich, A. Skorupa, W.,
Ion beam induced nanocrystallization of SiC,
8th Int. Conf. on Silicon Carbide and Related Materials (ICSCRM 99), Research Triangle Park, NC, USA, Oct. 10-15, 1999

Hornauer U., Günzel R., Reuther H., Richter E., Wieser E., Möller W., Schumacher G.,
Dettenwanger F., Schütze M.,
Protection of γ-based TiAl against high temperature oxidation using ion implantation of chlorine,
EMRS 1999 Spring Meeting, Strasbourg, France, June 1 – 4, 1999

Hornauer U., Günzel R., Reuther H., Richter E., Wieser E. and Möller W.,
Inhibition of the oxidation of intermetallic TiAl by ion implantation,
8th Annual Conf. of Doctoral Students, WDS `99, Praha, CZ, June 22 – 25, 1999

Hornauer, U., Richter, E., Matz, Wieser, E., Möller, W., Schumacher, G., Schütze, M.,
Microstructure and oxidation kinetics of intermetallic TiAl after Si and Mo ion implantation,
SMMIB, Beijing, China, Sept 19-24, 1999

Hornauer, U., Günzel, R., Richter, E., Matz, W., Reuther, H., Mücklich, A., Wieser, E., Möller, W.,
Schumacher, G., Dettenwanger, F., Schütze, M.,
Application of implantation of Cl into TiAl alloys using PBII,
PBII '99, Kyoto, Japan, Dec. 13 – 16, 1999

Hornauer, U., Schumacher, G., Reuther, H., Matz, W., Wieser, E., Richter, E., Schütze, M.,
Influence of silicon ion-implantation on the microstructure and oxidation kinetics of Ti50Al,
Gordon Research Conf.: Corrosion dry, New London, USA, July 19 - 23, 1999

Huang, N., Günzel, R., Richter, E., Prokert, F., Matz, W., Grötzschel, R., Reuther, H.,
Surface characteristics of titanium oxide layer on titanium surface formed by plasma immersion ion implantation,
AEPSE, Beijing, China, Sept. 15-19, 1999

Huang, N., Günzel, R., Pham, M.T., Richter, E.,
Surface modification of titanium biomaterials by oxygen ion implantation using plasma immersion ion implantation,
PBII '99, Kyoto, Japan, Dec. 13 - 16, 1999

Jäger, H.U., Albe, K.,
Molecular dynamics simulations of steady state growth of ion deposited tetrahedral amorphous carbon films,
10th Europ. Conf. on Diamond, Diamond-Like Materials, Carbon Nanotubes, Nitrides and Silicon Carbide, Prague, Czech Republic, Sept. 12-17, 1999

Jäger, H.U., Albe, K.,
Molecular dynamics simulations of steady state growth of ion deposited tetrahedral amorphous carbon films,
MRS 1999 Fall Meeting, Boston, USA, Nov. 29 – Dec. 3, 1999

Jiang, W., Thevuthasan, S., Weber, W.J., Grötzschel, R.,
Deuterium channeling analysis for He-implanted 6H-SiC,
IBA-14/ECAART-6, Dresden, Germany, July 26-30, 1999

Khan, R.U.A., Silva, S.R.P., Gebel, T., Panknin, D.,
Bistability phenomena in ion implanted hydrogenated amorphous carbon films,
IBA-14/ECAART-6, Dresden, Germany, July 26-30, 1999

Klimenkov, M., Borany, J.von, Matz, W., Heinig, K.H.,
TEM study of Ge-nanoclusters in thin SiO_2 layers,
29. Tagung der Deutschen Gesellschaft für Elektronenmikroskopie, Dortmund, Sept. 5 - 10, 1999

Kögler, R., Peeva, A., Anwand, W., Werner, P., Danilin, A.B., Skorupa, W.,
Gettering centres for metals and oxygen formed in MeV-ion-implanted and annealed Si,
8th Int. Autumn Mtg.: Gettering and Defect Engineering in Semiconductor Technology (GADEST´99), Höör, Sweden, Sept. 25-28, 1999

Kögler, R.,
Punktdefekte in Silizium nach Ionenimplantation und Ausheilung außerhalb der projizierten Ionenreichweite,
Deusche Arbeitstagung zu Punktdefekten in Halbleitern, Max Planck Institut für Festkörperphysik, Stuttgart, Germany, June 23-24, 1999

Kolitsch, A.,
Development of a user data base system for ion implanter operation,
6th DANFYSIK User Meeting, Sesimbra, Portugal, Sept. 1999

Kolitsch, A., Fukarek, W., Fitz, C., Möller, W.,
Real time stress analysis of deposition and implantation processes at DANFYSIK 1090 machines,
6th DANFYSIK User Meeting, Sesimbra, Portugal, Sept. 1999

Kolitsch, A., Möller, W., Malkow, Th., Bull, S.J., Magula, V.,
Growth and characterization of hard and elastic carbon nitride films,
SMMIB, Beijing, China, Sept. 19 - 24, 1999

Kruse, O., Parascandola, S., Möller, W.,
In-situ real-time depth profiling by elastic recoil detection analysis and its applications to ion nitriding of stainless steel,
MRS Spring Meeting '99, San Francisco, USA, April 5 - 9, 1999

Mäder, M., Neelmeijer, C., Schreiner, M.,
Non-destructive composition analysis of glass artefacts,
IBA-14/ECAART-6, Dresden, Germany, July 26-30, 1999

Mändl, S., Günzel, R., E. Richter, E., Möller, W., Rauschenbach, B.,
Annealing behaviour of nitrogen implanted stainless steel,
SMMIB, Beijing, China, Sept. 19 – 24, 1999

Markwitz, A., Grambole, D., Herrmann, F., Trompetter B., Dioses, T., Gauldie, R. W.,
Reliable micro-measurement of Sr is the key to cracking the life-history code in the fish otolith,
IBA-14/ECAART-6, Dresden, Germany, July 26-30, 1999

Martin, J., Wannemacher, R., Sigle, W., Bischoff, L., Teichert, J.,
Konfokale Mikroskopie an elektronen- und ionenstrahlinduzierten Farbzentrenverteilungen in Diamant,
DPG-Frühjahrstagung, Münster, Germany, March 22 – 26, 1999

Martin, J., Teichert, J., Bischoff, L., Sigle, W., Köhler, B., Wannemacher, R.,
Confocal microscopy of color center distributions in diamond,
12th Int. Conf. on Dynamical Processes in the Excited State of Solids, Humacao, Puerto Rico, 1999

Matz, W., (invited)
ROBL - a CRG Beam Line at the ESRF dedicated to Radiochemistry and Materials Research,
Europ. Round Table SR and FEL '99, Krakow, Poland, Nov. 9 - 10, 1999

Matz, W., Schell, N., Prokert, F., Eichhorn, F., Berberich, F.,
ROBL - a synchrotron research facility for the Institute of Ion Beam Physics and Materials Research of the Forschungszentrum Rossendorf,
Symp. 25 Jahre Strukturforschung, Munich, Nov. 12 - 13, 1999

Möller, W.,
Nitridieren von Metalloberflächen mit Puls-Plasma-Immersion,
Workshop „Gepulste Plasmen in der Praxis", Wuppertal, Germany, Feb. 1, 1999

Möller, W.,
Plasma immersion ion implantation for the treatment of metal surfaces,
52nd Annual Gaseous Electronics Conference, Norfolk, Virginia, USA, Oct. 7, 1999

Möller, W.,
Surface processes and diffusion mechanisms during ion nitriding of stainless steel and aluminium alloys,
5th Int. Workshop on Plasma Based Ion Implantation, Kansai Science City, Japan, Dec. 15, 1999

Mrotschek, I., Günzel, R., Richter, E., Möller, W.,
Ion assisted surface modifications of hard metals,
SMMIB, Beijing, China, Sept. 19 – 24, 1999

Neelmeijer, C., Mäder, M., Pietsch, U., Ulbricht, H., Walcha, H.-M.,
PIXE fingerprints of Böttger stoneware,
IBA-14/ECAART-6, Dresden, Germany, July 26-30, 1999

Neelmeijer, C.,
Paint layer studies – performances of X-ray fluorescence and ion beam techniques,
6th Int. Conf. on Non-Destructive Testing and Microanalysis for the Diagnostics and Conservation of the Cultural and Environmental Heritage (Art'99), Rome, Italy, May 17 – 20, 1999

Nepijko, S.A., Klimenkov, M., Kuhlenbeck, H., Freund, H.-J.,
Local melting of the NiAl-support under deposited Pd-cluster in the $Pd/Al_2O_3/NiAl_{(110)}$-system during electron irradiation in TEM,
3rd Int. Conf. Modification of Properties of Surface Layers (MPSL 99), Sumy, Ukraine,
May 25 - 29, 1999

Noetzel, J., Geisler, H., Gorbunov, A., Tselev, A., Brand, K., Lehmann, M., Mücklich, A., Dobler, M., Wieser, E., Möller, W.,
Strukturelle Veränderungen in laserdeponierten Fe/Al Multischichten durch Ionenstrahlmischen und thermische Behandlung,
DPG-Frühjahrstagung, Münster, Germany, March 22-26, 1999

Noetzel, J., Handstein, A., Gorbunov, A.,Tselev, A., Mücklich, A., Prokert, F., Wieser, E., Möller, W.,
Ionenstrahlinduzierte Strukturbildung im System Co/Cu,
DPG-Frühjahrstagung, Münster, Germany, March 22-26, 1999

Oswald, S., Schmidt, B., Heinig, K.H.,
XPS investigations for the study of Ge clustering in SiO_2,
Europ. Conf. on Applied Surface and Interface Analysis, Sevilia, Spain, Oct. 4-8, 1999

Panknin, D., Wirth, H., Skorupa, W.,
Flash lamp annealing for efficient p-type doping of SiC,
10^{th} Int. Conf. Radiation Effects in Insulators-REI 10, Jena, Germany, July 18-23, 1999

Panknin, D., Skorupa, W., Wirth, H., Voelskow, M., Mücklich, A., Anwand, W., Brauer, G., Gonzalez-Varona, O., Perez-Rodriguez, A., Morante, J.M. ,
Ion beam doping of 6H-SiC for high concentration P-type layers,
8th Int. Autumn Mtg.: Gettering and Defect Engineering in Semiconductor Technology (GADEST´99), Höör, Sweden, Sept.25-28, 1999

Panknin, D., Wirth, H., Skorupa, W.,
High concentration doping of 6H-SiC by ion implantation: flash versus furnace annealing,
8^{th} Int. Conf. on Silicon Carbide and Related Materials (ICSCRM 99), Research Triangle Park, NC, USA, Oct. 10-15, 1999

Parascandola, S., Kruse, O., Möller, W.,
Retention und Emission von Stickstoff während der Implantation niederenergetischer Stickstoffionen in AISI 316,
DPG-Frühjahrstagung, Münster, Germany, March 17 - 21, 1999

Parascandola, S., Telbizova, T., Kruse, O., Möller, W.,
Nitrogen transport during ion nitriding of aluminium,
MRS Spring Meeting '99, San Francisco, USA, April 5 - 9, 1999

Parascandola, S., Telbizova, T., Kruse, O., Richter, E., Möller, W.,
Ion nitriding of aluminium - the influence of oxygen on the nitriding kinetics,
ICMCTF '99, San Diego, USA, April 12 - 15, 1999

Parascandola, S., Telbizova, T., Kruse, O., Möller, W.,
The influence of the oxygen partial pressure on the ion nitriding of aluminium – an investigation by means of real time elastic recoil detection analysis,
IBA-14/ECAART-6, Dresden, Germany, July 26 – 30, 1999

Parascandola, S., Kruse, O., Richter, E., Möller, W.,
Nitrogen transport during nitriding austenitic stainless steel by low energy ion implantation,
SMMIB, Beijing, China, Sept. 19 – 24, 1999

Peeva, A., Kögler, R., Brauer, G., Skorupa, W., Werner, P.,
Experimental evidence for interstitial defects in the $R_P/2$ region of MeV-ion implanted and annealed silicon,
DPG-Frühjahrstagung, Münster, Germany, March 22-26, 1999

Peeva, A., Kögler, R., Brauer, G., Skorupa, W., Werner, P.,
Metallic impurity gettering to defects remaining in the $R_P/2$ region of MeV-ion implanted and annealed silicon,
1st ENDEASD (European Network on Defect Engineering of Advanced Semiconductor Devices) Workshop, Santorini, Greece, April 21-22, 1999

Peeva, A., Kögler, R., Werner, P., de Mattos, A.A.D., Fichtner P.F.P., Skorupa, W.,
Evidence for interstitial defects remaining in the Rp/2 region of MeV-ion implanted silicon,
IBA-14/ECAART-6, Dresden, Germany, July 26-30, 1999

Penzhorn, R.-D., Bekris, N., Coad, P., Doerr, L., Friedrich, M., Glugla, M., Haigh, A.,
Lässer, R., Peacock, A.,
Status and research progress at the tritium laboratory Karlsruhe,
5th Int. Symp. on Fusion Nuclear Technology, Rome, Italy, Sept. 19-24, 1999

Pezoldt, J., Rybin, P.V., Kulikov, D.V., Trushin, Yu.V., Yankov, R.A., Voelskow, M., Kreissig, U.,
The influence of the implantation sequence on the formation of thin $(SiC)_{1-x}(AlN)_x$ layers by ion beam synthesis,
10th Int. Conf. Radiation Effects in Insulators-REI 10, Jena, Germany, July 18-23, 1999

Pham, M.T., Matz, W., Reuther, H., Richter, E., Steiner, G., Oswald, S.,
Ion beam sensitizing of titanium surfaces to hydroxyapatite formation,
SMMIB, Beijing, China, Sept. 19-24, 1999

Pham, M.T., Reuther, H., Matz, W., Richter, E., Wieser, E., Steiner, G., Oswald, S.,
Ionenstrahlgestützte Hydroxylapatitbildung zur Verbesserung der Biokompatibilität von Titanimplantaten,
Wiss. Konf. der Wissenschaftsgemeinschaft Gottfried Wilhelm Leibniz, München, Oct. 1999

Pham, M.T., Reuther, H., Matz, W., Richter, E., Wieser, E., Steiner, G., Salzer, R., Oswald, S.,
Sensibilisierung von Titanimplantaten zur Hydroxylapatitbildung,
2nd Interdisciplinary Essen-Symposium of the Working Group on "Biomaterials and Tissue Compatibility", Essen, Oct. 6-8, 1999

Pham, M.T., Steiner, G., Salzer, R.,
Silber-Cluster in Dünnfilmen: AFM-Charakterisierung,
Scanning Probe Microscopy, European Users Meeting, Dresden, Germany, Oct. 28-28, 1999

Posselt, M.,
Prediction of the morphology of the as-implanted damage in silicon using a novel combination of BCA and MD simulations,
First ENDEASD (European Network on Defect Engineering of Advanced Semiconductor Devices) Workshop, Santorini, Greece, April 21-22, 1999

Posselt, M., (invited)
A novel method to investigate ion-beam-induced defect evolution in Si,
5th Int. Symp. on Process Physics and Modeling in Semiconductor Technology, ECS 1999 Spring Meeting, Seattle, WA, USA, May 2-6, 1999

Posselt, M., Schmidt, Br., Feudel, T., Strecker, N., (invited)
Atomistic simulation of ion implantation and its application in Si technology,
E-MRS 1999 Spring Meeting, Strasbourg, France, June 1-4, 1999

Posselt, M.,
Determination of the as-implanted defect structure in silicon by a combined simulation method,
IUMRS-ICAM 99 Conference, Beijing, China, June 13-18, 1999

Rebohle, L., Tyschenko, I.E., von Borany, J., Skorupa, W., Fröb, H.,
Strong violet light emission from Ge^+-implanted SiO_2 layers,
SPIE's Int. Symp., Optoelectronics 1999, San Jose, California, USA, Jan. 25-29, 1999

Rebohle, L., Revesz, A.G., Skorupa, W., Hughes, H.L.,
The effects of preparation conditions of SIMOX samples on the photoluminescence spectra of their buried oxide layer,
11. Conf. on Insulating Films on Semiconductors (INFOS´99), Kloster Banz, Germany,
June 16-19, 1999

Rebohle, L., von Borany, J., Skorupa, W., Fröb, H., Tyschenko, I.E.,
Strong light emission from Ge^+-implanted SiO_2 films,
8th Annual Conference of Doctoral Students WDS'99, Praha, CZ, June 22-25, 1999

Reiche, R., Oswald, S., Wetzig, K., Dobler, M., Reuther, H.,
XPS und Faktorenanalyse zur Untersuchung von Eisensilizidproben,
10. Tagung Festkörperanalytik, Wien, Austria, July 5 - 7, 1999

Reinert, T., Reibetanz, U., Vogt, J., Butz, T., Grambole, D., Herrmann, F.,
Pressure-induced calcium redistribution in articular cartilage,
IBA-14/ECAART-6, Dresden, Germany, July 26-30, 1999

Reuther, H., Betzl, M., Richter, E.,
Phase formation and annealing behaviour of aluminium implanted with iron ions,
SMMIB, Beijing, China, Sept. 19 – 24, 1999

Reuther, H., Betzl, M.,
Annealing behaviour of magnesium and aluminium implanted with iron ions,
Int. Conf. Applications Mössbauer Effect, Garmisch-Partenkirchen, Aug. 29 - Sept. 3, 1999

Richter, E., Günzel, R., Parascandola, S., Telbizova, T., Kruse, O., Möller, W.,
Nitriding of stainless steel and aluminium alloys by plasma immersion ion implantation,
SMMIB, Beijing, China, Sept. 19 –2 4, 1999

Rybin, P.V., Kulikov, D.V., Trushin, Yu.V., Pezoldt, J., Yankov, R.A., Skorupa, W.,
The influence of internal stress fields due to point defect clusters on interstitial diffusion in SiC under irradiation ,
3. Int. Workshop on New Approaches to High Tech Materials: Nondestructive Testing and Computer Simulations in Science and Engineering, St. Petersburg, Russia, June, 1999

Sass, J., Mazur, K., Eichhorn, F.,
Lateral ordering in semiconductor hetero layers studied by high resolution diffraction and specular reflectivity,
4th Autumn School on X-ray scattering from surfaces and thin layers, Smolenice, Slovakia,
Sept. 22 - 25, 1999

Scheerschmidt, K., Conrad, D., Belov, A.,
Kristalldefekte an gebondeten Grenzflächen: MD-Strukturrelaxation und HREM Bildsimulation,
29. Tagung der Deutschen Gesellschaft für Elektronenmikroskopie, Dortmund, Germany,
Sept. 5-10, 1999

Scheerschmidt, K., Belov, A., Conrad, D.,
Structure modelling by molecular dynamics: Analysis of TEM images of bonded interfaces,
IoP Conf. Ser., Electron Microscopy and Analysis Group Conference (EMAG'99), Sheffield, UK,
August 25-27, 1999

Sendezera, E.J., Davidson, A.T., Anwand, W., Brauer, G. Nicht, E.-M.,
Characterization of Ar^+ implanted LiF by a variable energy slow positron beam,
44th Annual Meeting of the South African Institute of Physics (SAIP99), Port Elizabeth, July 6-9,1999

Sendezera, E.J., Davidson, A.T., Anwand, W., Brauer, G. Nicht, E.-M.,
Depth profiling of defects in Mg^+ implanted LiF using a slow positron beam,
44th Annual Meeting of the South African Institute of Physics (SAIP99), Port Elizabeth, July 6-9,1999

Sendezera, E.J., Davidson, A.T., Anwand, W., Brauer, G. Nicht, E.-M.,
A comparative defect study of LiF implanted with 100 keV argon, magnesium, and aluminium ions by slow positron annihilation spectroscopy,
44th Annual Meeting of the South African Institute of Physics (SAIP99), Port Elizabeth, July 6-9,1999

Serre, C., Perez-Rodriguez, A., Romano-Rodriguez, A., Morante, J.R., Esteve, J., Acero, M.C., Koegler, R., Skorupa, W.,
Ion beam synthesis of polycrystalline SiC on SiO_2 structures for MEMS applications,
IBA-14/ECAART-6, Dresden, Germany, July 26-30, 1999

Serre, C., Perez-Rodriguez, A., Romano-Rodriguez, A., Morante, J. R., Fonseca, L., Acero, M. C., Esteve, J., Kögler, R., Skorupa, W.,
ß-SiC on SiO_2 formed by ion implantation and bonding for micromechanics applications,
NATO Advanced Research Workshop, Kiev, Ukraine, Oct. 12 – 15, 1999

Skorupa, W., (invited)
Ion beam processing of single crystalline silicon carbide,
Second Vietnamese-German Meeting, Heidelberg, Germany, May 17-21, 1999

Skorupa, W., (invited)
Si-Technologie basierter UV-Lichtemitter für die optische Interchip-Kommunikation,
Fach-und Expertengespräch Lösungen der Intra-und Interconnect-Krise in der Mikroelektronik,
BMBF, Bonn, Sept.8, 1999

Skorupa, W., (invited)
Ion beam processing for silicon-based light emission: The Rossendorf approach,
Dutch Mtg. on Physics with Ion Beams, Eindhoven, The Netherlands, Oct. 27, 1999

Soltani-Farshi, M., Kreissig, U., Richter, E., Möller, W.,
Detrapping of implanted He and accumulated H in Ti,
IBA-14/ECAART-6, Dresden, Germany, July 26-30, 1999

Stoemenos, J., Pecz, B., Heera, V.,
Consequences of high dose, high temperature Al^+ implantation in 6H-SiC,
8th Int. Conf. on Silicon Carbide and Related Materials (ICSCRM 99), Research Triangle Park, NC, USA, Oct. 10-15, 1999

Strobel, M., Heinig, K-H., Möller, W.,
"Inverse" Ostwald ripening due to ion irradiation: An athermal process studied by Monte Carlo simulations,
Gordon Research Conference on Materials Processes Far From Equilibrium, Plymouth, NH, USA, July 11-16, 1999

Teichert, J., Bischoff, L., Hausmann S., Hobert, H.,
Raman investigation of lattice defects in the $CoSi_2$ synthesis using focused ion beam implantation,
Europ. Workshop for Advanced Metallization MAM, Oostende, Belgium, March 8-10, 1999

Teichert, J., Bischoff, L., Hausmann S., (invited)
Maskenlose Implantation von Mikrostrukturen mit feinfokussierten Ionenstrahlen,
DPG-Frühjahrstagung, Münster, Germany, March 22-26, 1999

Teichert, G., Panknin, D., Petzoldt, J.,
Photothermal measurements of Al and Al/N implanted 6H-SiC,
HI-TECH 99, St. Petersburg, Russia, June 7 - 11, 1999

Telbizova, T., Parascandola, S., Kreissig, U., Richter, E., Möller, W.,
Observation of the thermal transport during ion nitriding of aluminium,
SMMIB, Beijing, China, Sept. 19 – 24, 1999

Thees, H.-J., Wittmaack, M., Stegemann, K.-H., Borany, J. von, Heinig, K.-H., Gebel, T.,
Microstructure and electrical properties of gate SiO_2 containing Ge nanoclusters for memory applications,
10^{th} Workshop on Dielectrics in Microelectronics, Barcelona, Spain, Nov. 3-5, 1999

Trushin, Yu.V., Kulikov, D.V., Rybin, P.V., Pezoldt, J., Yankov, R.A., Voelskow, M., Kreissig, U.,
Experimental and theoretical studies of the defect structure evolution in SiC after implantation of Al and N ions,
4th Russ. Conf. on Physics of Semiconductors, Novosibirsk, Russia, Oct. 25-29, 1999

Tsyganov, I., Wieser, E., Matz, W., Mücklich, A., Reuther, H.,
Formation of the phases Ti_3Al and TiAl by high dose implantation of aluminium into titanium,
IBA-14/ECAART-6, Dresden, Germany, July 26-30, 1999

Turos, A., Gawlik, G., Jagielski, J., Stonert, A., Madi, N., Matz, W., Mücklich, A.,
Atomic transport effects in Kr-ion bombarded ZrO_2/Fe ternary system,
Int. Conf. on Radiation Effects in Insulators, Jena, Germany, July 19-23, 1999

Ueda, M., Gomes, G., Berni, L.A., Rosso, J.O., Barroso, J.J., Abramof, E., Beloto, A.F., Reuther, H.,
Plasma immersion ion implantation using a glow discharge source with controlled plasma potential,
IBA-14/ECAART-6, Dresden, Germany, July 26 - 30, 1999

Walterfang, M., Kruijer, S., Dobler, M., Reuther, H., Keune, W.,
Phase analysis in α-Fe after high-dose Si ion implantation by depth-selective conversion electron Mössbauer spectroscopy (DCEMS),
Int. Conf. Applications Mössbauer Effect, Garmisch-Partenkirchen, Germany, Aug. 29 - Sept. 3, 1999

Weber, R., Skorupa, W.,
Precipitation kinetics in formation of SiO_2 layers: The role of spatial correlation functions,
9^{th} Int. Symp. on Silicon-on-Insulator Technology and Devices, within: 195. Meeting of
The Electrochemical Society, Seattle, USA, May 2-7, 1999

Wieser, E., Schreiber, J., Wenzel, C., Bartha, J.W., Bendjus, B., Melov, V., Peikert, M., Matz, W., Adolphi, B., Fischer, D.,
Modification of Ta-based thin film barriers by ion implantation of nitrogen and oxygen,
Int. Conf. Advanced Metallization for ULSI Application, AMC '99, Orlando, USA, Sept. 26 -28, 1999

Lectures

Borany, J. von,
Implantation doping of Ge for detector applications- State of the Art,
Eurysis Mesures, Lingolsheim, France, July 13, 1999

Brauer, G.,
Characterization of Al^+ and Ni^+ co-implanted and annealed 6H-SiC by positron annihilation spectroscopy and Rutherford backscattering/channeling,
Pennsylvania State University, University Park /PA, USA, April 15, 1999

Brauer, G.,
Intentions for the construction of an intense positron beam line at Forschungszentrum Rossendorf,
Universita' di Trento, Trento, Italy, May 25, 1999

Brauer, G.,
Characterization of Al^+ and Ni^+ co-implanted and annealed 6H-SiC by positron annihilation spectroscopy and Rutherford backscattering/channeling,
Brookhaven National Laboratory,Upton/NY, USA, March 31, 1999

Brauer, G.,
Plans for the assembly, construction and use of an intense positron source at ELBE,
University of Hong Kong ,Hong Kong, Sept. 28, 1999

Brauer, G.,
Characterization of Al^+ and Ni^+ co-implanted and annealed 6H-SiC by positron annihilation spectroscopy and Rutherford backscattering/channeling,
University of Hong, Hong Kong, Sept. 30, 1999

Brauer, G.,
Effects of neutron irradiation on positron lifetime and micro-Vickers hardness of Fe-Cu model alloys and reactor pressure vessel steel,
University of Hong Kong, Hong Kong, Nov. 25, 1999

Fontaine, F.,
Implantationsdotierung von Diamantschichten,
Universität Ulm, Germany, June 9, 1999

Friedrich, M.,
Tritium detection by accelerator mass spectrometry,
University of Helsinki, Dept. of Physics, Oct. 13, 1999

Friedrich, M.,
Tritium depth profiling in carbon by accelerator mass spectrometry,
MPI für Plasmaphysik, Garching, Dec. 12, 1999

Fukarek, W.,
Application of RTSE, gSE and PIRR in PVD, CVD and ion implantation,
Materials Research Laboratory at The Pennsylvania State University, May 10, 1999

Fukarek, W.,
In-situ-Messung mechanischer Spannungen in BN-Schichten,
TU Chemnitz, 26 Nov 1999

Fukarek, W.,
In situ diagnostics of thin film deposition,
2nd Year Coordination Meeting of TMR network, Rossendorf, 18-19 Nov 1999

Fukarek, W.,
In situ diagnostic capabilities at IIM,
LSF user meeting, Rossendorf, 10 Dec 1999

Gebel, T.,
Non-volatile memory effects of ion-beam synthesized Ge and Si nanoclusters,
California Institute of Technology, Pasadena (CA), USA, Oct.18, 1999

Gebel, T.,
Electrical Characterization of SiO_2 layers containing Ge and Si nanoclusters,
Naval Research Laboratory, Washington DC, USA, Nov.17, 1999

Gebel, T.,
Electrical properties of Si and Ge nanoclusters in SiO_2 layers,
PhD-Symposium, Charles University, Prague, Czech Republic; June 22-25, 1999

Grötzschel, R.,
Möglichkeiten und Probleme der modernen Ionenstrahlanalytik,
Universität Bochum, January 1999

Grötzschel, R., Kruse, O., Kreißig, U., Parascandola, S., Grigull, S.,
Atomic transport studies by in-situ ERDA,
Universität Helsinki, October 1999

Grötzschel, R., Kreissig, U., Kruse, O., Parascandola, S., Grigull, S., Schmidt, B.,
In-situ Ionenstrahlanalytik zur Untersuchung atomarer Transportprozesse in Festkörpern,
HMI Berlin, October 1999

Günzel, R.,
Verschleißfester Edelstahl durch Plasmaimmersions-Ionenimplanmtation,
Robert Bosch GmbH, Crailsheim, March 9, 1999

Günzel, R., Richter, E., Möller, W.,
Verschleißminderung bei Aluminiumlegierungen,
Werkstoff-Forum Hannover-Messe, Hannover, April 20 – 24, 1999

Hausmann, S.,
Strahlenschäden und Ionenstrahlsynthese mit fokussierten Ionenstrahlen,
ETH Zürich, Schweiz, January 19, 1999

Hausmann, S.,
Strahlenschäden und Ionenstrahlsynthese mit fokussierten Ionenstrahlen,
Universität Osnabrück, Surface Science Seminar, August 20, 1999

Hausmann, S.,
Strahlenschäden und Ionenstrahlsynthese mit fokussierten Ionenstrahlen,
Ruhr-Universität Bochum, November 4, 1999

Heinig, K.-H.,
Synthesis of new materials by ion beams,
CSNSM, ORSAY Campus, France, May 3, 1999

Kolitsch, A., Möller, W.,
Preparation of CN_x films by ion beam assited deposition,
Honfleur, France: First Annual Meeting of the TMR Network „Synthesis, structure and properties of new carbon based hard materials“, March 4 – 7, 1999

Malhouitre, S., Kolitsch, A., Möller, W.,
Preparation of Si_3N_4 films by ion beam assited deposition,
Honfleur, France: First Annual Meeting of the TMR Network „Synthesis, structure and properties of new carbon based hard materials“, March 4 – 7, 1999

Malhouitre, S., Kolitsch, A., Möller, W.,
Preparation of Si_3N_4, CN_x / Si_3N_4 multilayers and Si-C-N films by ion beam assited deposition,
Second Year Coordination Meeting of the TMR Network „Synthesis, structure and properties of new carbon based hard materials“, Dresden, Nov. 18 - 21, 1999

Matz, W.,
Possibilities for real-time experiments at ROBL,
Workshop on real-time studies with x-ray synchrotron radiation, HMI Berlin, June 21, 1999

Matz, W., Seidel, W.,
Elektronenbeschleuniger als Quellen elektromagnetischer Strahlung,
Public lectures for Teachers (Lehrerfortbildung ‘99), Rossendorf, Aug. 26, 1999

Matz, W.,
ROBL - Synchrotronstrahlung für Ökologie- und Materialforschung,
Public lecture (Tag der offenen Tür), Rossendorf, Sept. 11, 1999

Matz, W.,
The Materials Research End-station at ROBL - Possibilites for Synchrotron Radiation Studies,
Institute of Electronic Materials Technology, Warsaw, Nov. 12, 1999

Möller, W.,
Festkörperspektroskopie mit Ionen,
TU Dresden, W.E.Heraeus-Ferienkurs für Physik, Sept. 28, 1999

Möller, W.,
Ionen-Festkörper-Wechselwirkung,
Sommerschule „Nukleare Sonden und Ionenstrahlen“, Bad Blankenburg, Germany, Oct. 6, 1999

Möller, W.,
Echtzeit-in-situ-Ionenstrahlanalysen zum Nitrieren von Metalloberflächen,
Festkörpertag des SFB 345 "Festkörper weitweg vom Gleichgewicht", Universität Göttingen,
Oct. 22, 1999

Neelmeijer, C.,
Non-destructive analysis of pigments on paper,
Università degli Studi di Firenze, Dipartimento di Fisica, Italy, March 25, 1999

Neelmeijer, C.,
Ein Kern aus Gold,
Workshop „Modellhaftes Konservierungskonzept für umweltgeschädigte Email-Pretiosen im Grünen Gewölbe/Dresden“ (DBU-Projekt „Grünes Gewölbe“), Dresden, March 8 – 9, 1999

Neelmeijer, C.,
External PIXE measurements,
Symposium “Limoges painted enamels”, Kunstgewerbemuseum Berlin, Rathgen-Forschungslabor/ Staatliche Museen zu Berlin, May 21, 1999

Panknin, D.,
Ion beam doping of 6H-SiC for high concentration p- and n-type layers,
Univ. of Barcelona, Dept. of Appl. Phys., Spain, Dec. 3, 1999

Parascandola, S.,
Ion nitriding of aluminum - the influence of oxygen on the nitriding kinetics,
Sandia National Lab, Albuquerque, NM, USA, April 19, 1999

Parascandola, S.,
Ion nitriding of aluminum - the influence of oxygen on the nitriding kinetics,
Los Alamos National Lab, Los Alamos, NM, USA, April 21, 1999

Parascandola, S.,
Ion nitriding of aluminum - the influence of oxygen on the nitriding kinetics,
National Renewable Energy Lab, Golden, Co, USA, April 22, 1999

Peeva, A.,
Gettering centers for metals away from the projected ion range in high energy ion implanted and annealed silicon,
Fed. Univ. of Rio Grande do Sul, Porto Alegre, Brasilien, Nov. 18, 1999

Posselt, M.,
Atomistische Simulation der Ionenimplantation und ihre Anwendung in der Si-Technologie,
Institut für Physik der Universität Augsburg, January 28, 1999

Posselt, M.,
Computer simulation of ion-beam-induced processes in solids: An overview of the activities at the FZ Rossendorf,
Environmental Molecular Science Laboratory at Pacific Northwest National Laboratory, Richland, WA, USA, May 7, 1999

Prokert, F.,
Röntgenreflektometrie an Dünnschichtsystemen,
TU Chemnitz, Graduiertenkolleg, Chemnitz, June 8, 1999

Rebohle, L.,
Strong violet light emission from Ge^+-implanted SiO_2 layers,
California Institute of Technology, Pasadena, CA, USA, January 22, 1999

Rebohle, L.,
Strong violet light emission from Ge^+-implanted SiO_2 layers,
Naval Research Laboratory, Washington, D.C., USA, February 1, 1999

Richter, E., Günzel, R.,
Randschichthärten von Edelstahl und Leichtwerkstoffen,
3. Industriefachtagung “Oberflächen- und Wärmebehandlung” Chemnitz, June 1 – 2, 1999

Richter, E.,
Nitrieren von Aluminiumlegierungen mit Plasma-Immersions-Implantation,
Werkstoff-Forum Hannover-Messe, Hannover, April 20 – 24, 1999

Skorupa, W.,
Semiconductor related work at the Institute of Ion Beam Physics and Materials Research, Forschungszentrum Rossendorf,
California Institute of Technology, Pasadena, CA, USA, January 22, 1999

Skorupa, W.,
Semiconductor related work at the Institute of Ion Beam Physics and Materials Research at the Forschungszentrum Rossendorf,
Naval Research Laboratory, Washington, D.C., USA, February 1, 1999

Skorupa, W.,
Ion beam processing of single crystalline silicon carbide,
Pacific Northwest Laboratory, Richland, WA, USA, May 7, 1999

Skorupa, W.,
Silicium basierte Lichtemission durch Ionenstrahlsynthese,
Inst. für Physikalische Hochtechnologien, Jena, Germany, June 11, 1999

Skorupa, W.,
Recent advances of ion beam processing of electronic materials at the FZ Rossendorf,
Fed. Univ. of Rio Grande dol Sul, Porto Alegre, Brasilien, Nov. 19, 1999

Skorupa, W.,
Ion beam modification of advanced electronic materials-Activities at the FZ Rossendorf,
Comision Nacional de Energia Atomica, Centro Atomico Constituyentes, San Martín, Pcia. de Buenos Aires, Argentinien, Nov. 26, 1999

Soltani-Farshi, M.,
Herstellung von TiN-Schichten,
Werkstoff-Forum Hannover-Messe, Hannover, April 20 – 24, 1999

Strobel, M.
Modeling and Computer Simulation of Ion Beam Synthesis of Nanostructures,
University of Catania, Italy, December 13, 1999

Wieser, E.,
Phasenbildung in Metallen bei Hochdosisimplantation,
Seminar des IFW Dresden, Dresden, May 21, 1999

Wieser, E.,
Phasenbildung in Metallen bei Hochdosisimplantation,
TU Chemnitz, Kolloquium des Institutes für Physik, Chemnitz, Nov. 10, 1999

Reports

Borany, J. von,
Erzeugung von Ge Nanoclustern in dünnen SiO_2- Schichten für nichtflüchtige Speicherzellen,
Zwischenbericht zum SMWK/SMWA-Verbundprojekt: Nanokristall-Speicher, 20.03.1999

Borany, J. von,
Untersuchungen zur Stabilität von Ge-Nanoclustern in dünnen Gateoxiden in einer Prozeßtechnologie für nichtflüchtige Speicherzellen,
Zwischenbericht zum SMWK/SMWA-Verbundprojekt: Nanokristall-Speicher, 31.10.1999

Brauer, G.,
Materialforschung mittels Positronen-Annihilationsspektroskopie,
SMWK: 4-7533-70-FZR/705, Zwischenbericht 10.07.1999

Köhler, B., Teichert, J.,
Entwicklung einer neuen Technologie zur Probenpräparation für die Transmissions-Elektronenmikroskopie (TEM) auf der Basis der Ionenfeinstrahlbearbeitung,
SMWK/4-7533-70-864-98/3, Zwischenbericht 30.06.1999

Skorupa, W.,
Ion beam processing of single crystalline silicon carbide,
Pacific Northwest Laboratory, Richland, WA, USA, May 7, 1999

Skorupa, W.,
Silicium basierte Lichtemission durch Ionenstrahlsynthese,
Inst. für Physikalische Hochtechnologien, Jena, Germany, June 11, 1999

Skorupa, W.,
Recent advances of ion beam processing of electronic materials at the FZ Rossendorf,
Fed. Univ. of Rio Grande dol Sul, Porto Alegre, Brasilien, Nov. 19, 1999

Skorupa, W.,
Ion beam modification of advanced electronic materials-Activities at the FZ Rossendorf,
Comision Nacional de Energia Atomica, Centro Atomico Constituyentes, San Martín, Pcia. de Buenos Aires, Argentinien, Nov. 26, 1999

Soltani-Farshi, M.,
Herstellung von TiN-Schichten,
Werkstoff-Forum Hannover-Messe, Hannover, April 20 – 24, 1999

Strobel, M.
Modeling and Computer Simulation of Ion Beam Synthesis of Nanostructures,
University of Catania, Italy, December 13, 1999

Wieser, E.,
Phasenbildung in Metallen bei Hochdosisimplantation,
Seminar des IFW Dresden, Dresden, May 21, 1999

Wieser, E.,
Phasenbildung in Metallen bei Hochdosisimplantation,
TU Chemnitz, Kolloquium des Institutes für Physik, Chemnitz, Nov. 10, 1999

Reports

Borany, J. von,
Erzeugung von Ge Nanoclustern in dünnen SiO_2- Schichten für nichtflüchtige Speicherzellen,
Zwischenbericht zum SMWK/SMWA-Verbundprojekt: Nanokristall-Speicher, 20.03.1999

Borany, J. von,
Untersuchungen zur Stabilität von Ge-Nanoclustern in dünnen Gateoxiden in einer Prozeßtechnologie für nichtflüchtige Speicherzellen,
Zwischenbericht zum SMWK/SMWA-Verbundprojekt: Nanokristall-Speicher, 31.10.1999

Brauer, G.,
Materialforschung mittels Positronen-Annihilationsspektroskopie,
SMWK: 4-7533-70-FZR/705, Zwischenbericht 10.07.1999

Köhler, B., Teichert, J.,
Entwicklung einer neuen Technologie zur Probenpräparation für die Transmissions-Elektronenmikroskopie (TEM) auf der Basis der Ionenfeinstrahlbearbeitung,
SMWK/4-7533-70-864-98/3, Zwischenbericht 30.06.1999

Matz, W., Schell, N., Bernhard, G., Prokert, F., Reich, T., Claußner, J., Oehme, W., Schlenk, R., Dienel, S., Funke, H., Eichhorn, F., Betzl, M., Pröhl, D., Strauch, U., Hüttig, G., Krug, H., Neumann, W., Brendler, V., Reichel, P., Denecke, M.A., Nitsche, H.,
ROBL - a CRG Beamline for Radiochemistry and Materials Research at the ESRF,
Wissenschaftlich-Technische Berichte FZR-256, Apr. 1999

Skorupa, W.,
Blaue Elektrolumineszenz aus nanoskaligen Halbleiteranordnungen,
SMWK/4-7531.50-03-844-98/1, Zwischenbericht 30.06.1999

Teichert, J., Borany, J.v.,
Entwicklung einer Niederenergie- Implantationskammer mit einem neuartigen Bremslinsensystem,
FZR-Report 1999

Laboratory Visits

Berberich, F.,
European Synchrotron Radiation Facility, Grenoble, Feb. 10 - 28, 1999

Bischoff, L.,
AMD Saxony, November 23-24, 1999

Brauer, G.,
Brookhaven National Laboratory, March 27-April 1, 1999

Brauer, G.,
Pennsylvania State University, April 6-16, 1999

Brauer, G.,
University of Hong Kong, Sept. 21 – Oct. 07, 1999; Nov. 9-30, 1999

Eichhorn, F.,
European Synchrotron Radiation Facility, Grenoble, Feb. 18-March 1; June 22–28;
Oct. 25-Nov. 2, 1999

Eichhorn, F.,
Institute of Electronic Materials Technology, Warsaw, Nov. 15 - 19, 1999

Fontaine, F.,
Fernuniversität Hagen, Lehrgebiet Bauelemente der Elektrotechnik,
April 13-14; April 21-22, 1999

Fontaine, F.,
Universität Ulm, Abteilung Festkörperphysik, June 8-10, 1999

Friedrich, M.,
University of Helsinki, Dept. of Physics, Accelerator Laboratory, Oct. 12-16, 1999

Fukarek, W.,
Materials Research Laboratory at Pennsylvania State University, State College, USA,
April 17 – May 15, 1999

Gebel, T.,
Fernuniversität Hagen, July 7-8, 1999

Matz, W., Schell, N., Bernhard, G., Prokert, F., Reich, T., Claußner, J., Oehme, W., Schlenk, R., Dienel, S., Funke, H., Eichhorn, F., Betzl, M., Pröhl, D., Strauch, U., Hüttig, G., Krug, H., Neumann, W., Brendler, V., Reichel, P., Denecke, M.A., Nitsche, H.,
ROBL - a CRG Beamline for Radiochemistry and Materials Research at the ESRF,
Wissenschaftlich-Technische Berichte FZR-256, Apr. 1999

Skorupa, W.,
Blaue Elektrolumineszenz aus nanoskaligen Halbleiteranordnungen,
SMWK/4-7531.50-03-844-98/1, Zwischenbericht 30.06.1999

Teichert, J., Borany, J.v.,
Entwicklung einer Niederenergie- Implantationskammer mit einem neuartigen Bremslinsensystem,
FZR-Report 1999

Laboratory Visits

Berberich, F.,
European Synchrotron Radiation Facility, Grenoble, Feb. 10 - 28, 1999

Bischoff, L.,
AMD Saxony, November 23-24, 1999

Brauer, G.,
Brookhaven National Laboratory, March 27-April 1, 1999

Brauer, G.,
Pennsylvania State University, April 6-16, 1999

Brauer, G.,
University of Hong Kong, Sept. 21 – Oct. 07, 1999; Nov. 9-30, 1999

Eichhorn, F.,
European Synchrotron Radiation Facility, Grenoble, Feb. 18-March 1; June 22–28;
Oct. 25-Nov. 2, 1999

Eichhorn, F.,
Institute of Electronic Materials Technology, Warsaw, Nov. 15 - 19, 1999

Fontaine, F.,
Fernuniversität Hagen, Lehrgebiet Bauelemente der Elektrotechnik,
April 13-14; April 21-22, 1999

Fontaine, F.,
Universität Ulm, Abteilung Festkörperphysik, June 8-10, 1999

Friedrich, M.,
University of Helsinki, Dept. of Physics, Accelerator Laboratory, Oct. 12-16, 1999

Fukarek, W.,
Materials Research Laboratory at Pennsylvania State University, State College, USA,
April 17 – May 15, 1999

Gebel, T.,
Fernuniversität Hagen, July 7-8, 1999

Gebel, T.,
CCR Beschichtungstechnologie GmbH, Rheinbreitbach, Sept.9-10, 1999

Gebel, T.,
California Institute of Technology, Pasadena/CA, USA, Oct.10-Nov.13, 1999

Gebel, T.,
Naval Research Laboratory, Washington DC, USA, Nov.15-27, 1999

Grötzschel, R.,
University of Helsinki, Accelerator laboratory, Oct. 12-16, 1999

Hausmann, S.,
Ruhr-Unversität Bochum, Nov. 3-5, 1999

Heinig, K.-H.,
CSNSM, Orsay, France, May 2-6, 1999

Heinig, K.-H.,
University Aarhus, Denmark, October 29 -30, 1999

Kolitsch, A.,
City University of Hong Kong, 27-29 Sept., 1999

Kreher, J.,
European Synchrotron Radiation Facility, Grenoble, June 14 – 22; Sept. 27 - Oct. 3, 1999

Mäder, M.,
Laboratoire de Recherche des Musées de France, Le Louvre, Paris, France, Oct. 2 – 9, 1999

Matz, W.,
European Synchrotron Radiation Facility, Grenoble, March 1 – 3; May 3 – 11; Sept. 16 - 23;
Nov. 29 - Dec. 3, 1999

Matz, W.,
Institute of Electronic Materials Technology, Warsaw, Nov. 11 - 13, 1999

Neelmeijer, C.,
Restoration Lab.of Opificio delle Pietre Dure, Lab. of the Physics Department: INFN and LENS,
Firenze, Italy, March 25 – 26, 1999

Neelmeijer, C.,
Hahn-Meitner-Institut, ISL, Berlin, Germany, Oct. 29 – 30, 1999

Neelmeijer, C.,
Laboratoire de Recherche des Musées de France, Le Louvre, Paris, France, Oct. 2 – 9, 1999

Parascandola, S.,
Colorado School of Mines, Dept. of Physics, Golden, USA, April 22 - 24, 1999

Peeva, A.,
Fed. Univ. of Rio Grande do Sul, Porto Alegre, Nov. 2 - Dec. 13, 1999

Peeva, A.,
MPI für Mikrostrukturphysik , Halle, several weeks during February, April, and June 1999

Posselt, M.,
Environmental Molecular Science Laboratory at Pacific Northwest National Laboratory, Richland, WA, USA, May 7, 1999

Posselt, M.,
Materials Research Laboratory, University of Illinois at Urbana-Champaign, IL, USA, May 10, 1999

Posselt, M.,
Institut für Integrierte Systeme der ETH Zürich, Switzerland, June 9, 1999

Prokert, F.,
European Synchrotron Radiation Facility, Grenoble, May 11 – 18; June 22 – 28; Sept. 14 - 22, 1999

Rebohle, L.,
Thomas J. Watson Laboratory of Applied Physics, California Institute of Technology, Pasadena, CA, USA, January 21-24, 1999

Rebohle, L.,
Naval Research Laboratory, Washington, D.C., USA, Jan. 30-Feb. 2, 1999

Reichel, P.,
European Synchrotron Radiation Facility, Grenoble, March 23 - Apr. 1; June 14 - 22, 1999

Skorupa, W.,
Thomas J. Watson Laboratory of Applied Physics, California Institute of Technology, Pasadena, CA, USA, January 21-24, 1999

Skorupa, W.,
Naval Research Laboratory, Washington, D.C., USA, Jan. 30-Feb. 2, 1999

Skorupa, W.,
Pacific Northwest Laboratory, Richland, WA, USA, May 7-8, 1999

Skorupa, W.,
Inst. für Physikalische Hochtechnologien, Jena, Germany, June 10-11, 1999

Skorupa, W.,
CCR Beschichtungstechnologie GmbH, Rheinbreitbach, Sept.9-10, 1999

Skorupa, W.,
Fed. Univ. of Rio Grande dol Sul, Porto Alegre, Brasilien, Nov. 15-20, 1999

Skorupa, W.,
Comision Nacional de Energia Atomica, Centro Atomico Constituyentes,
Laboratorio TANDAR, San Martín, Pcia. de Buenos Aires, Argentinien, Nov. 23-26, 1999

Strobel, M.,
CSNSM, Orsay, France, May 2-6, 1999

Strobel, M.,
CSN-IMETEM and University of Catania, Italy, December 13-14, 1999

Teichert, J.,
Ruhr-Unversität Bochum, Nov. 3-5, 1999

Patents

Günzel, R.,
Modulator für die Plasmaimmersions – Ionenimplantation,
PCT/DE 98/00144

Heera, V.,
Verfahren zur Herstellung von Kontakten und Leitbahnen in oder auf kristallinen Siliziumkarbid-Halbleitersubstraten
Erfindungsanmeldung beim Deutschen Patentamt, AZ 199 44 144.8, 15.09.1999

Heinig, K.-H., Schmidt, B.,
Verfahren zur Verringerung der Breite der Größenverteilung von Nanoclustern in Festkörpern,
Erfindungsanmeldung beim Deutschen Patentamt, AZ 199 31 971.5, 09.07.1999

Schmidt, B., Heinig, K.-H.,
Verfahren zur Herstellung von Monolagen aus Silizium-Nanoclustern in Siliziumoxid,
Erfindungsanmeldung beim Deutschen Patentamt, AZ 199 33 632.6, 17.07.1999

PhD Theses

Rebohle, L.,
Lumineszenzeigenschaften ionenimplantierter nanokristalliner SiO_2-Schichten,
TU Dresden, 04.11.1999

Strobel, M.,
Modeling and Computer Simulation of Ion Beam Synthesis of Nanostructures,
TU Dresden, 13.10.1999

Weber, R.,
Präzipitation von SiO_2 in Silicium nach einer Sauerstoff-Hochdosisimplantation,
TU Dresden, 26.04.1999

Awards

Hauschild, T.,
Best poster contribution at HERCULES 1999, Grenoble, France, March, 1999

Parascandola, S.,
ICMCTF'99 Student Scholarship, ICMCTF'99, San Diego, Ca, USA, April 12 - 15, 1999

Strobel, M.,
Doktorandenpreis des FZ-Rossendorf 1999

Guests

M. Alfaro,
Max-Planck-Inst. für Kernphysik Heidelberg, Dec. 13 - 14, 1999

V. M. Anishchik,
Belarussian State Univeristy, Minsk, Belarus, Dec. 17 – 24, 1999

Hydroxyapatite Nucleation on Na Ion Implanted Titanium Surfaces

M.T. Pham, W. Matz, H. Reuther, E. Richter, G. Steiner*
* Institut für Analytische Chemie, Technische Universität Dresden

Hydroxyapatite (HA) coating is the common approach to improve the biocompatibility of orthopaedic and dental titanium-based implants. Low-temperature processses are of current interest. In these processes, biologically active HA having the chemistry and structure of mineralized tissue may be formed under *in vivo* simulated conditions. One key problem is to impart Ti surfaces with the ability to nucleate HA formation from an aqueous solution. An enhanced HA nucleation can be achieved by (i) functionalized surfaces acting as molecular blueprints for site-directed nucleation, (ii) elevated supersaturation of HA at the surface, and (iii) surface topography providing confined reaction microenvironments and geometrically matched nucleating sites. Ti surfaces treated with NaOH have been shown to induce HA formation upon exposing to simulated body fluid (SBF) [1,2]. The effect is closely related to the above criteria: generation of hydroxylated surface Ti–OH groups and increased supersaturation of HA by increased surface pH resulted from Na_2TiO_3 hydrolysis, and etching-generated rugged surface morphology.

This paper presents the surface treatment involving ion implantation of Na into Ti to show that surface-incorporated Na_2TiO_3 and a microporous rugged surface topography are formed by reactions of Na with Ti, and such surfaces are reactive to induce HA nucleation upon exposing to SBF. The present experiments used plates of commercially pure Ti (10 × 10 × 1 mm^3). Standard procedures of polishing and cleaning were applied before use. Na ions were implanted at doses ranging from 8×10^{16} to 4×10^{17} ions cm^{-2}. The ion energies were set at 18 to 22 keV to deposit Na within a surface layer of (22 – 28) ± 14 nm thickness. Exposure experiments in SBF of pH 7.4 were conducted at 37 °C in polystyrene vials. The surfaces were characterized by XRD, FTIR, XPS, SEM, and light microscopy (LM).

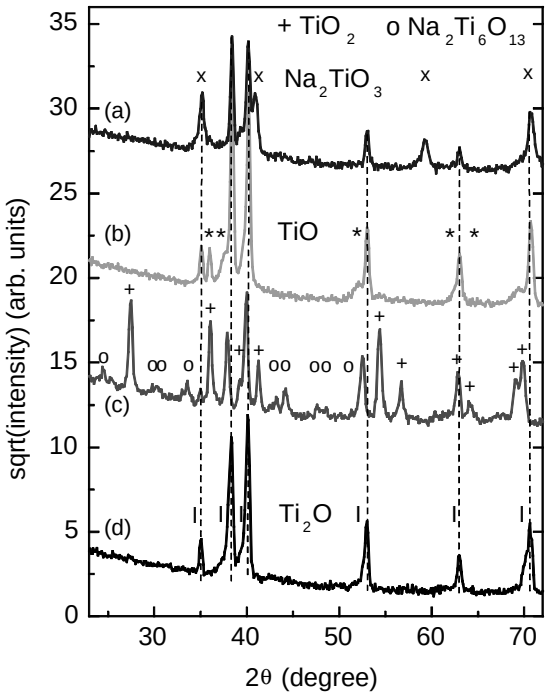

The new major phase introduced into the surface after Na implantation is Na_2TiO_3 as evidenced from the XRD analysis (Fig. 1a). The signal intensity increases with the ion dose indicating the increased concentration formed by ion implantation. The substrate Ti signal is attenuated correspondingly, confirming that the Ti surface becomes covered by the implanted layer.

Fig. 1: XRD patterns of (a) an as-implanted Ti sample, 2.4×10^{17} Na^+ cm^{-2}, showing the formation of Na_2TiO_3, (b) a sample implanted with 1.6×10^{17} Na^+ cm^{-2} followed by a heat treatment at 400 °C in air for 20 min, (c) like b with heat treatment at 700 °C producing $Na_2Ti_6O_{13}$, and (d) a preoxidized Ti surface implanted with 2.4×10^{17} Na^+ cm^{-2}. The different phases are marked by symbols. The vertical dashed lines indicate the titanium Bragg reflections of the substrate.

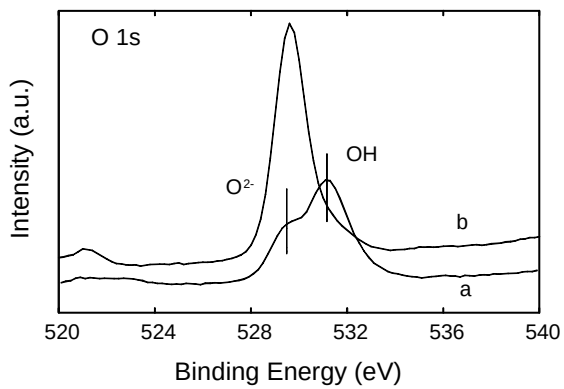

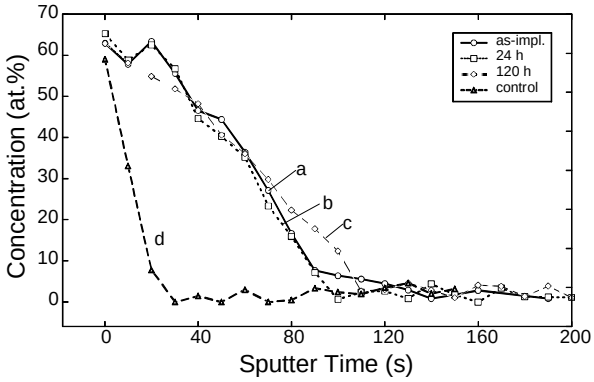

Fig. 2 (left): O 1s XPS spectra from a Ti sample implanted with 1.6×10^{17} Na^+ cm^{-2}: (a) as-implanted, (b) after heat treatment at 700 °C in air for 20 min. O 1s subpeaks reveal oxide-bound O^{2-} species at 530.0 eV and hydroxide-bound OH species at 531.3 eV. 700 °C heat treatment leads to an enhanced development of the oxide part and removal of the hydroxide part.

Fig. 3 (right): Sputter depth profiles of O determined from XPS of (a:❍) an as-implanted Ti sample (2.4×10^{17} Na^+ cm^{-2}), (b:❑) like a after 24 h incubation in a 137 mM NaCl solution at 37 °C, (c:◇) like b after 120 h incubation, and (d: Δ) a control sample without Na implantation after incubation treatment like c.

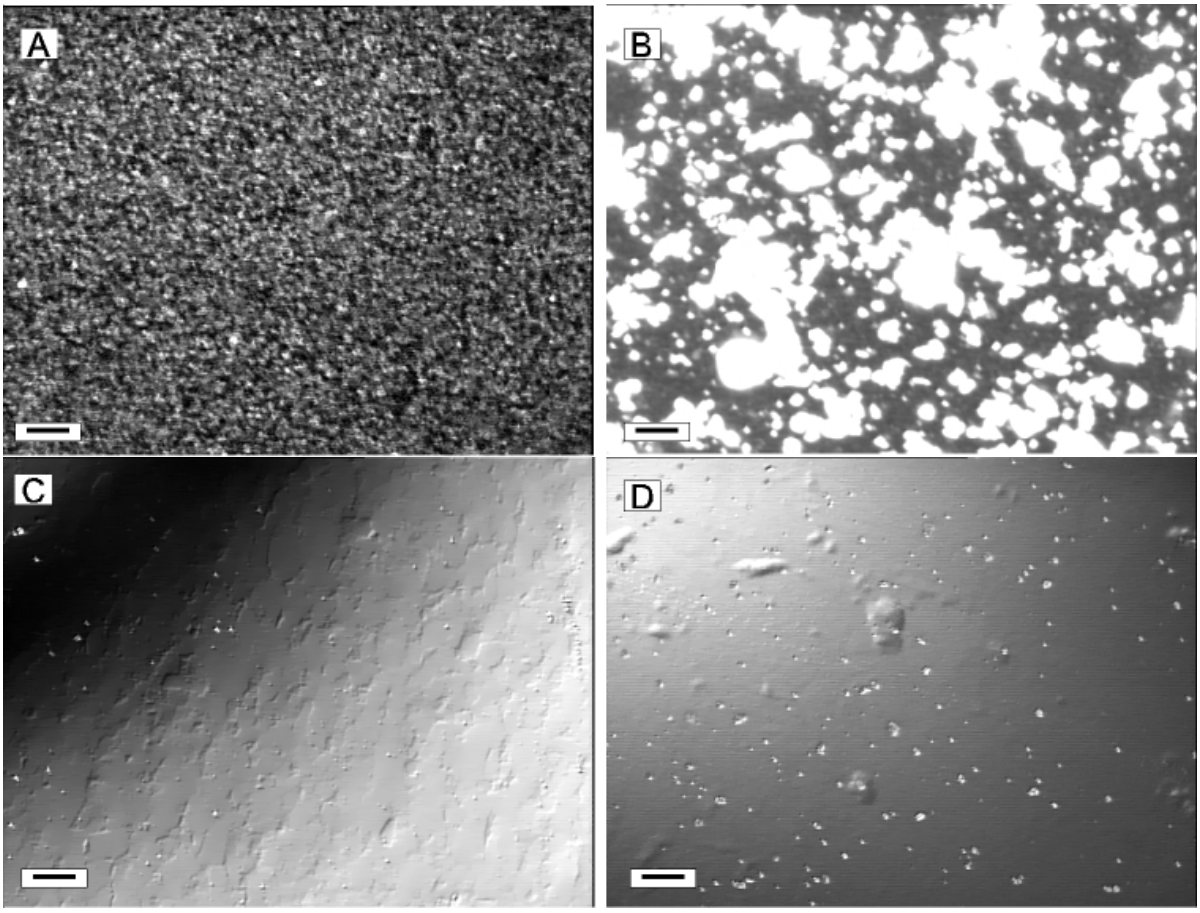

Fig. 4: Light microscopic images showing the evolution of surface morphology: (A) Ti implanted with 2.4×10^{17} Na^+ cm^{-2}, (B) sample A after 24 h incubation in SBF, (C) original Ti surface, and (D) sample C after 24 h incubation in SBF. Bright features in B and D are hydroxyapatite precipitates. Scale bars: 10 µm.

XPS measurements, Fig. 2, revealed that the surface contains oxide- and hydroxide-bound oxygen. This indicates the propencity for hydroxylating and is consistent with the presence of sodium oxide/titanate. Na_2TiO_3 is incorporated within the surface layer. The penetration of Na was seen to follow that of O, suggesting that Na ions are active oxygen-carrying species during implantation. Fig. 3 shows the depth profiles of O indicating the formed titanate layer. Heat treatment was shown to strongly modify the composition of the implanted layer. Heating to 400 °C in air for 20 min results in the formation of TiO and reduction of the Na_2TiO_3 amount (Fig. 1b). $Na_2Ti_6O_{13}$ occurs at 700 °C (Fig. 1c). These reactions can be related to the reduced power of Na and its peroxide and hyperoxide formed during the heat treatment. This is confirmed when Na was implanted into a rutile-coated (preoxidized) Ti surface showing the formation of Ti_2O, but no crystalline phase of any Na-Ti compounds (Fig. 1d).

Sodium ion implantation results in roughening the Ti surface. The roughness increases with the ion dose. Fig. 4a shows surface features produced at an ion dose of 2.4×10^{17} Na^+ cm^{-2} revealing µm-scaled porous structures homogeneously distributed over the entire surface. A rigorous reaction of Na with Ti, in addition to the ion implantation induced sputtering, can account for this large scale in roughness. The ability for HA nucleation was assessed by incubation tests in SBF. A 24 h exposure to SBF evidently revealed the enhanced deposition of calcium phosphate (Ca-P) from the solution into a Na implanted surface. Fig. 4b demonstrates this result: precipitate features covering a large part of the surface. Resolved imaging by SEM exhibited that the surface is densely seeded with precipitate nuclei. The large aggregates seen in Fig. 4b indicate the spontaneous precipitation and the rapid growth on these reactive Ca-P nuclei. The precipitates from SBF were identified by XRD and FTIR to be hydroxyapatite.

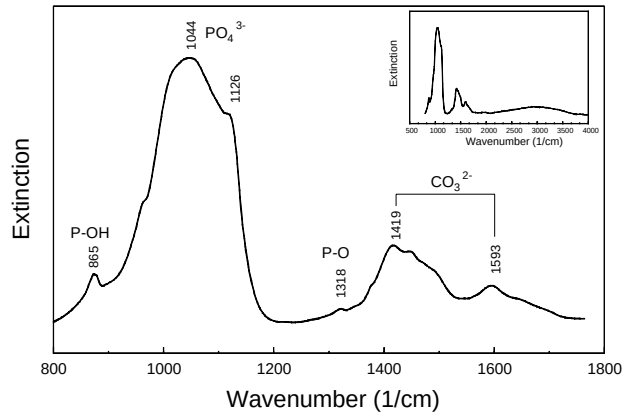

Fig. 5: IR spectra of a Na implanted Ti surface after 120 h incubation in SBF revealing characteristics of a typical carbonated hydroxyapatite. The inset shows a survey spectrum displaying the apatite OH absorption band at around 3579 cm^{-1}.

Fig. 5 shows the FTIR spectra of such precipitates formed on a Na implanted Ti surface. As shown by XRD, HA is formed while Na_2TiO_3 disappears, suggesting the active involvement of the latter in the reactions. The hydrolysis of Na_2TiO_3 produces hydroxylated surface -Ti-OH and increase in pH, two factors encouraging the HA nucleation. The morphology of a control sample is also presented for reference (Figs. 4c and d). The control surface displays only some scattered precipitates (Fig. 4d), implying that the HA nucleation on pure Ti surface is greatly inhibited.

References

[1] H.M. Kim, F. Miyaji, T. Kokubo, T. Nakamura, J. Biomed. Mater. Res. 32 (1996) 409; H.M. Kim, F. Miyaji, T. Kokubo, S. Nishiguchi, T. Nakamura, J. Biomed. Mater. Res. 45 (1999) 100

[2] H.B. Wen, J.R. de Wijn, F.Z. Cui, K. de Groot, Biomaterials 19 (1998) 215

Patents

Günzel, R.,
Modulator für die Plasmaimmersions – Ionenimplantation,
PCT/DE 98/00144

Heera, V.,
Verfahren zur Herstellung von Kontakten und Leitbahnen in oder auf kristallinen Siliziumkarbid-Halbleitersubstraten
Erfindungsanmeldung beim Deutschen Patentamt, AZ 199 44 144.8, 15.09.1999

Heinig, K.-H., Schmidt, B.,
Verfahren zur Verringerung der Breite der Größenverteilung von Nanoclustern in Festkörpern,
Erfindungsanmeldung beim Deutschen Patentamt, AZ 199 31 971.5, 09.07.1999

Schmidt, B., Heinig, K.-H.,
Verfahren zur Herstellung von Monolagen aus Silizium-Nanoclustern in Siliziumoxid,
Erfindungsanmeldung beim Deutschen Patentamt, AZ 199 33 632.6, 17.07.1999

PhD Theses

Rebohle, L.,
Lumineszenzeigenschaften ionenimplantierter nanokristalliner SiO_2-Schichten,
TU Dresden, 04.11.1999

Strobel, M.,
Modeling and Computer Simulation of Ion Beam Synthesis of Nanostructures,
TU Dresden, 13.10.1999

Weber, R.,
Präzipitation von SiO_2 in Silicium nach einer Sauerstoff-Hochdosisimplantation,
TU Dresden, 26.04.1999

Awards

Hauschild, T.,
Best poster contribution at HERCULES 1999, Grenoble, France, March, 1999

Parascandola, S.,
ICMCTF'99 Student Scholarship, ICMCTF'99, San Diego, Ca, USA, April 12 - 15, 1999

Strobel, M.,
Doktorandenpreis des FZ-Rossendorf 1999

Guests

M. Alfaro,
Max-Planck-Inst. für Kernphysik Heidelberg, Dec. 13 - 14, 1999

V. M. Anishchik,
Belarussian State Univeristy, Minsk, Belarus, Dec. 17 – 24, 1999

W. Assmann,
Universität München, Oct. 28 -29, 1999

V. T. Astrelin,
Budker Institute of Nuclear Physics, Novosibirsk, Russia, Nov. 5 – Dec. 19, 1999

M. Behar,
Dept. of Physics, Univ. of Rio Grande dol Sul, Porto Allegre, Brazil, July 11-Aug. 7, 1999

V.I. Belko,
Belarussian State University, Minsk, Belarus, March 14 - June 12; Sept. 27 – Dec. 26, 1999

V. Borodin
Russian Research Centre "Kurchatov Institute", Moscow, Russia, Sept. 25 – Nov. 16, 1999

G. Catchen,
Pennsylvania State University, USA, May 20-21, 1999

A. A. Deshkovskaya,
Belarussian State University, Minsk, Belarus, Nov. 16 – Dec. 23, 1999

B. Dev
Institute of Physics, Bhubaneswar, India, Aug. 3 - 11, 1999

N. Donkov,
Institute of Electronics, Bulgarian Academy of Science Sofia, Bulgaria, Nov. 15 – Dec. 1, 1999

J. Engeldinger,
Univ. des Saarlandes, Inst. für Physikalische Chemie, Nov. 29 – Dec. 3, 1999

P. Fichtner,
Dept. of Physics, Univ. of Rio Grande dol Sul, Porto Allegre, Brazil, July 25-Aug. 14, 1999

C. Fiebiger,
Fachhochschule Köln, Fachbereich Restaurierung/Konservierung, Köln, Germany, Nov. 9 – 11, 1999

G. Gawlik,
Institute of Electronic Materials Technology, Warsaw, Poland, Oct. 3-10, 1999

B. Groß,
Univ. des Saarlandes, Inst. für Physikalische Chemie, Nov.29 – Dec. 3, 1999

D. K. Gupta,
Institute for Plasma Research, India, June 25 – July 7, 1999

M. Hecker,
Institut für Festkörper- und Werkstoffforschung, Dresden, June 19 - 22, 1999

B. Heisel,
Univ. des Saarlandes, Inst. für Physikalische Chemie, Nov. 29 – Dec. 3, 1999

N. Huang,
Southwest Jiaotong University, Chengdu, China, Jan. 1 – Sept. 26, 1999

R. Jarjis,
University of Oxford, Dept. of Materials, Oxford, UK, June 20 – July 4, 1999

D. Jembrich,
Technische Universität, Institut für analytische Chemie, Wien, Austria, Nov. 20 – Dec. 3, 1999

R.U.A. Khan,
University of Surrey, Guildford, UK, May 1- July 31, 1999

M.Kokkoris,
National Technical University of Athens, Greece, Aug. 2 - 6, 1999

J.Krynicki,
Institute of Chemistry and Nuclear Technology, Warsaw, Poland, Nov. 8 - 12, 1999

V. Kh. Liechtenstein,
Institute of Nuclear Fusion, Russian Research Centre „Kurchatov Institute“, Moscow,
July 31 – Aug. 6, 1999

Dr. Xuan Luo,
Institute of Physics, Chinese Academy of Sciences, Beijing, China, June 21 – Sept. 20, 1999

K.N. Madhusoodanan,
Univ. Cochin, India, May 5-July 28, 1999

V.V. Makarov,
Centre for Analysis of Substances, Moskau, March 24-26, 1999; Dec. 3-9, 1999

K. Mazur,
Institute of Electronic Materials Technology, Warsaw, Poland, July 12 - 17, 1999

B.K. Panda,
Humboldt-Stipendiat, April 29, 1998 -April 30, 1999

A. Perez-Rodriguez,
Dept. Appl.Phys. and Electronics, Univ. Barcelona, Spain, Dec. 9-14, 1999

A. Piatkowsa,
Institute of Electronic Materials Technology, Warsaw, Poland, Oct. 3-10, 1999

J. Piekoszewski,
Soltan Institute for Nuclear Studies, Otwock, Poland, March, May and November 1999

F. Priolo,
Univ. of Catania, Italy, July 21-25, 1999

I. Prochaska,
Charles University Prague, Dec. 6-7, 1999

J. Raisanen,
University of Jyväskylä, Dept. of Physics, Nov. 1-3, 1999

E. Rauhala,
University of Helsinki, Dept. of Physics, Nov. 1-3, 1999

A. G. Revesz,
Revesz Associates and Naval Research Laboratories, Washington D.C., USA, June 19-23, 1999

R. Riehn,
University Kapstadt, South Africa, Feb. 1-March 26, 1999

A. I. Rogozin,
Budker Institute of Nuclear Physics, Novosibirsk, Russia, Jan 22 – May 23; Sept. 26 – Dec. 26, 1999

J. Sass,
Institute of Electronic Materials Technology, Warsaw, Poland, July 12 - 17, 1999

M. Schreiner,
Akademie der Bildenden Künste, Institut für Farbenchemie, Wien, Austria, Nov. 20 – 25, 1999

F. Schrempel,
Friedrich-Schiller-Universität Jena, Inst. für Festkörperphysik, Nov. 22 – 24, 1999

T. Schwendler,
TU Chemnitz, Feb. 1-4; March 10-12; June 14 –17; Oct.25-26, 1999

N. Shevchenko,
Tomsk State University, Russia, Nov. 26 – Dec. 24, 1999

E. Sendezera,
University of Zululand, South Africa, April 9-26, 1999

Ch. Serre,
Dept. Appl.Phys. and Electronics, University Barcelona, Spain, April 19-25, 1999; Dec. 9-15, 1999

T. Som,
Nuclear Science Centre, New Delhi, India, July 15 – Oct. 12, 1999

A. Ster,
MTA-KFKI, Research Institute for Technical and Materials Science, Budapest, Hungary,
Feb. 21 - March 13; Sept. 28 – Oct. 31, 1999

J. Stoemenos,
Univ. Thessaloniki, Greece, May 17-21, 1999

M. Swart,
University of the North, Sovenga/Pietersburg, South Africa, Oct. 11 – Dec. 10, 1999

M.Toulemonde,
CIRIL, Caen,France, Oct. 28-29, 1999

A.Turos,
Institute of Electronic Materials Technology, Warsaw, Poland, March 4 - 7, Oct. 3-10,
Dec. 6 - 14, 1999

T. Tzvetkova,
Institute of Solid State Physics, Bulgarian Academy of Science Sofia, Bulgaria, Nov.28–Dec.23, 1999

M.Ueda,
Instituto Nacional de Pesquisas Espaciais, S. Paulo, Brasilien, July 30 - Aug. 11, 1999

R. Vlastou,
National Technical University of Athens, Greece, Aug. 2- 6, 1999

A. Volkov,
Russian Research Centre “Kurchatov Institute“, Moscow, Russia, Sept. 25 – Nov. 16, 1999

A. Wallianos,
Max-Planck-Inst. für Kernphysik Heidelberg, April 12 - 16; Dec. 13 - 14, 1999

D. L. Williamson,
Colorado School of Mines, Dept. of Physics, USA, Sept. 4 – 7, 1999

Young-Suk Kim,
Friedrich-Schiller-Universität Jena, Inst. für Festkörperphysik, Nov. 22 – 24, 1999

Meetings Organized by the Institute

14th International Conference on Ion Beam Analysis/6th European Conference on Accelerators in Applied Research and Technology, Dresden, July 26 – 30, 1999
Chairman: W. Möller

3rd Summer School "Nuclear Probes and Ion Beams“, Bad Blankenburg, Thuringia, Sept. 1999
(FZ Rossendorf/HMI Berlin)

Second Year Coordination Meeting of the TMR Network, "Synthesis, structure and properties of new carbon based hard materials", Nov. 18-21, 1999, Dresden

First Round Table Meeting of the Large-Scale Facility, „Center for Application of ion beams in materials research (AIM)“, Dec. 12, 1999, Dresden

Seminar of the Institute

Dr. P. Schaaf
Universität Göttingen
Laser-Nitrieren: Superschnelles Nitrieren von Eisen, untersucht mit schnellen Ionen und ergänzenden Methoden
Jan. 28, 1999

Dr. C. A. Straede
DTI Tribology Centre Aarhus
Development of advanced surface treatment with the aim of industrial use
Feb. 25, 1999

D. Fey
Architekturen für ein Photonisches VLSI
Gesamthochschule Siegen/ Univ. Jena
April 16,1999

Prof. S. Nepijko
FHI Berlin
Emissionseigenschaften von kleinen Teilchen (Schwerpunkt: Lichtemission)
April 22, 1999

Dr. H. Sachdev
Uni Saarbrücken
Die Gasphasenabscheidung von c-BN mittels CVD-Methoden
April 29, 1999

A. Wallianos,
Max-Planck-Inst. für Kernphysik Heidelberg, April 12 - 16; Dec. 13 - 14, 1999

D. L. Williamson,
Colorado School of Mines, Dept. of Physics, USA, Sept. 4 – 7, 1999

Young-Suk Kim,
Friedrich-Schiller-Universität Jena, Inst. für Festkörperphysik, Nov. 22 – 24, 1999

Meetings Organized by the Institute

14th International Conference on Ion Beam Analysis/6th European Conference on Accelerators in Applied Research and Technology, Dresden, July 26 – 30, 1999
Chairman: W. Möller

3rd Summer School "Nuclear Probes and Ion Beams“, Bad Blankenburg, Thuringia, Sept. 1999
(FZ Rossendorf/HMI Berlin)

Second Year Coordination Meeting of the TMR Network, "Synthesis, structure and properties of new carbon based hard materials", Nov. 18-21, 1999, Dresden

First Round Table Meeting of the Large-Scale Facility, „Center for Application of ion beams in materials research (AIM)“, Dec. 12, 1999, Dresden

Seminar of the Institute

Dr. P. Schaaf
Universität Göttingen
Laser-Nitrieren: Superschnelles Nitrieren von Eisen, untersucht mit schnellen Ionen und ergänzenden Methoden
Jan. 28, 1999

Dr. C. A. Straede
DTI Tribology Centre Aarhus
Development of advanced surface treatment with the aim of industrial use
Feb. 25, 1999

D. Fey
Architekturen für ein Photonisches VLSI
Gesamthochschule Siegen/ Univ. Jena
April 16,1999

Prof. S. Nepijko
FHI Berlin
Emissionseigenschaften von kleinen Teilchen (Schwerpunkt: Lichtemission)
April 22, 1999

Dr. H. Sachdev
Uni Saarbrücken
Die Gasphasenabscheidung von c-BN mittels CVD-Methoden
April 29, 1999

A. Wallianos,
Max-Planck-Inst. für Kernphysik Heidelberg, April 12 - 16; Dec. 13 - 14, 1999

D. L. Williamson,
Colorado School of Mines, Dept. of Physics, USA, Sept. 4 – 7, 1999

Young-Suk Kim,
Friedrich-Schiller-Universität Jena, Inst. für Festkörperphysik, Nov. 22 – 24, 1999

Meetings Organized by the Institute

14th International Conference on Ion Beam Analysis/6th European Conference on Accelerators in Applied Research and Technology, Dresden, July 26 – 30, 1999
Chairman: W. Möller

3rd Summer School "Nuclear Probes and Ion Beams“, Bad Blankenburg, Thuringia, Sept. 1999
(FZ Rossendorf/HMI Berlin)

Second Year Coordination Meeting of the TMR Network, "Synthesis, structure and properties of new carbon based hard materials", Nov. 18-21, 1999, Dresden

First Round Table Meeting of the Large-Scale Facility, „Center for Application of ion beams in materials research (AIM)“, Dec. 12, 1999, Dresden

Seminar of the Institute

Dr. P. Schaaf
Universität Göttingen
Laser-Nitrieren: Superschnelles Nitrieren von Eisen, untersucht mit schnellen Ionen und ergänzenden Methoden
Jan. 28, 1999

Dr. C. A. Straede
DTI Tribology Centre Aarhus
Development of advanced surface treatment with the aim of industrial use
Feb. 25, 1999

D. Fey
Architekturen für ein Photonisches VLSI
Gesamthochschule Siegen/ Univ. Jena
April 16,1999

Prof. S. Nepijko
FHI Berlin
Emissionseigenschaften von kleinen Teilchen (Schwerpunkt: Lichtemission)
April 22, 1999

Dr. H. Sachdev
Uni Saarbrücken
Die Gasphasenabscheidung von c-BN mittels CVD-Methoden
April 29, 1999

Dr. H. Stoeri
TU Wien
Dynamik gepulster Gleichstromentladungen
May 6, 1999

Dr. J. Meijer
Ruhr-Universität Bochum
Beschleuniger-Mikrostrahlanlage zur Materialmodifikation
June 10, 1999

Prof. W. Richter
TU Berlin
Real-Time-Kontrolle von Oberflächenmodifikationen
June 17, 1999

A.G. Revesz
Revesz Associates, Bethesda, MD, USA and Naval Research Lab., Washington, D.C., USA
Effects of heat treatments in inert ambients on Si/SiO_2 structures
June 21, 1999

Dr. A. Ohl
Institut für Niedertemperatur-Plasmaphysik, Greifswald
Plasmainduzierte chemische Mikrostrukturierung von Polymeroberflächen
July 15, 1999

Prof. F. Priolo
Univ. of Catania, Italy
Rare earth doped Si-nanocrystals for silicon-based optoelectronics
July 22, 1999

Dr. M. C. Ridgway
University of Canberra, Australia
Atomic scale structure in amorphized semiconductors
Oct. 14, 1999

Prof. W. Kutschera
Universität Wien, Austria
Beschleunigermassenspektrometrie am Vienna Environmental Research Accelerator
Oct. 21, 1999

Prof. P. Ziemann
Universität Ulm
Die Selbstorganisation von Blockcopolymeren – Ein vielversprechender Ansatz hin zur Nanolithographie
Dec. 2, 1999

V.V. Makarov
CAS Moscow, Russia
Selected problems of SIMS investigations for Cu-Gettering in silicon
Dec. 6, 1999

Project based on External Funds

The following overview is listed according to the starting dates and informs about the topic, the local project leader and the supporting institution. Additional projects with industrial partners are not included because of confidential agreements.

1.
04/1996 - 03/1999 Bundesministerium für Bildung und Forschung **BMBF**
Ion beam based characterization of silicatic materials for non-destructive analytical work on objects of historic glass and enamel
Dr. Christian Neelmeijer; Tel.: (0351) 260-3254; c.neelmeijer@fz-rossendorf.de

2.
06/1996 - 02/2000 Deutsche Forschungsgemeinschaft **DFG**
Entwicklung eines permeable base Transistors mit Kobaltsilicid-gate auf der Basis maskenloser Implantation mit fokussiertem Ionenstrahl
Dr. Jochen Teichert; Tel.: (0351) 260-3445; j.teichert@fz-rossendorf.de

3.
08/1996 - 10/1999 Deutsche Forschungsgemeinschaft **DFG**
Investigation of the corrosion behaviour of magnesium and magnesium alloys by oxygen ion implantation
Dr. Edgar Richter; Tel.: (0351) 260-3326; e.richter@fz-rossendorf.de

4.
09/1996 - 07/1999 Deutsche Forschungsgemeinschaft **DFG**
Depth selective analysis of the metallurgical phase formation and phase composition in ion implanted iron-silicon surface layers by Mössbauer spectroscopy
Dr. Helfried Reuther; Tel.: (0351) 260-2898; h.reuther@fz-rossendorf.de

5.
01/1997 - 12/1999 Deutsche Forschungsgemeinschaft (SFB 422) **DFG**
Nanostructures in ion irradiated interfaces of multilayers prepared by pulsed laser deposition
Prof. Dr. Egbert Wieser; Tel.: (0351) 260-3096; e.wieser@fz-rossendorf.de

6.
03/1997 - 02/1999 Deutsche Forschungsgemeinschaft **DFG**
Plasma immersion ion implantation: experiments and simulation of the sheet layer dynamics
Prof. Dr. Wolfhard Möller; Tel.: (0351) 260-2245; w.moeller@fz-rossendorf.de

7.
03/1997 - 02/2000 Deutsche Forschungsgemeinschaft **DFG**
Modification of the electrical and optical properties of implanted SiC layers by ion beam induced epitaxial crystallization, annealing and activation
Dr. Viton Heera; Tel.: (0351) 260-3343; v.heera@fz-rossendorf.de

8.
05/1997 - 04/2001 European Union, within the BRITE-EURAM Project **EU**
Plasma immersion ion implantation for enhancing high precision machining with tools of complex geometry
Dr. Reinhard Günzel; Tel.: (0351) 260-2462; r.guenzel@fz-rossendorf.de

9.
07/1997 - 06/2000 Volkswagen-Stiftung **VWSt.**
Improvement of the high-temperature oxidation behaviour of TiAl-based alloys by ion implantation
Prof. Dr. Egbert Wieser; Tel.: (0351) 260-3096; e.wieser@fz-rossendorf.de

10.
07/1997 - 12/2000 Sächsisches Staatsministerium für Wissenschaft und Kunst **SMWK**
Surface analysis of steels and silicon by positron annihilation spectroscopy
Dr. Gerhard Brauer; Tel.: (0351) 260-2117; g.brauer@fz-rossendorf.de

11.
08/1997 - 07/1999 European Union, within the Copernicus Research Program **EU**
Development of heavy duty reactor windows for industrial scale removal of NO_x and SO_2 from flue gas by electron beam treatment
Prof. Dr. Egbert Wieser; Tel.: (0351) 260-3096; e.wieser@fz-rossendorf.de

12.
09/1997 - 06/2000 Sächsisches Staatsministerium für Wirtschaft und Arbeit **SMWA**
Hardening of stainless steel using plasma immersion ion implantation
Dr. Edgar Richter; Tel.: (0351) 260-3326; e.richter@fz-rossendorf.de

13.
10/1997 - 10/1999 Deutsche Forschungsgemeinschaft **DFG**
Deposition of c-BN layers with thickness in the micrometer scale: Diagnostics and modeling of the film growth processes
Dr. Wolfgang Fukarek; Tel.: (0351) 260-2277; w.fukarek@fz-rossendorf.de

14.
11/1997 - 10/2001 European Union, within the TMR Network **EU**
Synthesis, structure and properties of new carbon based hard materials
Dr. Andreas Kolitsch; Tel.: (0351) 260-3348; a.kolitsch@fz-rossendorf.de

15.
01/1998 - 12/1999 Deutscher Akademischer Austauschdienst **DAAD**
Nb/NbN-layers on Ti produced by plasma immersion ion implantation
Dr. Edgar Richter; Tel.: (0351) 260-3326; e.richter@fz-rossendorf.de

16.
01/1998 - 12/1999 Deutsche Forschungsgemeinschaft **DFG**
Investigation of defects of the vacancy-type in ion beam treated silicon carbide by means of positron annihilation spectroscopy
Dr. Gerhard Brauer; Tel.: (0351) 260-2117; g.brauer@fz-rossendorf.de

17.
01/1998 - 12/1999 Deutscher Akademischer Austauschdienst **DAAD**
Nucleation, growth and gettering behavior of helium induced cavities in silicon
Dr. Wolfgang Skorupa; Tel.: (0351) 260-3612; w.skorupa@fz-rossendorf.de

18.
01/1998 - 12/1999 Deutscher Akademischer Austauschdienst **DAAD**
Installation of a negative helium ion source for the operation at the Rossendorf tandem accelerator
Dr. Manfred Friedrich; Tel.: (0351) 260-3284; m.friedrich@fz-rossendorf.de

19.
03/1998 - 02/2002 European Union, within the TMR Programme **EU**
European network on defect engineering of advanced semiconductor devices
Dr. Karl-Heinz Heinig; Tel.: (0351) 260 3288; kh.heinig@fz-rossendorf.de

20.
04/1998 - 03/2001 Bundesministerium für Bildung und Forschung **BMBF**
Nutzung der Rossendorfer Beschleuniger
Prof. Dr. Wolfhard Möller; Tel.: (0351) 260-2245; w.moeller@fz-rossendorf.de

21.
07/1998 - 06/2000 Sächsisches Staatsministerium für Wissenschaft und Kunst **SMWK**
Physical and technological fundamentals for the engineering of nanoclusters for nonvolatile memories
Dr. Johannes von Borany; Tel.: (0351) 260-3378; j.v.borany@fz-rossendorf.de

22.
07/1998 - 12/2000 Sächsisches Staatsministerium für Wissenschaft und Kunst **SMWK**
Blue electroluminescence from nanoscaled semiconductor structures
Dr. Wolfgang Skorupa; Tel.: (0351) 260-3612; w.skorupa@fz-rossendorf.de

23.
07/1998 - 12/2000 Sächsisches Staatsministerium für Wissenschaft und Kunst **SMWK**
Surface layers with structures in nanometer scales used for medical implants
Dr. Edgar Richter; Tel.: (0351) 260-3326; e.richter@fz-rossendorf.de

24.
07/1998 - 12/2000 Sächsisches Staatsministerium für Wissenschaft und Kunst **SMWK**
Preparation of TEM samples by means of focused ion beam milling
Dr. Jochen Teichert; Tel.: (0351) 260-3445; j.teichert@fz-rossendorf.de

25.
07/1998 - 12/2000 Sächsisches Staatsministerium für Wissenschaft und Kunst **SMWK**
Optimization of Ta barrier layers for copper metallization of microelectronic devices
Prof. Dr. Egbert Wieser; Tel.: (0351) 260-3096; e.wieser@fz-rossendorf.de

26.
10/1998 - 04/2000 European Union, within the TMR Programme **EU**
(Large Scale Facility) Center for application of ion beams in materials research
Prof. Dr. Wolfhard Möller; Tel.: (0351) 260-2245; w.moeller@fz-rossendorf.de

27.
10/1998 - 11/2001 Deutsche Forschungsgemeinschaft **DFG**
Ion-acoustic microscopy using focused ion beams
Dr. Lothar Bischoff; Tel.: (0351) 260-2963; l.bischoff@fz-rossendorf.de

28.
11/1998 - 10/2001 Deutsche Forschungsgemeinschaft **DFG**
Modeling and computer simulation of amorphous hard carbon film growth by energetic particle impact
Dr. Hans-Ulrich Jäger; Tel.: (0351) 260-3373; h.u.jaeger@fz-rossendorf.de

29.
01/1999 - 12/1999 Deutscher Akademischer Austauschdienst **DAAD**
DLTS- and PAS-Studies of ion implanted silicon carbide
Dr. Gerhard Brauer; Tel.: (0351) 260-2117; g.brauer@fz-rossendorf.de

30.
01/1999 - 12/2000 Deutscher Akademischer Austauschdienst **DAAD**
Development of a technology of high temperature sensors based on SiCOI substrates
Dr. Dieter Panknin; Tel.: (0351) 260-3613; d.panknin@fz-rossendorf.de

31.
01/1999 - 12/2001 Bundesministerium für Bildung und Forschung **BMBF**
Nanoclusterbildung durch Ionenimplantation, Zusammenarbeit mit Russland
Dr. Karl-Heinz Heinig, Tel.: (0351) 260-3288; k.h.heinig@fz-rossendorf.de

32.
07/1999 - 06/2002 WTZ mit Bulgarien **WTZ**
Investigation of the clusters emission characteristics of liquid metal ion source with the aim to produce focused ionized cluster beams
Dr. Jochen Teichert; Tel.: (0351) 260-3445; j.teichert@fz-rossendorf.de

33.
09/1999 - 09/2001 Deutsche Forschungsgemeinschaft **DFG**
Dynamische in situ-Untersuchung der Entstehung von kompressiven Spannungen in Bornitridschichten und des Einflusses von Verunreinigungen und Wachstums-parametern
Dr. Wolfgang Fukarek; Tel.: (0351) 260 2277; w.fukarek@fz-rossendorf.de

34.
11/1999 - 12/2001 Deutsche Forschungsgemeinschaft **DFG**
Preparation of stacked monolayers of semiconductor nanoclusters
Dr. Bernd Schmidt, Tel.: (0351 260-2726 ; bernd.schmidt@fz-rossendorf.de

Experimental Equipment

1. Accelerators, Ion Implanters and Ion-Assisted-Deposition

²	van de Graaf accelerator	1,8 MeV	
²	Tandem accelerator [EGP 10-1]	5 MV	*NIIEFA, Russia*
²	Tandetron accelerator	3 MV	*HIGH VOLTAGE, NL*
²	Ion implanter	80 kV	Own construction
²	Ion implanter	180 kV, medium current	*SCANIBAL, FL*
²	High current ion implanter	200 kV, high current	*DANFYSIK, DK*
²	High energy ion implanter	500 kV	*HIGH VOLTAGE, NL*
²	Plasma-immersion ion implantation	5-60 keV	
²	Fine focused ion beam	50 keV, 100 nm, 10 A/cm^2	
²	Ion beam assisted deposition		
²	Plasma enhanced chemical vapour deposition		

2. Particle and Photon Based Analytical Techniques

²	RBS	Rutherford backscattering	p," : 1-6 MeV	
²	ERDA	Elastic recoil detection analysis	35 MeV, ^{35}Cl	
²	PIXE	Proton induced X-ray analysis	+ PIGE-option, external beam	
²		Nuclear microprobe	MeV, > 2 µm	
²	NRA	Nuclear reaction analysis	^{1}H (^{15}N," ( ) ^{12}C	
²	SEM	Scanning electron microscope	+ EDX-option	*ZEISS, D*
²	TEM	Transmission electron microscope	300 kV, LaB_6	*PHILIPS, NL*
			+ EDX-option	
²	STM	Scanning tunneling microscope	+ AFM-option	*DME, DK*
²	AES	Auger electron spectroscopy	+ XPS-option	*FISONS, GB*
²	CEMS	Mössbauer spectroscopy		
²	XRD	X-ray diffraction	laboratory + synchrotron (ROBL)	
²	SE	Spectroscopic ellipsometry	250-1700 nm	*WOOLLAM, USA*
²	FTIR	Fourier transform infrared spectrometry	600-7000 cm^{-1}	*NICOLET, USA*

3. Other Analytical and Measuring Techniques

²	Dektak surface profilometer	*VEECO, USA*
²	Micro indenter	*SHIMATSU, J*
²	Scratch tester	*SHIMATSU, J*
²	Spreading resistance measuring station	*SENTECH, D*
²	Hall-effect equipment	*BIO-RAD, GB*
²	I-U and C-U- analyzer	*KEITHLEY, USA*

4. Preparation Techniques

²	Wet chemical etching and cleaning	including anisotropic selective KOH-etching
²	Photolithographic patterning	5 µm-level
²	Thermal treatment	Room Temperature - 2000°C Furnace, Flash lamp unit, Rapid thermal annealing, RF-Heating (Vacuum)
²	Physical deposition	Sputtering DC / RF, Evaporation
²	Dry etching	Plasma and RIE mode
²	Bonding techniques	Anodic, Si-Si and Wire Bonding

List of Personnel

Director: Prof. W. Möller

Deputy Director: Prof. E. Wieser

Scientific Staff:

Permanent:

Dr. L. Bischoff
Dr. J. von Borany
Dr. W. Bürger
Dr. F. Eichhorn
Dr. M. Friedrich
Dr. W. Fukarek
Dr. D. Grambole
Dr. R. Grötzschel
Dr. R. Günzel
Dr. V. Heera
Dr. K.-H. Heinig
Dr. H.-U. Jäger
Dr. R. Kögler
Dr. A. Kolitsch
Dr. U. Kreißig
Dr. W. Matz
Dr. A. Mücklich
Dr. C. Neelmeijer
Dr. D. Panknin
Dr. M.T. Pham
Dr. M. Posselt
Dr. F. Prokert
Dr. H. Reuther
Dr. E. Richter
Dr. B. Schmidt
Dr. H. Seifarth
Dr. W. Skorupa
Dr. J. Teichert
Dr. H. Tyrroff
Dr. M. Voelskow

Post Docs:

Dr. A. Belov
Dr. T. Chevolleau
Dr. F. Fontaine
Dr. M. Klimenkov
Dr. S. Malhouitre
Dr. M. Soltani-Farshi

Projects:

W. Anwand
Dr. G. Brauer
Dr. V. Ermel
Dr. O. Kruse
M. Mäder
E.-M. Nicht
M. Peikert
Dr. M. Seidel

PhD Students:

F. Berberich
E. Chagarov
C. Fitz
T. Gebel
T. Hauschild
S. Hausmann
A. Höfgen
U. Hornauer
C. Klein
I. Mrotschek
J. Noetzel
S. Parascandola
A. Peeva
L. Rebohle
Br. Schmidt
M. Strobel
T. Telbizova

Technical Staff:

Permanent:

J. Altmann
R. Aniol
G. Anwand
I. Beatus
T. Betzl
W. Boede
K.-D. Butter
E. Christalle
K. Fukarek
W. Gäßner
B. Gebauer
H.-J. Grahl
P. Hartmann
F. Herrmann
G. Hofmann
M. Iseke
S. Klare
R. Kliemann
J. Kreher
A. Kunz
G. Küster
D. Maul
M. Mißbach
K. Müller
F. Nötzold
W. Probst
E. Quaritsch
P. Reichel
B. Richter
M. Roch
B. Scheumann
H. Schluttig
E. Schmidt
G. Schnabel
J. Schneider
A. Scholz
C. Schulenberg
K. Thiemig
S. Turuc
A. Vetter
A. Weise
I. Winkler

Projects:

J. Born
H. Felsmann
G. Grunert
A. Schneider
H. Seifert
G. Winkler